



Universiteit  
Leiden  
The Netherlands

## Integer and fractional quantum hall effects in lattice magnets

Venderbos, J.W.F.

### Citation

Venderbos, J. W. F. (2014, March 25). *Integer and fractional quantum hall effects in lattice magnets*. *Casimir PhD Series*. Retrieved from <https://hdl.handle.net/1887/24911>

Version: Corrected Publisher's Version

License: [Licence agreement concerning inclusion of doctoral thesis in the Institutional Repository of the University of Leiden](#)

Downloaded from: <https://hdl.handle.net/1887/24911>

**Note:** To cite this publication please use the final published version (if applicable).

Cover Page



Universiteit Leiden



The handle <http://hdl.handle.net/1887/24911> holds various files of this Leiden University dissertation.

**Author:** Venderbos, Jörn Willem Friedrich

**Title:** Integer and fractional quantum hall effects in lattice magnets

**Issue Date:** 2014-03-25

# CHAPTER 9

---

## DENSITY-WAVE STATES FROM A SYMMETRY PERSPECTIVE IN TWO DIMENSIONS

---

### 9.1 Electronic lattice symmetries

The present section will discuss in detail the mathematical prerequisites for studying the effect of lattice symmetries. We will introduce relevant notation which will be used throughout the paper. Some aspects presented below may be rather technical (even though conceptually straightforward) and upon first reading this section may just be glossed over.

#### 9.1.1 Space group symmetries

In this work we will be mainly concerned with two-dimensional systems and we therefore describe the necessary formalism in this setting. The material presented in this section is very straightforwardly generalized to  $3D$  or even arbitrary dimension, and at the very end of this work we comment on how the content and conclusions of this work may carry over to  $3D$ .

We denote the atomic positions in the crystal lattice by  $\vec{r}_i$ , where  $i$  is a label for the atomic site. The atomic position can be decomposed in terms of the Bravais lattice as

$$\vec{r}_i = \vec{x} + \vec{l}_i, \quad (9.1)$$

where  $\vec{x}$  is a Bravais lattice vector and  $\vec{l}_i$  denotes the position of the  $i$ -th atom with respect to the unit cell vector  $\vec{x}$ . The latter can be written in terms of its generators as

$$\vec{x} = \vec{x}_{n_1 n_2} = n_1 \vec{x}_1 + n_2 \vec{x}_2. \quad (9.2)$$

Here the vector  $\vec{n} = (n_1, n_2) \in \mathbb{Z}^2$  is integer-valued and specifies a given Bravais lattice site. In the following we will occasionally use vectors  $\vec{n}, \vec{m}, \dots$  to refer to unit cells. For a lattice with  $N_{\text{sl}}$  different sublattices, i.e.  $N_{\text{sl}}$  atoms in the unit cell, there are  $N_{\text{sl}}$  distinct  $\vec{l}$  vectors.

Space groups consist of all spatial symmetries of the crystal lattice and here we assume that the space group is symmorphic, meaning that we can always find an origin such that all space group elements are generated by translations and point group operations, which are themselves symmetries. Translations will be written as  $T(\vec{x})$ , representing a translation over lattice vector  $\vec{x}$  and point group operations will be written as  $R$ . In two dimension, to which we particularize unless stated otherwise, and for spinless fermions the dihedral groups  $D_n$  are identical to the groups  $C_{nv}$ , which instead of an in-plane twofold rotation axis, contain a mirror reflection. In the rest of this paper we assume the symmetry group to be  $C_{nv}$ . For spinful fermions the two symmetry groups must be distinguished as the twofold rotation and reflection act differently on the spin degree of freedom. For the most part, this difference is not important for our purposes, we have however included some details on it in Appendix C.3. In the following we will assume the equivalence of  $D_n$  and  $C_{nv}$ , but whenever appropriate or necessary we will comment on the differences. For a  $C_{nv}$  symmetric system, any element of the space group can be written in terms of the four generators  $T(\vec{x}_1), T(\vec{x}_2), C_n$  and  $\sigma_v$ , where  $C_n$  is the  $n$ -fold rotation and  $\sigma_v$  is a reflection. Any element may then be specified by  $T(\vec{x}_1)^{m_1} T(\vec{x}_2)^{m_2} C_n^{m_3} \sigma_v^{m_4}$  and point group operations  $R$  can be written as  $R = C_n^{m_1} \sigma_v^{m_2}$ .

The effect of a point group symmetry on an atomic position is represented as  $R\vec{r}_i = R\vec{x} + R\vec{l}_i$ . As this operation is a symmetry,  $R\vec{r}_i$  is another atomic position, but possibly an inequivalent one. Hence we have  $R\vec{r}_i = \vec{r}'_j = \vec{x}' + \vec{l}'_j$ . It is not necessarily true that  $\vec{x}' = R\vec{x}$ , the difference must however be some lattice vector  $\vec{t}_i$ ,  $\vec{x}' = R\vec{x} + \vec{t}_i$ .  $\vec{t}_i$  depends on the atom in the unit cell, hence the label  $i$ . It thus follows that  $R\vec{r}_i = R\vec{x} + \vec{t}_i + \vec{l}'_j$ .

We now wish to find the transformation properties of the field operators and the

Hamiltonian. The creation and annihilation field operators are given by

$$\begin{aligned}\hat{\psi}_\sigma(\vec{r}_i) &= \hat{\psi}_\sigma(\vec{x} + \vec{l}_i) = \hat{\psi}_{i\sigma}(\vec{x}) \equiv \hat{\Psi}(\vec{x}), \\ \hat{\psi}_\sigma^\dagger(\vec{r}_i) &= \hat{\psi}_\sigma^\dagger(\vec{x} + \vec{l}_i) = \hat{\psi}_{i\sigma}^\dagger(\vec{x}) \equiv \hat{\Psi}^\dagger(\vec{x})\end{aligned}\quad (9.3)$$

Here we use the index  $\sigma$  to denote any additional internal degree of freedom, which in this work will invariably be the electron spin, but in principle one may think of  $\sigma$  as representing the collection of internal degrees of freedom including also an electron orbital degree of freedom ( $p$ , or  $d$ -orbitals for instance). For convenience we also collect the operators  $\hat{\psi}_{i\sigma}(\vec{x})$  in the vector operator  $\hat{\Psi}(\vec{x})$ . Note again that  $i$  labels the sublattice degree of freedom, which we explicitly distinguish from the other degrees of freedom. Defining  $N$  as the number of unit cells, the Fourier transform of the field operators is given by

$$\hat{\psi}_{i\sigma}(\vec{k}) = \frac{1}{\sqrt{N}} \sum_{\vec{x}} \hat{\psi}_\sigma(\vec{x} + \vec{l}_i) e^{-i\vec{k}\cdot\vec{x}} = \frac{1}{\sqrt{N}} \sum_{\vec{x}} \hat{\psi}_{i\sigma}(\vec{x}) e^{-i\vec{k}\cdot\vec{x}}, \quad (9.4)$$

We choose this definition of the Fourier transform, as opposed to the common tight binding Fourier exponentials  $e^{-i\vec{k}\cdot(\vec{x}+\vec{l}_i)}$ , to ensure that  $\mathcal{H}(\vec{k} + \vec{G}) = \mathcal{H}(\vec{k})$ . Below we briefly discuss this gauge choice, which one should be aware of when evaluating symmetry properties. We define the operators  $\hat{U}_R$  and their Hermitian conjugates as acting on the field operators to implement the point group symmetry  $R$ . Then one has

$$\hat{U}_R \hat{\psi}_\sigma(\vec{r}_i) \hat{U}_R^\dagger = \sum_{\sigma'} U_{R\sigma\sigma'}^o \hat{\psi}_{\sigma'}(R\vec{r}_i) = \sum_{j,\sigma'} U_{R\sigma\sigma'}^o U_{Rij}^{sl} \hat{\psi}_{j\sigma'}(\vec{x}') \quad (9.5)$$

Here  $U_R^o$  is a unitary matrix that acts in the space of internal orbital degrees of freedom (hence the superscript  $o$ ). The matrix  $U_R^{sl}$  acts in sublattice space. One observes easily that the combined effect on the orbital and sublattice space can be represented as  $\hat{U}_R^\dagger = U_R^o \otimes U_R^{sl}$ . To deduce the transformation properties of the field operators in momentum space, we note that  $\vec{x} + \vec{l}_i = R^{-1}(\vec{x}' + \vec{l}_j)$ , where  $\vec{x}' = R\vec{x} + \vec{l}_i$ . Thus we get

$$\begin{aligned}\hat{U}_R \hat{\psi}_{i\sigma}(\vec{k}) \hat{U}_R^\dagger &= \sum_{j,\sigma'} \sum_{\vec{x}} U_{R\sigma\sigma'}^o U_{Rij}^{sl} \hat{\psi}_{j\sigma'}(\vec{x}') e^{-i\vec{k}\cdot\vec{x}} \\ &= \sum_{j,\sigma'} \sum_{\vec{x}} U_{R\sigma\sigma'}^o U_{Rij}^{sl} \hat{\psi}_{j\sigma'}(\vec{x}') e^{-iR\vec{k}\cdot R\vec{x}} \\ &= \sum_{j,\sigma'} \sum_{\vec{x}} U_{R\sigma\sigma'}^o U_{Rij}^{sl} \hat{\psi}_{j\sigma'}(\vec{x}') e^{-iR\vec{k}\cdot(\vec{x}' - \vec{l}_i)} \\ &= \sum_{j,\sigma'} U_{R\sigma\sigma'}^o U_{Rij}^{sl} e^{iR\vec{k}\cdot\vec{l}_i} \hat{\psi}_{j\sigma'}(R\vec{k})\end{aligned}\quad (9.6)$$

For convenience we define the new matrix  $U_R^{\text{sl}}(\vec{k})$  to include the  $\vec{k}$ -dependencies  $U_R^{\text{sl}}(\vec{k}) = \text{diag}(e^{iR\vec{k}\cdot\vec{t}_1}, \dots, e^{iR\vec{k}\cdot\vec{t}_{N_{\text{sl}}}}) \times U_R^{\text{sl}}$ . Then we can write concisely  $\hat{U}_R \hat{\Psi}(\vec{k}) \hat{U}_R^\dagger = U_R^{\text{o}} \otimes U_R^{\text{sl}}(\vec{k}) \hat{\Psi}(R\vec{k}) \equiv \mathcal{U}_R^\dagger \hat{\Psi}(R\vec{k})$ , with a proper redefinition of  $\mathcal{U}_R$  to incorporate the  $\vec{k}$  dependence.

The translationally invariant Hamiltonian is generically written as

$$\begin{aligned} \hat{H} &= \sum_{i,j,\sigma,\sigma'} \sum_{\vec{x},\vec{x}'} \hat{\psi}_{i\sigma}^\dagger(\vec{x}) \mathcal{H}_{i\sigma,j\sigma'}(\vec{x} - \vec{x}') \hat{\psi}_{j\sigma'}(\vec{x}') \\ &= \sum_{i,j,\sigma,\sigma'} \sum_{\vec{k}} \hat{\psi}_{i\sigma}^\dagger(\vec{k}) \mathcal{H}_{i\sigma,j\sigma'}(\vec{k}) \hat{\psi}_{j\sigma'}(\vec{k}) \equiv \sum_{\vec{k}} \hat{\Psi}^\dagger(\vec{k}) \mathcal{H}(\vec{k}) \hat{\Psi}(\vec{k}) \end{aligned} \quad (9.7)$$

Under the symmetry operation the Hamiltonian transforms as

$$\hat{U}_R \hat{H} \hat{U}_R^\dagger = \sum_{i,j,\sigma,\sigma'} \sum_{\vec{k}} (\mathcal{U}_R \mathcal{H} \mathcal{U}_R^\dagger)_{i\sigma,j\sigma'}(\vec{k}) \hat{\psi}_{i\sigma}^\dagger(R\vec{k}) \hat{\psi}_{j\sigma'}(R\vec{k}), \quad (9.8)$$

and since this is a symmetry we must have  $\hat{U}_R \hat{H} \hat{U}_R^\dagger = \hat{H}$ , which implies

$$\mathcal{U}_R(\vec{k}) \mathcal{H}(\vec{k}) \mathcal{U}_R^\dagger(\vec{k}) = \mathcal{H}(R\vec{k}). \quad (9.9)$$

The composition of two point group symmetries gives another element of the point group, i.e. if  $R_1$  and  $R_2$  are symmetries, then so is  $R_3 = R_2 R_1$ . This is of particular importance if we think of the point group as being generated by just two elements. The effect of such a product of symmetries (first applying  $R_1$ , then  $R_2$ ) on the field operator is, using equation (9.6),

$$\hat{U}_{R_3} \hat{\Psi}(\vec{k}) \hat{U}_{R_3}^\dagger = \hat{U}_{R_2} \hat{U}_{R_1} \hat{\Psi}(\vec{k}) \hat{U}_{R_1}^\dagger \hat{U}_{R_2}^\dagger = \mathcal{U}_{R_1}^\dagger(\vec{k}) \mathcal{U}_{R_2}^\dagger(R_1 \vec{k}) \hat{\Psi}(R_2 R_1 \vec{k}). \quad (9.10)$$

Not only does this demonstrate that one should be careful with the order in which matrix multiplications must take place, it also shows that if and only if  $R\vec{k}^* = \vec{k}^*$  for some  $\vec{k}^*$  in the Brillouin zone and *all*  $R$  of the point group, do the  $\mathcal{U}_R$  form a representation of the group, i.e.  $\mathcal{U}_{R_3} = \mathcal{U}_{R_2} \mathcal{U}_{R_1}$ . If a proper subgroup of the point group leaves a certain  $\vec{k}^*$  invariant, then the  $\mathcal{U}_R$  will form a representation of that subgroup.

## 9.1.2 Gauge dependencies

We now examine in more detail the gauge choice that is contained in the definition of the Fourier transform of the creation and annihilation operators. The choice of the previous section, as mentioned, reflects the requirement  $\mathcal{H}(\vec{k} + \vec{G}) = \mathcal{H}(\vec{k})$ . A

common choice in tight-binding analyses is (suppressing generalized orbital indices for clarity)

$$\begin{aligned}\hat{\psi}_i(\vec{k}) &= \frac{1}{\sqrt{N}} \sum_{\vec{x}} \hat{\psi}(\vec{x} + \vec{l}_i) e^{-i\vec{k} \cdot (\vec{x} + \vec{l}_i)} \\ &= \frac{1}{\sqrt{N}} \sum_{\vec{x}} \hat{\psi}_i(\vec{x}) e^{-i\vec{k} \cdot (\vec{x} + \vec{l}_i)} = \frac{e^{-i\vec{k} \cdot \vec{l}_i}}{\sqrt{N}} \sum_{\vec{x}} \hat{\psi}_i(\vec{x}) e^{-i\vec{k} \cdot \vec{x}}.\end{aligned}\quad (9.11)$$

It is easy to see that the two choices are indeed related by gauge transformation of the form

$$\begin{aligned}\mathcal{A}(\vec{k}) &= \text{diag}(e^{i\vec{k} \cdot \vec{l}_1}, \dots, e^{i\vec{k} \cdot \vec{l}_{N_{\text{sl}}}}), \\ \mathcal{A}^\dagger(\vec{k}) &= \text{diag}(e^{-i\vec{k} \cdot \vec{l}_1}, \dots, e^{-i\vec{k} \cdot \vec{l}_{N_{\text{sl}}}})\end{aligned}\quad (9.12)$$

We immediately deduce that the momentum dependent Hamiltonian in the new basis is written in terms of the previous choice as

$$\mathcal{H}'(\vec{k}) = \mathcal{A}^\dagger(\vec{k}) \mathcal{H}(\vec{k}) \mathcal{A}(\vec{k}) \quad (9.13)$$

The vectors  $\vec{l}_i$  describe structures within the unit cell and it is therefore obviously not true that inner products with reciprocal lattice vectors will give multiples of  $2\pi$ . Hence,  $\mathcal{H}'(\vec{k} + \vec{G}) \neq \mathcal{H}'(\vec{k})$ . This has the following consequence. Since the two Hamiltonians are unitarily equivalent, the spectrum is unaltered and will be fully revealed in the first Brillouin zone. The eigenstates however will not be periodic as expected, and show a repetitive pattern not equal to the first Brillouin zone. This should be taken into account when doing calculations, but will not be reflected in quantities of physical significance.

Repeating the same calculation as above to find the transformation properties of state operators, we deduce that

$$\begin{aligned}\hat{U}_R \hat{\psi}_i(\vec{k}) \hat{U}_R^\dagger &= \sum_j \sum_{\vec{x}} U_{Rij}^{\text{sl}} \hat{\psi}_j(\vec{x}') e^{-i\vec{k} \cdot (\vec{x} + \vec{l}_i)} = \sum_j \sum_{\vec{x}} U_{Rij}^{\text{sl}} \hat{\psi}_{j\sigma'}(\vec{x}') e^{-i\vec{k} \cdot R^{-1}(\vec{x}' + \vec{l}_j)} \\ &= \sum_j \sum_{\vec{x}} U_{Rij}^{\text{sl}} \hat{\psi}_j(\vec{x}') e^{-iR\vec{k} \cdot (\vec{x}' + \vec{l}_j)} = \sum_j U_{Rij}^{\text{sl}} \hat{\psi}_{j\sigma'}(R\vec{k}),\end{aligned}\quad (9.14)$$

From which we conclude that with this gauge choice the matrix  $\mathcal{U}_R$  is completely momentum independent and only contains the permutation of all the atoms in the unit cell:  $\mathcal{U}_R' \mathcal{H}'(\vec{k}) \mathcal{U}_R'^\dagger = \mathcal{H}'(R\vec{k})$ .

It is important to be aware of this difference when studying invariant  $\vec{k}$ -points, i.e. momenta for which  $R\vec{k}^* = \vec{k}^* \text{ mod } \vec{G}$ . In that case one often needs precisely

$\mathcal{H}(\vec{k} + \vec{G}) = \mathcal{H}(\vec{k})$ , so that

$$\mathcal{U}_R(\vec{k}^*) \mathcal{H}(\vec{k}^*) \mathcal{U}_R^\dagger(\vec{k}^*) = \mathcal{H}(R\vec{k}^*) = \mathcal{H}(\vec{k}^* \bmod \vec{G}) = \mathcal{H}(\vec{k}^*). \quad (9.15)$$

### 9.1.3 Lattice symmetries and translational symmetry breaking

When translational invariance is lost due to the interaction-induced formation of a density-wave state, the explicit operation of lattice symmetries is slightly altered. Here we show explicitly how translational symmetry breaking affects the action of lattice operations (which may even no longer be symmetries) within the formalism developed above. In light of content of this work, we demonstrate this for a specific case of translational symmetry breaking, where the generators of the remaining translations are at most doubled with respect to the fully symmetric ones, i.e.  $\vec{x}_1 \rightarrow 2\vec{x}_1$  and/or  $\vec{x}_2 \rightarrow 2\vec{x}_2$ . This amounts to a quadrupled unit cell at most. The considerations are completely general however, and apply equivalently to situations where the unit cell is tripled, which is natural in systems with hexagonal symmetry.

The mean field Hamiltonian for given density-wave order is then written as

$$\hat{H} = \sum_{\vec{k} \in \text{rbz}} \hat{\chi}^\dagger(\vec{k}) \mathcal{H}(\vec{k}) \hat{\chi}(\vec{k}). \quad (9.16)$$

where the spinor  $\hat{\chi}$  is given by

$$\hat{\chi}(\vec{k}) = \hat{\chi}_{\mu j}(\vec{k}) = \begin{bmatrix} \hat{\chi}_{0j}(\vec{k}) \\ \hat{\chi}_{1j}(\vec{k}) \\ \hat{\chi}_{2j}(\vec{k}) \\ \hat{\chi}_{3j}(\vec{k}) \end{bmatrix} = \begin{bmatrix} \hat{\psi}_j(\vec{k}) \\ \hat{\psi}_j(\vec{k} + \vec{Q}_1) \\ \hat{\psi}_j(\vec{k} + \vec{Q}_2) \\ \hat{\psi}_j(\vec{k} + \vec{Q}_3) \end{bmatrix}. \quad (9.17)$$

The momenta  $\vec{Q}_\mu$  satisfy the relations  $2\vec{Q}_\mu = \vec{0} \bmod \vec{G}$  and  $\vec{Q}_1 + \vec{Q}_2 + \vec{Q}_3 = \vec{0} \bmod \vec{G}$ . For convenience we set  $\vec{Q}_0 = \vec{0}$ . Note that these algebraic relations pertain to the case of unit cell quadrupling. Different algebraic relations hold for other patterns of translational symmetry breaking, the scheme does not depend on the specific form of these relations.

We derive that a point group operation acts on the spinor components as

$$\begin{aligned} \hat{U}_R \hat{\chi}_{\mu i}(\vec{k}) \hat{U}_R^\dagger &= \hat{U}_R \hat{\psi}_i(\vec{k} + \vec{Q}_\mu) \hat{U}_R^\dagger = U_{Rij}^{\text{sl}}(\vec{k} + \vec{Q}_\mu) \hat{\psi}_j(R\vec{k} + R\vec{Q}_\mu) = \\ U_{Rij}^{\text{sl}}(\vec{k} + \vec{Q}_\mu) \hat{\psi}_j(R\vec{k} + \vec{Q}_\nu) &= U_{Rij}^{\text{sl}}(\vec{k} + \vec{Q}_\mu) U_{R\mu\nu}^{\text{sb}} \hat{\chi}_{\nu j}(R\vec{k}) = \\ &\begin{bmatrix} U_R^{\text{sl}}(\vec{k}) & & & \\ & \ddots & & \\ & & & U_R^{\text{sl}}(\vec{k} + \vec{Q}_3) \end{bmatrix}_{\mu\nu} U_{R\nu\eta}^{\text{sb}} \hat{\chi}_\eta(R\vec{k}), \end{aligned} \quad (9.18)$$

Here  $U_R^{\text{sb}}$  is a matrix that acts on the momentum components  $\mu$  of the spinor  $\hat{\chi}$ . The point group operation  $R$  generally permutes the momenta  $\vec{Q}_\mu$  that represent the translational symmetry breaking (sb) and the symmetry breaking matrix  $U_R^{\text{sb}}$  implements this permutation. We stress that in the case of translational breaking we do not have the freedom to multiply the matrix  $U_R^{\text{sl}}(\vec{k}) = \text{diag}(e^{iR\vec{k}\cdot\vec{t}_1}, \dots, e^{iR\vec{k}\cdot\vec{t}_{N_{\text{sl}}}}) \times U_R^{\text{sl}}$  by an overall factor  $e^{-iR\vec{k}\cdot\vec{t}_1}$ . The latter is allowed in the absence of translational symmetry breaking since an overall global displacement of the unit cell is immaterial. When translational symmetry is broken  $\vec{t}_j$  may no longer be good translations.

Based on the above we can write down an expression for the symmetry condition of the translationally broken mean-field Hamiltonian in momentum space. If we denote the mean-field Hamiltonian as  $\mathcal{H}(\vec{k})$  and the matrix representing the symmetry operation by  $\tilde{U}^\dagger(\vec{k})$ , which is defined as  $\tilde{U}_R \hat{\chi}(\vec{k}) \tilde{U}_R^\dagger = \tilde{U}^\dagger(\vec{k}) \hat{\chi}(R\vec{k})$ , then we have

$$\tilde{U}_R(\vec{k}) \mathcal{H}(\vec{k}) \tilde{U}_R^\dagger(\vec{k}) = \mathcal{H}(R\vec{k}) \quad (9.19)$$

Here  $\vec{k}$  is restricted to the reduced BZ (RBZ). Care must be taken when analyzing invariant  $\vec{k}$ -points in the reduced BZ, as these points are not invariant points in the original BZ. Using the periodicity of the RBZ is consequently nontrivial. To demonstrate this, let us imagine that we are considering a momentum  $\vec{k}^*$  that is left invariant in the RBZ by the symmetry operation  $R$ . Then we would naively have  $\hat{\chi}_\mu(R\vec{k}^*) = \hat{\chi}_\mu(\vec{k}^*)$ . This is not correct however. The correct relation reads  $\hat{\chi}_\mu(R\vec{k}^*) = \hat{\chi}_\mu(\vec{k}^* + \vec{G}_{\text{rbz}})$ , where  $\vec{G}_{\text{rbz}}$  is a reciprocal lattice vector of the RBZ. For the cases we have restricted ourselves to from the outset, which is commensurate  $\vec{Q}_\mu$ , the reciprocal lattice vectors of the RBZ are precisely the  $\vec{Q}_\mu$  vectors. To see this one observes that they all get folded onto  $\Gamma$  by definition and thus must correspond to reciprocal lattice vectors. This means that we must have  $\vec{G}_{\text{rbz}} = \vec{Q}_\mu$ . In addition we know that given the commensurability assumptions the vectors  $\vec{Q}_\mu$  form a group under addition. From this we conclude that the addition of a RBZ reciprocal lattice vector just permutes the  $\hat{\chi}_\mu$ , i.e.  $\hat{\chi}_\mu(\vec{k}^* + \vec{G}_{\text{rbz}}) = U_{\mu\nu}^{\text{eq}\dagger} \hat{\chi}_\nu(\vec{k}^*)$ . The matrix  $U_{\mu\nu}^{\text{eq}}$  implements the equivalence of momenta in the RBZ. In particular, this means for a symmetry operation  $R$  that

$$\mathcal{H}(R\vec{k}^*) = \mathcal{H}(\vec{k}^* + \vec{G}_{\text{rbz}}) = U^{\text{eq}\dagger} \mathcal{H}(\vec{k}^*) U^{\text{eq}} \quad (9.20)$$

and hence that

$$U^{\text{eq}} \tilde{U}_R(\vec{k}^*) \mathcal{H}(\vec{k}^*) \tilde{U}_R^\dagger(\vec{k}^*) U^{\text{eq}\dagger} = \mathcal{H}(\vec{k}^*). \quad (9.21)$$

We note in passing that it is a straightforward, albeit possibly tedious, matter to change to a gauge for which  $\mathcal{H}(\vec{k} + \vec{G}_{\text{rbz}}) = \mathcal{H}(\vec{k})$ , where  $\mathcal{H}(\vec{k})$  is the mean-field

Hamiltonian of the translational symmetry broken state. One may choose  $\vec{Q}_1$  and  $\vec{Q}_2$  as generators of the reciprocal lattice, for which we have  $\hat{\chi}(\vec{k} + \vec{Q}_1) = U_1^{\text{eq}\dagger} \hat{\chi}(\vec{k})$  and  $\hat{\chi}(\vec{k} + \vec{Q}_2) = U_2^{\text{eq}\dagger} \hat{\chi}(\vec{k})$ . Clearly  $\hat{\chi}(\vec{k} + \vec{Q}_1 + \vec{Q}_2) = U_1^{\text{eq}\dagger} U_2^{\text{eq}\dagger} \hat{\chi}(\vec{k}) = U_2^{\text{eq}\dagger} U_1^{\text{eq}\dagger} \hat{\chi}(\vec{k})$ , implying that  $U_1^{\text{eq}\dagger}$  and  $U_2^{\text{eq}\dagger}$  commute and are simultaneously diagonalizable. For  $2\vec{Q}_1 = 2\vec{Q}_2 = 0$  we have in addition  $(U_1^{\text{eq}})^2 = (U_2^{\text{eq}})^2 = 1$  mandating the eigenvalues to be  $e^{i\phi_\mu}$  with  $\phi_\mu = 0, \pi$ . One now sets  $\phi_\mu = \vec{k} \cdot \vec{x}_{1,2}$  so as to match correct value for  $\vec{Q}_1 \cdot \vec{x}_{1,2} = 0, \pi$  and  $\vec{Q}_2 \cdot \vec{x}_{1,2} = 0, \pi$  simultaneously. This then defines the gauge transformation needed to compensate the eigenvalues of  $U_1^{\text{eq}}$  and  $U_2^{\text{eq}}$ .

We close this section by showing that an analogous expression can be derived for the tight-binding gauge, i.e.  $\hat{\mathcal{H}}(\vec{k}) = \mathcal{A}^\dagger(\vec{k}) \mathcal{H}(\vec{k}) \mathcal{A}(\vec{k})$ . In that case we obtain

$$\begin{aligned} \hat{U}_R \hat{\chi}_{\mu i}(\vec{k}) \hat{U}_R^\dagger &= \hat{U}_R \hat{\psi}_i(\vec{k} + \vec{Q}_\mu) \hat{U}_R^\dagger = \\ U_{Rij}^{\text{sl}} \hat{\psi}_j(R\vec{k} + R\vec{Q}_\mu) &= U_{Rij}^{\text{sl}} \hat{\psi}_j(R\vec{k} + \vec{Q}_\nu + \vec{G}_\mu) = \\ U_{Rij}^{\text{sl}}(\vec{G}_\mu) U_{R\mu\nu}^{\text{sb}} \hat{\psi}_j(R\vec{k} + \vec{Q}_\nu) &= U_{Rij}^{\text{sl}}(\vec{G}_\mu) U_{R\mu\nu}^{\text{sb}} \hat{\chi}_{\nu j}(R\vec{k}) = \\ \left[ \begin{array}{ccc} U_R^{\text{sl}} \mathcal{A}^\dagger(\vec{0}) & & \\ & \ddots & \\ & & U_R^{\text{sl}} \mathcal{A}^\dagger(\vec{G}_3) \end{array} \right]_{\mu\nu} & U_{R\nu\eta}^{\text{sb}} \hat{\chi}_\eta(R\vec{k}), \end{aligned} \quad (9.22)$$

where the crucial point to notice here is that  $R\vec{Q}_\mu = \vec{Q}_\nu + \vec{G}_\mu$  with  $\vec{G}_\mu$  some reciprocal lattice vector which has an effect on the state operator via  $\mathcal{A}^\dagger(\vec{G}_\mu)$ . This fully specifies the action of symmetry operations on state operators in the tight-binding gauge.

### 9.1.4 Topological characteristics of fermionic states

We now come to a brief discussion of the topological character of fermionic states. One of the main purposes of this work was to shed light on the connection between lattice symmetry and spectral properties. Symmetry broken density wave states may cause a spectral gap to open, in which case the ground state will be insulating for the appropriate filling. The presence of discrete symmetries can give rise to additional topological quantum numbers of the ground state and here we are interested in the topological structure based on lattice symmetries [172, 176, 181]. The symmetry classification of particle hole condensates proposed and worked out here allows for a characterization of these condensates in terms of additional topological quantum numbers. In characterizing the condensates we will rely on the theoretical framework developed in Refs. [172, 182]. Here we will merely summarize some the results reported in those works and adapt them slightly to the language and definitions presented here.

It is convenient to rewrite the real space basis functions as  $|\vec{x}, j\rangle = \hat{\psi}_j^\dagger(\vec{x})|0\rangle$ , where for convenience we collect all local degrees of freedom (sublattice, orbital, spin) in the label  $j$ . After diagonalization of the Bloch Hamiltonian  $\mathcal{H}(\vec{k})$  one obtains the spectrum  $E_n(\vec{k})$  where  $n$  labels the band. The eigenstates are  $|\vec{k}, n\rangle = \hat{\gamma}_n^\dagger(\vec{k})|0\rangle$ . The normal mode operators and orbital operators are related by a matrix  $U(\vec{k})$  that contains the eigenvectors of the matrix  $\mathcal{H}(\vec{k})$  in its columns,  $\hat{\gamma}_n^\dagger(\vec{k}) = \hat{\psi}_j^\dagger(\vec{k})U_{jn}(\vec{k})$  with  $\mathcal{H}_{ij}(\vec{k})U_{jn}(\vec{k}) = E_n(\vec{k})U_{in}(\vec{k})$ . For the orbital operators we have the relation

$$\begin{aligned}\hat{U}_R\hat{\psi}_i(\vec{k})\hat{U}_R^\dagger &= \mathcal{U}_{Rij}^\dagger(\vec{k})\hat{\psi}_j(R\vec{k}), \\ \hat{U}_R\hat{\psi}_i^\dagger(\vec{k})\hat{U}_R^\dagger &= \hat{\psi}_j^\dagger(R\vec{k})\mathcal{U}_{Rji}(\vec{k})\end{aligned}\quad (9.23)$$

which implies for the normal mode operators

$$\begin{aligned}\hat{U}_R\hat{\gamma}_n\hat{U}_R^\dagger &= U_{ni}^\dagger(\vec{k})\mathcal{U}_{Rij}^\dagger(\vec{k})U_{jm}(R\vec{k})\hat{\gamma}_m(R\vec{k}), \\ \hat{U}_R\hat{\gamma}_n^\dagger(\vec{k})\hat{U}_R^\dagger &= \hat{\gamma}_m^\dagger(R\vec{k})U_{mj}^\dagger(R\vec{k})\mathcal{U}_{Rji}(\vec{k})U_{in}(\vec{k})\end{aligned}\quad (9.24)$$

These relations hold in an equivalent way for the mean-field normal modes  $\hat{\gamma}_n^\dagger(\vec{k}) = \hat{\chi}(\vec{k})U_{jn}(\vec{k})$  (we use the same symbols as no confusion is expected), resulting from the mean-field Hamiltonian. Based on the expressions for the operation of symmetries on  $\hat{\chi}(\vec{k})$  given in the previous sections, we simply have to substitute  $\tilde{\mathcal{U}}_R(\vec{k})$  for  $\mathcal{U}_R(\vec{k})$ . To establish a connection with results of [172], we define the sewing matrix  $\mathcal{B}_R(\vec{k})$  corresponding to an operation  $R$  as

$$\hat{U}_R\hat{\gamma}_n^\dagger(\vec{k})\hat{U}_R^\dagger \equiv \hat{\gamma}_m^\dagger(R\vec{k})\mathcal{B}_{Rmn}(\vec{k})\quad (9.25)$$

which may be expressed alternatively as

$$\mathcal{B}_{Rmn}(\vec{k}) = \langle R\vec{k}, m | \hat{U}_R | \vec{k}, n \rangle. \quad (9.26)$$

For condensate state which have an energy gap at the relevant filling (and under the assumption that  $R$  is indeed a symmetry) the sewing matrix will not mix occupied and unoccupied bands and therefore it is block diagonal. One can use equation (9.1.4) to write an expression for the sewing matrix in terms  $\mathcal{U}_R$ ,

$$\mathcal{B}_R(\vec{k}) = U^\dagger(R\vec{k})\mathcal{U}_R(\vec{k})U(\vec{k}). \quad (9.27)$$

Note that the three matrix appearing in the product are not individually block diagonal in the space of (occupied and unoccupied) bands. From this specific expression it is however immediately obvious that the sewing matrix is unitary. Hence, due to the

block diagonal structure, the sewing matrix is unitary when restricted to the space of occupied bands. In accordance with custom we restrict ourselves to the space of occupied bands.

There are two distinct types of additional quantum numbers an insulating state can, or cannot, acquire in two dimensions as a consequence of lattice point group symmetries. The first is the Chern number  $C$ , an integer which labels the Quantum Hall universality class of the insulating state. Nonzero Chern number will lead to a quantized Hall response when an electric field is applied, expressing the fact that the Chern number, a topological index, physically corresponds to the Hall conductivity  $\sigma_{xy}$ . The Chern number is defined as

$$C = \frac{1}{2\pi} \int_{\text{bz}} d\vec{k} \text{Tr} [F_{xy}(\vec{k})], \quad (9.28)$$

where  $F_{xy}(\vec{k})$  is the momentum space field strength corresponding to the non-Abelian Berry gauge connection  $A_i^{nm}(\vec{k})$ ,  $i = x, y$ . The latter is given by the expression

$$A_i^{nm}(\vec{k}) = -i \langle \vec{k}, n | \partial_i | \vec{k}, m \rangle \quad (9.29)$$

and the field strength is calculated in the standard way as

$$F_{ij}(\vec{k}) = \partial_i A_j(\vec{k}) - \partial_j A_i(\vec{k}) + i[A_i(\vec{k}), A_j(\vec{k})] \quad (9.30)$$

where  $i, j = x, y$  and  $\partial_i \equiv \partial/\partial k_i$ . The non-Abelian nature of the connection  $A_i$  and the field strength  $F_{ij}$  comes from the band indices  $n, m$ , which refer to the occupied bands only. The trace in equation (9.28) should therefore be understood as restricted to the space of occupied bands.

To see how point group symmetries constrain the Chern number one first derives the transformation of the field strength  $F_{ij}$  under such a point group operation, which is

$$F_{i'j'}(R\vec{k}) = \partial_{i'} A_{j'}(R\vec{k}) - \partial_{j'} A_{i'}(R\vec{k}) + i[A_{i'}(R\vec{k}), A_{j'}(R\vec{k})] = R_{i'i} R_{j'j} \mathcal{B}_R(\vec{k}) F_{ij}(\vec{k}) \mathcal{B}_R^\dagger(\vec{k}). \quad (9.31)$$

From this general transformation rule it follows that

$$F_{x'y'}(R\vec{k}) = \text{Det} [R] \mathcal{B}_R(\vec{k}) F_{xy}(\vec{k}) \mathcal{B}_R^\dagger(\vec{k}), \quad (9.32)$$

which yields when tracing over the occupied bands

$$\text{Tr} [F_{x'y'}(R\vec{k})] = \text{Det} [R] \text{Tr} [F_{xy}(\vec{k})]. \quad (9.33)$$

This relation can be directly used to deduce that if the system has a symmetry which is improper, i.e.  $\text{Det}[R] = -1$ , the Chern number must vanish [172]. Hence, in  $2D$  only insulating states which have rotational symmetries  $C_n$  are allowed to have nonzero Chern number. Incidentally, as was demonstrated earlier [177], the presence of time-reversal symmetry leads to the relation  $\text{Tr}[F_{xy}(-\vec{k})] = -\text{Tr}[F_{xy}(\vec{k})]$  and mandates vanishing Chern number in the same way. Physically this is not surprising as the quantum Hall response equation itself is time-reversal odd.

Point group symmetries not only force the Chern number to be zero in some cases, they can also be used to calculate it modulo an integer number [172]. For instance, in case of  $C_4$  symmetry, the Chern number is given by a product of eigenvalues of  $C_4$  and  $C_2$  modulo 4. Specifically, if we label the eigenvalue of  $C_4$  at the square lattice Brillouin zone center  $\Gamma$  by  $\eta_4(\Gamma)$ , the  $C_4$ -eigenvalue at the Brillouin zone corner, denoted as  $Q_1$  (see Fig. 9.1), by  $\eta_4(Q_2)$ , and the  $C_2$  eigenvalue at  $Q_2$  by  $\eta_{2i}(Q_2)$  (or equivalently  $Q_3$ ), then we have

$$e^{i\pi C/2} = \prod_{i \in \text{occ}} \eta_{4i}(\Gamma) \eta_{4i}(Q_1) \eta_{2i}(Q_2) \quad (9.34)$$

( $i$  indexing the bands) which shows that the Chern number  $C$  is determined by the eigenvalues of point group operations. Due to the exponential  $e^{i\pi C/2}$  it is only determined modulo 4 in case of a  $C_4$  symmetric insulating state. More generally, for a  $C_n$  invariant system ( $n = 2, 3, 6$ ), the Chern number is determined by the rotational eigenvalues  $\eta_n$  at high symmetry point modulo  $n$  [172, 183]. In case of a  $C_3$  invariant state the expression reads

$$e^{i2\pi C/3} = \prod_{i \in \text{occ}} \eta_{3i}(\Gamma) \eta_{3i}(K_+) \eta_{3i}(K_-) \quad (9.35)$$

where  $K_+$  and  $K_-$  are the vertices of the hexagonal Brillouin zone, see Fig. 9.4. We note in passing that the presence of inversion symmetry alone ( $C_2$ ) the parity of the Chern number  $C$  can be obtained from the inversion eigenvalues.

In order to evaluate these expressions in the context of translational symmetry broken density wave states, it is helpful to realize that the product eigenvalues originates from the determinant of the sewing matrix, for example  $\prod_{i \in \text{occ}} \eta_{3i}(\Gamma) = \text{Det}[\mathcal{B}_{C_3}(\Gamma)]$ . In general, suppose that  $\vec{k}^*$  is one of the invariant momenta, i.e.  $R\vec{k}^* = \vec{k}^*$ , then we know from section 9.1.3 that  $\hat{U}_R \hat{\gamma}^\dagger(\vec{k}^*) \hat{U}_R^\dagger = \hat{\gamma}^\dagger(R\vec{k}^*) \mathcal{B}_R(\vec{k}^*) = \hat{\gamma}^\dagger(\vec{k}^*) U^{\text{eq}} \mathcal{B}_R(\vec{k}^*) \equiv \hat{\gamma}^\dagger(\vec{k}^*) \tilde{\mathcal{B}}_R(\vec{k}^*)$ . Using the expression for the sewing matrix as given in equation 9.27, we have

$$\tilde{\mathcal{B}}_R(\vec{k}^*) = U^{\text{eq}} U^\dagger(R\vec{k}^*) \tilde{\mathcal{U}}_R(\vec{k}^*) U(\vec{k}^*) = U^\dagger(\vec{k}^*) U^{\text{eq}} \tilde{\mathcal{U}}_R(\vec{k}^*) U(\vec{k}^*). \quad (9.36)$$

From equation 9.21 it follows that  $U^{\text{eq}}\tilde{\mathcal{U}}_R(\vec{k}^*)$  commutes with the Hamiltonian, meaning that  $U(\vec{k})$  diagonalizes  $U^{\text{eq}}\tilde{\mathcal{U}}_R(\vec{k}^*)$  as well (or can be chosen to do so). This shows that  $\text{Det}[\tilde{\mathcal{B}}_R(\vec{k}^*)]$  is equal to the product of eigenvalues of  $U^{\text{eq}}\tilde{\mathcal{U}}_R(\vec{k}^*)$ . The matrix  $U^{\text{eq}}$  should not be overlooked here.

The second kind of quantum numbers point group symmetric insulators can have in two dimensions is a set of two fractionally quantized numbers  $p_1$  and  $p_2$  which correspond to the electric charge polarization in the unit cell [172], defined as

$$\vec{P} = p_1\vec{x}_1 + p_2\vec{x}_2. \quad (9.37)$$

As polarization is generally only well-defined up to a lattice constant, one has  $0 \leq p_i < 1$ . The expression for the polarization parameters is

$$p_i = \frac{1}{2\pi} \int_0^1 dk_1 \int_0^1 dk_2 \text{Tr} [A_i(k_1\vec{G}_1 + k_2\vec{G}_2)]. \quad (9.38)$$

It should be stressed that these are only meaningful if the Chern number vanishes. This is a priori guaranteed for states with reflection symmetries or time-reversal symmetry. Ref. [172] discusses exhaustively how symmetry constrains the allowed values for  $p_1$  and  $p_2$ . That lattice symmetries should put constraints on electric polarization is most easily seen in one dimension, where the only symmetry is inversion. If the polarization is  $p$  the inversion requires  $p = -p + en$  with  $n$  integer due to fact that polarization is only defined up to a lattice vector. It follows that there are only two allowed values of electric polarization, 0 and  $e/2$ , which constitute distinct topological classes. Very similar reasoning using symmetries restricts the values of electric polarization in two dimensions. For instance, for  $C_6$  symmetry  $p_1$  and  $p_2$  are necessarily integer and therefore there is no nontrivial charge polarization. Other constraints will be discussed and applied directly when specific lattice symmetry groups are considered in following sections. If symmetry allows for nontrivial polarization then appropriate symmetry eigenvalues at high symmetry points in the Brillouin zone can be used to calculate the  $p_i$ . In case of  $C_2$  these eigenvalues formulas read

$$(-1)^{2p_1} = \prod_{i \in \text{occ}} \frac{\eta_{2i}(Q_2)}{\eta_{2i}(\Gamma)}, \quad (-1)^{2p_2} = \prod_{i \in \text{occ}} \frac{\eta_{2i}(Q_3)}{\eta_{2i}(\Gamma)} \quad (9.39)$$

These may be used as well in case of  $C_4$  insulating states, in which case  $p_1 = p_2$ . In case of a  $C_3$  invariant system the formula reads

$$e^{i2\pi p_{1,2}} = \prod_{i \in \text{occ}} \frac{\eta_{3i}(K_+)}{\eta_{3i}(K_-)}. \quad (9.40)$$

Yet a third topological number is given by the  $\mathbb{Z}_2$  number which distinguishes time-reversal invariant trivial insulators from the QSH state in two dimensions (a generalization exists for 3D) [1, 3, 184]. The crucial symmetry that allows for the definition of this number is time-reversal symmetry, i.e. time-reversal symmetry needs to be preserved to give rise to a meaningful  $\mathbb{Z}_2$  topological classification of 2D (and 3D) insulators. A  $\mathbb{Z}_2$  classification implies there are only two flavors: trivial insulators and nontrivial insulators. The  $\mathbb{Z}_2$  index  $\nu$  is obtained as follows

$$(-1)^\nu = \prod_{n=1}^4 \delta_n. \quad (9.41)$$

In general the  $\delta_n$ , which take values  $\pm 1$  and where  $n$  labels one of the four time-reversal invariant momenta of the 2D BZ, are not easy to obtain, however, the presence of inversion symmetry ( $C_2$  in 2D) allows for a straightforward determination based on the formula

$$\delta_n = \prod_{i \in \text{occ}} \eta_{2i}(\Gamma_n). \quad (9.42)$$

Here  $\Gamma_n$  denote the time-reversal invariant momenta,  $\eta_{2i}$  is again the  $C_2$  eigenvalue of the  $i$ -th band and the sum is over all occupied bands with the understanding that we only sum over one of the degenerate Kramers partners, which necessarily have the same eigenvalues. We will use this formula in Section 10.

## 9.2 Interactions and mean-field theory

The particle-hole condensates discussed in this paper are candidate ground states for interacting Hamiltonians on the respective lattices. It is therefore time to take a closer look into interacting lattice fermion models and build a general mean-field theory which may be used to test which condensates appear in the mean-field phase diagram for a given choice of interaction.

### 9.2.1 General formalism

We start from the assumption that the lattice has a basis, but neglect the internal orbital degree of freedom. The non-interacting part of the Hamiltonian is then written as

$$\hat{H}_0 = \sum_{ij} \sum_{\vec{k}} \hat{\psi}_i^\dagger(\vec{k}) \mathcal{H}_{ij}(\vec{k}) \hat{\psi}_j(\vec{k}). \quad (9.43)$$

Here and in the rest of this section we will explicitly write the sums over indices  $i, j$  as adherence to the summation convention may be confusing. For the interacting part of the Hamiltonian we take a density-density interaction of the form

$$\begin{aligned}\hat{H}_{\text{int}} &= \frac{1}{2} \sum_{ij} \sum_{\vec{x}, \vec{x}'} V_{ij}(\vec{x} - \vec{x}') \hat{n}_i(\vec{x}) \hat{n}_j(\vec{x}') \\ &= \frac{1}{2} \sum_{ij} \sum_{\vec{q}} \tilde{V}_{ij}(\vec{q}) \hat{\rho}_i(\vec{q}) \hat{\rho}_j(-\vec{q}),\end{aligned}\quad (9.44)$$

Here  $\hat{n}_i(\vec{x}) = \hat{\psi}_i^\dagger(\vec{x}) \hat{\psi}_i(\vec{x})$  and we have assumed translational invariance of interactions, expressed in  $V_{ij}(\vec{x} - \vec{x}')$  which only depends on the difference  $\vec{x} - \vec{x}'$ . Observe that we have suppressed spin indices here and excluded an onsite interaction of the type  $U \hat{n}_\uparrow(\vec{x}) \hat{n}_\downarrow(\vec{x})$ . This type of interaction is valid for spinless systems to which we will restrict ourselves in this section so as to avoid unnecessary complication at this stage. In the next section we treat the spinful case. As mentioned elsewhere, we will touch on triplet spin-density waves only occasionally in the bulk of this paper and in the last section we take more detailed but far from exhaustive look at triplet condensates. For now we particularize to spinless fermions. Note also the appearance of the factor  $1/2$  in front of the sum. This is due to the fact that we will find it convenient to enforce  $V_{ij}(\vec{x}) = V_{ji}(-\vec{x})$ , which has the consequence that each combination  $\hat{n}_i(\vec{x}) \hat{n}_j(\vec{x}')$  occurs twice.

The momentum dependent density-operator is defined as

$$\hat{\rho}_i(\vec{q}) = \sum_{\vec{k}} \hat{\psi}_i^\dagger(\vec{k} + \vec{q}) \hat{\psi}_i(\vec{k}), \quad (9.45)$$

and the Fourier transformed interaction reads explicitly

$$\tilde{V}_{ij}(\vec{q}) = \frac{1}{N} \sum_{\vec{x}} V_{ij}(\vec{x}) e^{-i\vec{q}\cdot\vec{x}}. \quad (9.46)$$

Note that so far we have not made any assumptions on the range of the interaction. The property  $V_{ij}(\vec{x}) = V_{ji}(-\vec{x})$  is expressed in momentum space as  $\tilde{V}_{ji}(\vec{q}) = \tilde{V}_{ij}^*(\vec{q}) = \tilde{V}_{ij}(-\vec{q})$ . As it is written now it generally contains interactions between nearest-neighbors, next nearest-neighbors, ect. In any specific model calculation one will always terminate this sequence somewhere and we therefore we write the interaction in momentum space as a series in which each term represents a distinct range,

$$\tilde{V}_{ij}(\vec{q}) = \frac{1}{N} \sum_n V_n \Gamma_{ij}^{(n)}(\vec{q}), \quad n = 1, 2, \dots \quad (9.47)$$

where, for instance,  $V_1$  corresponds to the interaction between nearest neighbors only. We stress that the nearest neighbor interaction pertains to the underlying lattice, and thus may be active between unit cells as well as within the unit cell.

Writing the the interaction term of equation (9.44) in terms of field operators explicitly we easily get

$$\sum_{ij} \sum_{\vec{q}, \vec{k}, \vec{k}'} \hat{\psi}_i^\dagger(\vec{k} + \vec{q}) \hat{\psi}_i(\vec{k}) \tilde{V}_{ij}(\vec{q}) \hat{\psi}_j^\dagger(\vec{k}' - \vec{q}) \hat{\psi}_j(\vec{k}'). \quad (9.48)$$

In the weak-coupling limit, anticipating density-wave order of some kind, it is legitimate to employ a Hubbard-Stratonovich (HS) decoupling of the interaction and look for the saddle-point solution. To that end we introduce two kinds of HS fields, one for charge order and one for bond order. At the same time, we make an assumption concerning the type of translational symmetry breaking, by specifying the set of ordering vectors  $\vec{Q}_\gamma$  which will feature in the expectation values  $\langle \hat{\psi}^\dagger(k + Q_\gamma) \hat{\psi}(k) \rangle$ . Consequently, the Ansatz for the HB fields corresponding to charge order are specified by the expression

$$\sum_{i, \gamma, \vec{k}} \Delta_{i\gamma}^* \hat{\psi}_i^\dagger(\vec{k} - \vec{Q}_\gamma) \hat{\psi}_i(\vec{k}) + \sum_{i, \gamma, \vec{k}} \hat{\psi}_i^\dagger(\vec{k} + \vec{Q}_\gamma) \hat{\psi}_i(\vec{k}) \Delta_{i\gamma} - \sum_{i, j, \gamma} \Delta_{i\gamma}^* \tilde{V}_{ij}^{-1}(\vec{Q}_\gamma) \Delta_{j\gamma}, \quad (9.49)$$

and the saddle-point equations read

$$\begin{aligned} \Delta_{i\gamma}^* &= \sum_{j, \vec{k}} \langle \hat{\psi}_j^\dagger(\vec{k} + \vec{Q}_\gamma) \hat{\psi}_j(\vec{k}) \rangle \tilde{V}_{ji}(\vec{Q}_\gamma) \\ \Delta_{i\gamma} &= \sum_{j, \vec{k}} \tilde{V}_{ij}(\vec{Q}_\gamma) \langle \hat{\psi}_j^\dagger(\vec{k}) \hat{\psi}_j(\vec{k} + \vec{Q}_\gamma) \rangle, \end{aligned} \quad (9.50)$$

which are obviously equivalent due to  $\tilde{V}_{ij}^* = \tilde{V}_{ji}$ . In general, the order parameters  $\Delta_{i\gamma}$  are complex, which suggests that the degrees contained in them are twice the number of lattice orbitals labeled by  $i$  times the number of ordering vectors labeled by  $\gamma$ . For site order this would not seem right, and indeed, given the set of  $\vec{Q}_\gamma$ , one may deduce relations showing the correct number of degrees of freedom. For instance, in case of  $2\vec{Q}_\gamma = 0$ , it is easy to show that the  $\Delta_{i\gamma}$  are real.

For bond order we follow a similar recipe, by first arranging the interaction in a suitable fashion

$$- \sum_{ij} \sum_{\vec{q}, \vec{k}, \vec{k}'} \hat{\psi}_i^\dagger(\vec{k} + \vec{q}) \hat{\psi}_j(\vec{k}) \tilde{V}_{ij}(\vec{k} - \vec{k}') \hat{\psi}_j^\dagger(\vec{k}') \hat{\psi}_i(\vec{k}' + \vec{q}). \quad (9.51)$$

Note the minus sign coming from the anti-commutation of fermion operators. For the interaction as given in (9.44) and (9.47), the functions  $\Gamma_{ij}^{(n)}(\vec{k} - \vec{k}')$  contained in  $\tilde{V}_{ij}(\vec{k} - \vec{k}')$  are separable. Specifically, one can write  $\Gamma_{ij}^{(n)}(\vec{k} - \vec{k}')$  as a sum of products of basis functions of irreducible representation of the lattice point group. This yields the expression

$$\Gamma_{ij}^{(n)}(\vec{k} - \vec{k}') = \sum_{\mathcal{I}, r} \lambda_{ij}^{(n, \mathcal{I}r)}(\vec{k}) \lambda_{ij}^{(n, \mathcal{I}r)*}(\vec{k}') \quad (9.52)$$

where the sum is over irreducible representations labeled by  $\mathcal{I}$  and its basis functions  $r$  (an irreducible representation may have more than one basis function). A term in the expansion defined by (9.47) then takes the form

$$-\frac{V_n}{N} \sum_{ij} \sum_{\vec{q}, \vec{k}, \vec{k}'} \sum_{\mathcal{I}, r} \hat{\psi}_i^\dagger(\vec{k} + \vec{q}) \hat{\psi}_j(\vec{k}) \lambda_{ij}^{(n, \mathcal{I}r)}(\vec{k}) \lambda_{ij}^{(n, \mathcal{I}r)*}(\vec{k}') \hat{\psi}_j^\dagger(\vec{k}') \hat{\psi}_i(\vec{k}' + \vec{q}). \quad (9.53)$$

Sticking with a term such as this one, we introduce the bond HS fields  $\Delta_{ij\gamma}^{(n, \mathcal{I}r)}$  and  $\Delta_{ij\gamma}^{(n, \mathcal{I}r)\dagger}$  as

$$\begin{aligned} & - \sum_{i, j, \gamma, \vec{k}} \sum_{\mathcal{I}, r} \left[ \Delta_{ij\gamma}^{(n, \mathcal{I}r)*} \lambda_{ij}^{(n, \mathcal{I}r)*}(\vec{k}) \hat{\psi}_j^\dagger(\vec{k}) \hat{\psi}_i(\vec{k} + \vec{Q}_\gamma) + \right. \\ & \quad \left. \hat{\psi}_i^\dagger(\vec{k} + \vec{Q}_\gamma) \hat{\psi}_j(\vec{k}) \lambda_{ij}^{(n, \mathcal{I}r)}(\vec{k}) \Delta_{ij\gamma}^{(n, \mathcal{I}r)} \right] \\ & \quad + \frac{N}{V_n} \sum_{\gamma, \mathcal{I}, r} \Delta_{ij\gamma}^{(n, \mathcal{I}r)*} \Delta_{ij\gamma}^{(n, \mathcal{I}r)} \end{aligned} \quad (9.54)$$

for which we have the saddle-point equations

$$\begin{aligned} \Delta_{ij\gamma}^{(n, \mathcal{I}r)*} &= \frac{V_n}{N} \sum_{\vec{k}} \langle \hat{\psi}_i^\dagger(\vec{k} + \vec{Q}_\gamma) \hat{\psi}_j(\vec{k}) \rangle \lambda_{ij}^{(n, \mathcal{I}r)}(\vec{k}) \\ \Delta_{ij\gamma}^{(n, \mathcal{I}r)} &= \frac{V_n}{N} \sum_{\vec{k}} \lambda_{ij}^{(n, \mathcal{I}r)*}(\vec{k}) \langle \hat{\psi}_j^\dagger(\vec{k}) \hat{\psi}_i(\vec{k} + \vec{Q}_\gamma) \rangle. \end{aligned} \quad (9.55)$$

As a consequence of translational symmetry breaking, we restrict the sum over momenta  $\vec{k}, \vec{k}'$  to momenta in the reduced Brillouin zone. At the same time we must include a sum over the momenta  $\vec{Q}_\mu$  for each of the momentum summations. For the

charge order parameter fields this yields explicitly

$$\begin{aligned}\Delta_{i\gamma} &= \sum_{j,\mu,\vec{k}\in\text{rbz}} \tilde{V}_{ij}(\vec{Q}_\gamma) \langle \hat{\psi}_j^\dagger(\vec{k} + \vec{Q}_\mu) \hat{\psi}_j(\vec{k} + \vec{Q}_\gamma + \vec{Q}_\mu) \rangle \\ &= \sum_{j,\mu,\vec{k}\in\text{rbz}} \tilde{V}_{ij}(\vec{Q}_\gamma) \langle \hat{\chi}_{\mu j}^\dagger(\vec{k}) \hat{\chi}_{[\mu+\gamma]j}(\vec{k}) \rangle.\end{aligned}\quad (9.56)$$

We have used the definition  $\hat{\chi}_{\mu i}(\vec{k}) = \hat{\psi}_i^\dagger(\vec{k} + \vec{Q}_\mu)$  already introduced in Section 9.1.3. By  $[\mu + \gamma]$  we mean the index  $\nu$  that is the result of  $\vec{Q}_\gamma + \vec{Q}_\mu = \vec{Q}_\nu$ . Hence, the momenta must be added and not the indices  $\mu$  and  $\gamma$  itself. The mean-field part of the Hamiltonian corresponding to charge order then reads

$$\sum_{i,\mu,\gamma,\vec{k}\in\text{rbz}} \left[ \Delta_{i\gamma}^* \hat{\chi}_{\mu i}^\dagger(\vec{k}) \hat{\chi}_{[\mu+\gamma]i}(\vec{k}) + \hat{\chi}_{[\mu+\gamma]i}^\dagger(\vec{k}) \hat{\chi}_{\mu i}(\vec{k}) \Delta_{i\gamma} \right] - \sum_{i,j,\gamma} \Delta_{i\gamma}^* \tilde{V}_{ij}^{-1}(\vec{Q}_\gamma) \Delta_{j\gamma}.\quad (9.57)$$

This mean field part of the Hamiltonian containing the coupling of (charge) order parameters to the spinors  $\hat{\chi}$ , together with the free part  $\mathcal{H}_0(\vec{k})$  constitutes the full mean field Hamiltonian of equation (9.16). The formalism laid out in the previous section can now be used to investigate the structure of symmetry breaking induced by the mean fields.

Clearly a similar expression may be written down for bond order, but instead of quoting the general result we think it will be illustrative to work out a specific case and see the formalism outlined above at work directly. We will do so in Section 9.2.3.

We close this section with some general remarks on the order parameters introduced above. By defining them such that they are labeled by the momenta  $\vec{Q}_\gamma$ , we have separated them automatically into translationally invariant and translational symmetry broken components. Both for bond and site order, the  $\gamma = 0$  component corresponds to translationally invariant orders, while nonzero  $\gamma \neq 0$  components signal the breaking of translational symmetry. The main purpose of the present mean-field theory is to find out which condensates transforming as irreducible representations of the relevant symmetry are contained in the solutions of the saddle-point equations, i.e. the site and bond order parameters. The translationally invariant components  $\gamma = 0$  are written in the sublattice space basis and in order to find the irreducible representations contained in the order parameters we only have to project on the sublattice functions.

## 9.2.2 Interactions with spin

In this section we present the generalities of a mean-field theory for spinful interacting lattice fermion models. Based on the work already done in the first part of this section,

it is rather straightforward to include the spin degree of freedom and thereby provide a way to discuss, classify and test the stability of triplet particle-hole condensates.

There is one main difference with the spinless case, and we already commented on this following equation (9.44), which is the presence of an on-site Hubbard repulsion. Fermionic statistics allows each site to be occupied by two electrons of opposite spin species, a situation which will however lead to an energetic penalty customarily labeled  $U$ . The onsite Hubbard Hamiltonian reads

$$\hat{H}_U = U \sum_{i, \vec{x}} \hat{n}_{i\uparrow}(\vec{x}) \hat{n}_{i\downarrow}(\vec{x}). \quad (9.58)$$

This term can be rewritten so as to allow for a decoupling in charge and spin order parameter fields separately. One easily finds that the onsite Hubbard term can be expressed as

$$\hat{H}_U \sim U \sum_{i, \vec{x}} [\hat{\psi}_{i\sigma}^\dagger(\vec{x}) \hat{\psi}_{i\sigma}(\vec{x})]^2 - U \sum_{i, \vec{x}} [\hat{\psi}_{i\sigma}^\dagger(\vec{x}) \vec{\sigma}_{\sigma\sigma'} \hat{\psi}_{i\sigma'}(\vec{x})]^2. \quad (9.59)$$

Here and in the following we adopt the convention that spin indices appearing twice are assumed to be summed over, as this should not cause any confusion. The first term of equation (9.59) is a product of density operators, i.e.  $\sum_{\sigma} \hat{n}_{i\sigma}(\vec{x})$ , and hence can be decoupled using a charge order field. The second term is written in terms of spin operators, i.e.  $\hat{\psi}_{i\sigma}^\dagger(\vec{x}) \vec{\sigma}_{\sigma\sigma'} \hat{\psi}_{i\sigma'}(\vec{x}) \sim \vec{s}_i$  with  $\sigma^i$  a set of Pauli matrices acting in spin space, and corresponds to spin ordering. Transforming to momentum space, the first term of equation (9.59) is written as

$$U \sum_i \sum_{\vec{q}, \vec{k}, \vec{k}'} \hat{\psi}_{i\sigma}^\dagger(\vec{k} + \vec{q}) \hat{\psi}_{i\sigma}(\vec{k}) \hat{\psi}_{i\sigma'}^\dagger(\vec{k}') \hat{\psi}_{i\sigma'}(\vec{k}' + \vec{q}), \quad (9.60)$$

while the second term, containing the spin operators, takes the form

$$U \sum_i \sum_{\vec{q}, \vec{k}, \vec{k}'} \hat{\psi}_{i\sigma_1}^\dagger(\vec{k} + \vec{q}) \sigma_{\sigma_1\sigma_2}^a \hat{\psi}_{i\sigma_2}(\vec{k}) \hat{\psi}_{i\sigma_3}^\dagger(\vec{k}') \sigma_{\sigma_3\sigma_4}^a \hat{\psi}_{i\sigma_4}(\vec{k}' + \vec{q}). \quad (9.61)$$

In the same way as before we anticipate translational symmetry breaking with ordering vectors  $\vec{Q}_\gamma$  forming a closed algebra under addition, and we proceed with the HS decoupling for the charge part to arrive at

$$\sum_{i, \gamma, \vec{k}} \Delta_{i\gamma}^{0*} \hat{\psi}_{i\sigma}^\dagger(\vec{k}) \hat{\psi}_{i\sigma}(\vec{k} + \vec{Q}_\gamma) + \sum_{i, \gamma, \vec{k}} \hat{\psi}_{i\sigma}^\dagger(\vec{k} + \vec{Q}_\gamma) \hat{\psi}_{i\sigma}(\vec{k}) \Delta_{i\gamma}^0 - \sum_{i, \gamma} \Delta_{i\gamma}^{0*} U^{-1} \Delta_{i\gamma}^0. \quad (9.62)$$

We introduce the spinful HS fields  $\Delta_{i\gamma}^a$  in the decoupling of the spin order term (9.61) as

$$\begin{aligned}
 & - \sum_{i,\gamma,\vec{k}} \Delta_{i\gamma}^{a*} \hat{\psi}_{i\sigma}^\dagger(\vec{k}) \sigma_{\sigma\sigma'}^a \hat{\psi}_{i\sigma'}(\vec{k} + \vec{Q}_\gamma) \\
 & - \sum_{i,\gamma,\vec{k}} \hat{\psi}_{i\sigma}^\dagger(\vec{k} + \vec{Q}_\gamma) \sigma_{\sigma\sigma'}^a \hat{\psi}_{i\sigma'}(\vec{k}) \Delta_{i\gamma}^a + \sum_{i,\gamma} \Delta_{i\gamma}^{a*} N U^{-1} \Delta_{i\gamma}^a. \quad (9.63)
 \end{aligned}$$

Here  $a = 1, 2, 3$  labels the direction in spin space and a sum over  $a$  is understood in expressions where the spin label appears twice. If we now let  $a$  take the values  $a = 0, 1, 2, 3$  and define  $\sigma^0$  as the identity matrix, then the self-consistent saddle-point equations for charge and spin order can be compactly written as

$$\begin{aligned}
 \Delta_{i\gamma}^{a*} &= \frac{U}{N} \sum_{\vec{k}} \langle \hat{\psi}_{i\sigma}^\dagger(\vec{k} + \vec{Q}_\gamma) \sigma_{\sigma\sigma'}^a \hat{\psi}_{i\sigma'}(\vec{k}) \rangle \\
 \Delta_{i\gamma}^a &= \frac{U}{N} \sum_{\vec{k}} \langle \hat{\psi}_{i\sigma}^\dagger(\vec{k}) \sigma_{\sigma\sigma'}^a \hat{\psi}_{i\sigma'}(\vec{k} + \vec{Q}_\gamma) \rangle. \quad (9.64)
 \end{aligned}$$

We observe that the onsite interaction  $U$  can induce charge density waves and spin density waves, which the current scheme treats on equal footing. Any form of bond order is not possible for an onsite interaction only, and in order to look for a spinful generalization of bond ordering, we revisit the longer range density-density interactions of equation (9.44) including the spin degree of freedom.

The starting point is straightforward, as we only need to write the spin labels explicitly,

$$\hat{H}_V = \frac{1}{2} \sum_{ij,\sigma\sigma'} \sum_{\vec{x},\vec{x}'} V_{ij}(\vec{x} - \vec{x}') \hat{n}_{i\sigma}(\vec{x}) \hat{n}_{j\sigma'}(\vec{x}'), \quad (9.65)$$

here the sum over spin indices is written explicitly due to the number operators. Transforming to momentum space we then have

$$\sum_{ij} \sum_{\vec{q},\vec{k},\vec{k}'} \hat{\psi}_{i\sigma}^\dagger(\vec{k} + \vec{q}) \hat{\psi}_{i\sigma}(\vec{k}) \tilde{V}_{ij}(\vec{q}) \hat{\psi}_{j\sigma'}^\dagger(\vec{k}') \hat{\psi}_{j\sigma'}(\vec{k}' + \vec{q}). \quad (9.66)$$

This term, which is quartic in the fermion operators, can be decoupled in charge order parameters and bond order parameters, something which we already demonstrated for the spinless case. In the presence of spin, the bond order parameters can be further categorized as order parameters with no spin structure and order parameters

corresponding to combined spin-bond order. The former is just a trivial generalization of equation (9.49) and the HS decoupling defining the order parameters  $\Delta_{i\gamma}^0$  reads

$$\sum_{i,\gamma,\vec{k}} \Delta_{i\gamma}^{0*} \hat{\psi}_{i\sigma}^\dagger(\vec{k}) \hat{\psi}_{i\sigma}(\vec{k} + \vec{Q}_\gamma) + \sum_{i,\gamma,\vec{k}} \hat{\psi}_{i\sigma}^\dagger(\vec{k} + \vec{Q}_\gamma) \hat{\psi}_{i\sigma}(\vec{k}) \Delta_{i\gamma}^0 - \sum_{i,\gamma} \Delta_{i\gamma}^0 V_{ij}^{-1}(\vec{Q}_\gamma) \Delta_{j\gamma}^0. \quad (9.67)$$

We have chosen the same notation  $\Delta_{i\gamma}^0$  for the order parameter fields as equation (9.62), since these two terms may indeed be collected into a single terms for charge order without spin structure. The self-consistent saddle-point equations for such charge order easily follow from equation (9.50) and take the form

$$\begin{aligned} \Delta_{i\gamma}^{0*} &= \sum_{j,\vec{k}} \langle \hat{\psi}_{j\sigma}^\dagger(\vec{k} + \vec{Q}_\gamma) \hat{\psi}_{j\sigma}(\vec{k}) \rangle \tilde{V}_{ji}(\vec{Q}_\gamma) \\ \Delta_{i\gamma}^0 &= \sum_{j,\vec{k}} \tilde{V}_{ij}(\vec{Q}_\gamma) \langle \hat{\psi}_{j\sigma}^\dagger(\vec{k}) \hat{\psi}_{j\sigma}(\vec{k} + \vec{Q}_\gamma) \rangle. \end{aligned} \quad (9.68)$$

Rearranging terms in equation (9.66) yields an interaction quartic in fermion operators which can be decoupled in the bond order channel,

$$- \sum_{ij} \sum_{\vec{q},\vec{k},\vec{k}'} \hat{\psi}_{i\sigma}^\dagger(\vec{k} + \vec{q}) \hat{\psi}_{j\sigma'}(\vec{k}) \tilde{V}_{ij}(\vec{k} - \vec{k}') \hat{\psi}_{j\sigma'}^\dagger(\vec{k}') \hat{\psi}_{i\sigma}(\vec{k}' + \vec{q}). \quad (9.69)$$

Further manipulations of this interaction term lead to a form which makes the spin structure of the bond order explicit. Again using the Pauli matrices  $\sigma^a = (\sigma^0, \sigma^1, \sigma^2, \sigma^3)$  we find the interaction to be equal to

$$-\frac{1}{2} \sum_{ij} \sum_{\vec{q},\vec{k},\vec{k}'} \hat{\psi}_{i\sigma_1}^\dagger(\vec{k} + \vec{q}) \sigma_{\sigma_1\sigma_2}^a \hat{\psi}_{j\sigma_2}(\vec{k}) \tilde{V}_{ij}(\vec{k} - \vec{k}') \hat{\psi}_{j\sigma_3}^\dagger(\vec{k}') \sigma_{\sigma_3\sigma_4}^a \hat{\psi}_{i\sigma_4}(\vec{k}' + \vec{q}). \quad (9.70)$$

Based on this interaction we can follow the same recipe for HS decoupling as in the spinless case, and apply it to each of the spin components  $a$ . Without explicitly writing the HS decoupling, we give the self-consistent saddle-point equations for the spinful bond order parameters, now labeled by  $a$  in addition to  $(n, \mathcal{I}_r, i, j, \gamma)$ ,

$$\begin{aligned} \Delta_{ij\gamma}^{a(n,\mathcal{I}_r)*} &= \frac{V_n}{N} \sum_{\vec{k}} \langle \hat{\psi}_{i\sigma}^\dagger(\vec{k} + \vec{Q}_\gamma) \sigma_{\sigma\sigma'}^a \hat{\psi}_{j\sigma'}(\vec{k}) \rangle \lambda_{ij}^{(n,\mathcal{I}_r)}(\vec{k}) \\ \Delta_{ij\gamma}^{a(n,\mathcal{I}_r)} &= \frac{V_n}{N} \sum_{\vec{k}} \lambda_{ij}^{(n,\mathcal{I}_r)*}(\vec{k}) \langle \hat{\psi}_{j\sigma}^\dagger(\vec{k}) \sigma_{\sigma\sigma'}^a \hat{\psi}_{i\sigma'}(\vec{k} + \vec{Q}_\gamma) \rangle. \end{aligned} \quad (9.71)$$

### 9.2.3 Example: honeycomb and triangular lattice

In order to show how the mean-field theory presented above may be used in a specific case we take the honeycomb lattice as an example. We will look at two sets of  $\vec{Q}_\mu$ , the  $K$ -points and the  $M$ -points. A mean-field theory incorporating translational symmetry breaking has been applied to the honeycomb lattice before [167, 168, 185] by working directly with a six site unit cell. This would correspond to  $\vec{Q}_\mu = \vec{K}_\pm$  in our case and we must of course obtain the same results in this case.

For the honeycomb lattice we first specify an explicit form for the interaction  $\tilde{V}_{ij}(\vec{q})$ . The honeycomb lattice has two sublattices,  $A$  and  $B$ , and the indices  $i, j$  run over these values. We take a nearest neighbor  $V_1$  and a next-nearest neighbor interaction  $V_2$  into account. In defining  $V_{ij}(\vec{x})$  (and consequently  $\tilde{V}_{ij}(\vec{q})$ ), we should be careful to comply with the counting convention specified by equation (9.44), and in case of the nearest neighbor interaction we set

$$\begin{aligned} V_{AB}(0) &= V_{AB}(\vec{x}_2) = V_{AB}(-\vec{x}_1) = \\ V_{BA}(0) &= V_{BA}(-\vec{x}_2) = V_{BA}(\vec{x}_1) = V_1 \end{aligned} \quad (9.72)$$

and all other matrix elements are zero. This leads to the Fourier transformed expression

$$\begin{aligned} \Gamma_{ij}^{(1)}(\vec{q}) &= \Gamma^{(1)}(\vec{q})\delta_{iA}\delta_{jB} + \Gamma^{(1)*}(\vec{q})\delta_{iB}\delta_{jA} \\ \Gamma^{(1)}(\vec{q}) &= 1 + e^{i\vec{q}\cdot\vec{x}_2} + e^{-i\vec{q}\cdot\vec{x}_1}. \end{aligned} \quad (9.73)$$

For the next-nearest neighbor interaction we make the following choice

$$\begin{aligned} V_{AA}(\vec{x}_1) &= V_{AA}(\vec{x}_2) = V_{AA}(\vec{x}_1 + \vec{x}_2) = \\ V_{AA}(-\vec{x}_1) &= V_{AA}(-\vec{x}_2) = V_{AA}(-\vec{x}_1 - \vec{x}_2) = V_2 \end{aligned} \quad (9.74)$$

and the same for  $V_{BB}$ . In Fourier space we then have

$$\Gamma_{ij}^{(2)}(\vec{q}) = \delta_{ij}\Gamma^{(2)}(\vec{q}) = 2\delta_{ij}(\cos q_1 + \cos q_2 + \cos q_3), \quad (9.75)$$

where  $q_i = \vec{q} \cdot \vec{x}_i$  and we have set  $\vec{x}_3 = -(\vec{x}_1 + \vec{x}_2)$ . Before going very specifically into the case of ordering at the  $K$ -points and subsequently  $M$ -points, we write down the decomposition of  $\Gamma_{ij}^{(1)}(\vec{k} - \vec{k}')$  and  $\Gamma_{ij}^{(2)}(\vec{k} - \vec{k}')$  in terms of the  $\lambda_{ij}^{(n, \mathcal{L}_r)}(\vec{k})$ , as these apply generally both to cases. It suffices to derive relevant expression for  $\Gamma^{(1)}(\vec{k} - \vec{k}')$  and  $\Gamma^{(2)}(\vec{k} - \vec{k}')$ . We obtain as a general expansion

$$\begin{aligned} \Gamma^{(1)}(\vec{k} - \vec{k}') &= \lambda^{(1, A_1)}(\vec{k})\lambda^{(1, A_1)*}(\vec{k}') + \vec{\lambda}^{(1, E_2)}(\vec{k}) \cdot \vec{\lambda}^{(1, E_2)*}(\vec{k}') \\ \Gamma^{(2)}(\vec{k} - \vec{k}') &= \lambda^{(2, A_1)}(\vec{k})\lambda^{(2, A_1)*}(\vec{k}') + \vec{\lambda}^{(2, E_2)}(\vec{k}) \cdot \vec{\lambda}^{(2, E_2)*}(\vec{k}') \\ &\quad \lambda^{(2, B_1)}(\vec{k})\lambda^{(2, B_1)*}(\vec{k}') + \vec{\lambda}^{(2, E_1)}(\vec{k}) \cdot \vec{\lambda}^{(2, E_1)*}(\vec{k}'). \end{aligned} \quad (9.76)$$

The functions  $\lambda^{(1, \mathcal{I}r)}(\vec{k})$  are given explicitly in Appendix A

With this preliminary work out of the way we are in a position to particularize to a certain set of ordering vectors. As advertised we focus on  $K$ -point ordering first, and as such we work with the state operator basis

$$\begin{bmatrix} \hat{\chi}_{0i}(\vec{k}) \\ \hat{\chi}_{1i}(\vec{k}) \\ \hat{\chi}_{2i}(\vec{k}) \end{bmatrix} = \begin{bmatrix} \hat{\psi}_i(\vec{k}) \\ \hat{\psi}_i(\vec{k} + \vec{K}_+) \\ \hat{\psi}_i(\vec{k} + \vec{K}_-) \end{bmatrix}. \quad (9.77)$$

Let's consider charge order first. It is straightforward to find that  $\Gamma_{ij}^{(1)}(0) = 3(\delta_{iA}\delta_{jB} + \delta_{iB}\delta_{jA})$  and that  $\Gamma_{ij}^{(1)}(\vec{K}_+) = \Gamma_{ij}^{(1)}(\vec{K}_-) = 0$ . As there is no contribution to  $\Delta_{i1}$  and  $\Delta_{i2}$  from the nearest neighbor interaction, the nearest neighbor interaction will cause translational symmetry breaking. For the next-nearest neighbor interaction we easily find that  $\Gamma_{ij}^{(2)}(0) = 6\delta_{ij}$  and  $\Gamma_{ij}^{(2)}(\vec{K}_+) = \Gamma_{ij}^{(2)}(\vec{K}_-) = -3\sqrt{3}\delta_{ij}$ . Observe that these are all real. The order parameters of equation (9.50) become

$$\begin{aligned} \Delta_{i0} &= 3\frac{V_1}{N} \sum_{\mu, \vec{k}} (\delta_{iA}\delta_{jB} + \delta_{iB}\delta_{jA}) \langle \hat{\chi}_{\mu j}^\dagger \hat{\chi}_{\mu j} \rangle + 6\frac{V_2}{N} \sum_{\mu, \vec{k}} \delta_{ij} \langle \hat{\chi}_{\mu j}^\dagger \hat{\chi}_{\mu j} \rangle \\ \Delta_{i1} &= -3\sqrt{3}\frac{V_2}{N} \sum_{\mu, \vec{k}} \delta_{ij} \langle \hat{\chi}_{\mu j}^\dagger \hat{\chi}_{[\mu+1]j} \rangle \\ \Delta_{i2} &= -3\sqrt{3}\frac{V_2}{N} \sum_{\mu, \vec{k}} \delta_{ij} \langle \hat{\chi}_{\mu j}^\dagger \hat{\chi}_{[\mu+2]j} \rangle, \end{aligned} \quad (9.78)$$

where we did not write the momentum dependence of the expectation values explicitly. From this it more or less directly follows that the order parameters  $\Delta_{i1}$  and  $\Delta_{i2}$  are not independent, but equivalent. Using the additive properties of the  $\vec{K}_\pm$  vectors we find that  $\Delta_{i1}^* = \Delta_{i2}$ . This is fully consistent with the expectation that the charge order parameters must contain six independent degrees of freedom, corresponding to the six sites in the enlarged unit cell.

We proceed in the same way for bond order. For the nearest neighbor bond order the order parameters read (again suppressing some momentum dependence)

$$\begin{aligned} \Delta_{ij\gamma}^{(1, A_1)} &= \frac{V_1}{N} \sum_{\mu, \vec{k}} \left[ \lambda^{(1, A_1)*}(\vec{k}) \delta_{iA} \delta_{jB} \langle \hat{\chi}_{\mu j}^\dagger \hat{\chi}_{[\mu+\gamma]i} \rangle + \lambda^{(1, A_1)}(\vec{k}) \delta_{iB} \delta_{jA} \langle \hat{\chi}_{\mu j}^\dagger \hat{\chi}_{[\mu+\gamma]i} \rangle \right], \\ \vec{\Delta}_{ij\gamma}^{(1, E_2)} &= \frac{V_1}{N} \sum_{\mu, \vec{k}} \left[ \vec{\lambda}^{(1, E_2)*}(\vec{k}) \delta_{iA} \delta_{jB} \langle \hat{\chi}_{\mu j}^\dagger \hat{\chi}_{[\mu+\gamma]i} \rangle + \vec{\lambda}^{(1, E_2)}(\vec{k}) \delta_{iB} \delta_{jA} \langle \hat{\chi}_{\mu j}^\dagger \hat{\chi}_{[\mu+\gamma]i} \rangle \right] \end{aligned} \quad (9.79)$$

For nearest neighbor bond order we expect nine complex degrees of freedom, corresponding to the nine bonds in the enlarged unit cell. Since we have three basis functions of irreducible representations and three degrees of freedom coming from  $\gamma$ , we immediately see that they represent the independent degrees of freedom. Note that  $\vec{\Delta}_{AB\gamma}^{(1,\mathcal{I})}$  and  $\vec{\Delta}_{BA\gamma}^{(1,\mathcal{I})}$  are not independent but related by complex conjugation. Very similar expressions hold for next-nearest neighbor bond order, which are all diagonal in sublattice space. For instance, the  $(2, A_1)$  order parameter reads

$$\Delta_{ij\gamma}^{(2,A_1)} = \frac{V_2}{N} \sum_{\mu, \vec{k}} \lambda^{(2,A_1)*}(\vec{k}) \delta_{ij} \langle \hat{\chi}_{\mu j}^\dagger \hat{\chi}_{[\mu+\gamma]i} \rangle, \quad (9.80)$$

For next-nearest neighbor bond order we expect nine complex order degrees of freedom for each of the sublattices. Since we now have six basis functions of irreducible representations, we seem to have twice too many. It is however straightforward to show that all the  $\Delta_{ij0}^{(2,\mathcal{I})}$  are real and that  $\Delta_{ij1}^{(2,\mathcal{I})}$  and  $\Delta_{ij2}^{(2,\mathcal{I})}$  are not independent. Hence, we have the correct number of degrees of freedom.

Instead of the ordering vectors  $\vec{K}_\pm$  we may anticipate a different pattern of translational symmetry breaking, and choose the three  $M$ -point ordering vectors, which we just label  $\vec{Q}_\mu$  (see Section 9.4.1). The mean field spinor then has four momentum components and reads

$$\begin{bmatrix} \hat{\chi}_{0i}(\vec{k}) \\ \hat{\chi}_{1i}(\vec{k}) \\ \hat{\chi}_{2i}(\vec{k}) \\ \hat{\chi}_{3i}(\vec{k}) \end{bmatrix} = \begin{bmatrix} \hat{\psi}_i(\vec{k}) \\ \hat{\psi}_i(\vec{k} + \vec{Q}_1) \\ \hat{\psi}_i(\vec{k} + \vec{Q}_2) \\ \hat{\psi}_i(\vec{k} + \vec{Q}_3) \end{bmatrix}. \quad (9.81)$$

Apart from this difference, we need to evaluate  $\tilde{V}_{ij}(\vec{Q}_\mu)$  for the three  $M$ -point momenta. Doing this we find that the charge order parameters take the form

$$\begin{aligned} \Delta_{i0} &= \frac{1}{N} \sum_{\mu, \vec{k}} [6V_2\delta_{ij} + 3V_1(\delta_{iA}\delta_{jB} + \delta_{iB}\delta_{jA})] \langle \hat{\chi}_{\mu j}^\dagger \hat{\chi}_{\mu j} \rangle \\ \Delta_{i1} &= \frac{1}{N} \sum_{\mu, \vec{k}} [-2V_2\delta_{ij} + V_1(\delta_{iA}\delta_{jB} + \delta_{iB}\delta_{jA})] \langle \hat{\chi}_{\mu j}^\dagger \hat{\chi}_{[\mu+1]j} \rangle \\ \Delta_{i2} &= \frac{1}{N} \sum_{\mu, \vec{k}} [-2V_2\delta_{ij} - V_1(\delta_{iA}\delta_{jB} + \delta_{iB}\delta_{jA})] \langle \hat{\chi}_{\mu j}^\dagger \hat{\chi}_{[\mu+2]j} \rangle \\ \Delta_{i3} &= \frac{1}{N} \sum_{\mu, \vec{k}} [-2V_2\delta_{ij} + V_1(\delta_{iA}\delta_{jB} + \delta_{iB}\delta_{jA})] \langle \hat{\chi}_{\mu j}^\dagger \hat{\chi}_{[\mu+3]j} \rangle. \end{aligned} \quad (9.82)$$

Note that in this case the nearest neighbor interaction in principle contributes to the order parameters describing translational symmetry breaking, which was different for ordering at  $\vec{K}$ . Insofar as bond order is concerned, we can simply copy the expressions from equations (9.2.3) and (9.80), but we must interpret the sum over ordering vectors to run over  $\vec{Q}_\mu$ .

As an illustrative example of a spinful mean field theory we apply the general expressions to the specific case of the triangular lattice. Choosing the triangular lattice we can for the moment avoid the additional complication of sublattice structure. We assume the presence of an onsite repulsion  $U$  and a nearest neighbor repulsion  $V_1 = V$ . For the nearest neighbor repulsion we find that the Fourier transform is given by  $\tilde{V}(\vec{q}) = V\Gamma^{(1)}(\vec{q})/N = 2V(\cos q_1 + \cos q_2 + \cos q_3)/N$ , and evaluated at the ordering momenta  $\vec{Q}_\mu$  it gives  $\Gamma^{(1)}(\vec{Q}_\mu) = -2$ , while clearly  $\Gamma^{(1)}(0) = 6$ . We therefore have for the charge order parameters

$$\begin{aligned}\Delta_0^0 &= \frac{U + 6V}{N} \sum_{\mu, \vec{k}} \langle \hat{\chi}_{\mu\sigma}^\dagger \hat{\chi}_{\mu\sigma} \rangle \\ \Delta_{\gamma=1,2,3}^0 &= \frac{U - 2V}{N} \sum_{\mu, \vec{k}} \langle \hat{\chi}_{\mu\sigma}^\dagger \hat{\chi}_{[\gamma+\mu]\sigma} \rangle,\end{aligned}\quad (9.83)$$

Where we have written the expectation values in terms of the mean field spinor components  $\hat{\chi}_{\mu\sigma} = \hat{\psi}_\sigma(\vec{k} + \vec{Q}_\gamma)$ , while suppressing the momentum dependence. Spin density wave order parameters can only originate from the onsite repulsion and we simply have

$$\Delta_\gamma^{a=1,2,3} = \frac{U}{N} \sum_{\mu, \vec{k}} \langle \hat{\chi}_{\mu\sigma}^\dagger \sigma_{\sigma\sigma'}^a \hat{\chi}_{[\gamma+\mu]\sigma'} \rangle. \quad (9.84)$$

We are left with bond order, which can be spinful or without any spin structure. The function  $\Gamma^{(1)}(\vec{k} - \vec{k}')$  is written as sum of products of irreducible representations in a manner exactly equal to the honeycomb lattice next nearest neighbor function  $\Gamma^{(2)}(\vec{k} - \vec{k}')$  given in equation (9.76). In total there are six irreducible representations to be summed over, for the sake of brevity we limit ourselves to writing down two of corresponding order parameters explicitly. For the triangular lattice they are

$$\begin{aligned}\Delta_\gamma^{a(1,A_1)} &= \frac{V}{N} \sum_{\vec{k}} \lambda^{(1,A_1)}(\vec{k}) \langle \hat{\chi}_{\mu\sigma}^\dagger \sigma_{\sigma\sigma'}^a \hat{\chi}_{[\gamma+\mu]\sigma'} \rangle, \\ \vec{\Delta}_\gamma^{a(1,E_2)} &= \frac{V}{N} \sum_{\vec{k}} \vec{\lambda}^{(1,E_2)}(\vec{k}) \langle \hat{\chi}_{\mu\sigma}^\dagger \sigma_{\sigma\sigma'}^a \hat{\chi}_{[\gamma+\mu]\sigma'} \rangle.\end{aligned}\quad (9.85)$$

### 9.3 Condensates of the square lattice

We now take a closer look at the density wave states of the square lattice. As advertised in previous sections, the focus will be on their symmetry and the way in which they alter the low-energy electronic properties of the band structure.

An important aspect of density-wave orders is the breaking of translational symmetry by modulations at finite wave vector. Condensation of particle-hole pairs at finite vector leads to a reduced group of invariant translations as one has to remove the broken translations from the Bravais lattice translational symmetry group. This enlarges the unit cell of the system. In case of the simple square lattice, it is well known that charge or spin density-waves at ordering vector  $\vec{Q} = (\pi, \pi)$  double the unit cell and, consequently, reduce the Brillouin zone to half of its size. When analyzing space group symmetries in such a situation it is appropriate to add the broken translations, which are no longer part of the set of invariant translations, to the point group of the Bravais lattice. This generates the extended point of the lattice, the point group of the enlarged unit cell, which has its own group structure and additional irreducible representations. We may put this differently by noting that generally, to find the point group of a given space group  $S$  one constructs the factor group  $G/T$  by factoring out all the translations  $T$ , the group of invariant translations. Translational symmetry breaking removes elements from  $T$ , which reappear as distinct cosets of  $G/T$ . A more detailed introduction of extended point groups is given in Appendix C. At this point it suffices to develop an intuitive understanding of the basic structure of extended point groups, so let us briefly consider an illustrative example of translational symmetry breaking. Suppose we anticipate ordering at wave vector  $\vec{Q} = (\pi, \pi)$ , a sensible expectation at half filling of the square lattice as  $Q$  nests the Fermi surface. In that case the generators of good translations, i.e. the group of invariant translations, are  $T(\vec{x}_1 + \vec{x}_2)$  and  $T(\vec{x}_1 - \vec{x}_2)$ . Hence,  $T(\vec{x}_1)$  is no longer a good translation and consequently becomes a member of the point group. The number of point group elements are doubled and new irreducible representations emerge, on top of the existing bare point group representations. Note that  $T(\vec{x}_1)$  is its own inverse, as  $2T(\vec{x}_1)$  belongs to the group of invariant translations. By the same token, even though  $T(\vec{x}_2)$  is no longer a good translation, it can be written as  $T(\vec{x}_1) - T(\vec{x}_1 - \vec{x}_2)$  and therefore belongs to the same coset as  $T(\vec{x}_1)$ .

In the following presentation of square lattice density waves, we will not restrict ourselves to the single ordering vector  $\vec{Q} = (\pi, \pi)$ , but instead consider more general multiple- $Q$  ordering using the triplet of ordering momenta  $\vec{Q}_1 = (\pi, \pi)$ ,  $\vec{Q}_2 = (\pi, 0)$  and  $\vec{Q}_3 = (0, \pi)$ , which are shown in Fig. 9.1. This set of ordering momenta has the useful property that it is closed under addition. Specifically, the additive algebraic properties are  $2\vec{Q}_\mu = 0$  (for each  $\mu = 1, 2, 3$ ), which makes them nicely commensu-

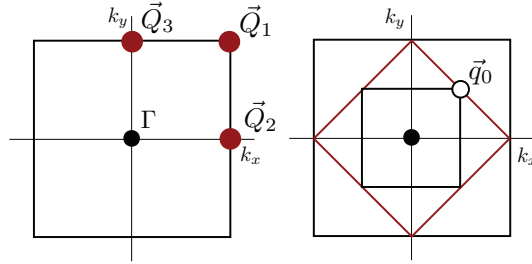


**Figure 9.1:** (Left) Brillouin zone of the square lattice. The momenta  $\vec{Q}_1 = (\pi, \pi)$ ,  $\vec{Q}_2 = (\pi, 0)$ , and  $\vec{Q}_3 = (0, \pi)$  are marked by bold red dots (Right) Outer black square represents the square lattice Brillouin zone. Red rotated square inscribed in the square lattice Brillouin zone marks the nested Fermi surface at half filling and at the same time corresponds to reduced Brillouin zone for translational symmetry breaking at wave vector  $\vec{Q}_1$ . Inner black square represents the reduced Brillouin zone for multiple  $\vec{Q}$  ordering and  $\vec{q}_0 = (\pi, \pi)/2$  denotes the location of the degeneracy point of the  $d_{x^2-y^2}$  density-wave state.

rate, and  $\pm\vec{Q}_1 \pm \vec{Q}_2 \pm \vec{Q}_3 = 0$ . This choice of ordering vectors immediately implies that the unit cell is at most four times as large and as a consequence the three translations  $T(\vec{x}_1)$ ,  $T(\vec{x}_2)$  and  $T(\vec{x}_3) \equiv T(\vec{x}_1 + \vec{x}_2)$  become members of the extended (point) symmetry group  $C_{4v}'''$ . The character table of this group listing the irreducible representations of this group is given in Appendix C and taken from [186]. Note that we altered notation with respect to [186] so as to conform to the definitions used in this work.

In this section dealing with the square lattice density waves, having fixed the set of commensurate ordering vectors, we start by listing all possible site, bond and flux ordered states by means of group theory. As advertised in Section 8.1 this will set the stage for establishing a connection between symmetry and electronic properties. We will demonstrate this in two separate subsections, the first of which provides a discussion of the specific form of the various density waves. The second then focuses on the way in which these density waves alter and affect the electronic (mean field) band structure.

There are three types of distinct orderings to consider in the context of lattice models and these are site or charge order, bond order, and time-reversal symmetry breaking flux order. Strictly speaking, the latter is also a form of bond ordering, as it is the hopping amplitudes which become complex. In order to properly account for gauge equivalence of seemingly different orderings, we distinguish them here

and treat them separately. Having specified the structure of translational symmetry breaking simple group theory arguments suffice to obtain a general organization of density-wave states according to symmetry, without having to write down explicit expression for them. For the square lattice with an enlarged unit cell containing four sites, we collect these four sites in a vector with elements  $\{s_i\}_{i=1}^4$  corresponding to the sites. Point group operations permute this set. A representation  $\mathcal{P}_s$  ( $s$  for site order) of the extended point is constructed by associating each element of the group with a permutation  $P_{ij}^s$  which acts on the  $s_i$ . In the same way we label the eight bonds by  $\{b_i\}_{i=1}^8$  and construct a representation  $\mathcal{P}_b$ . The permutations in both cases act explicitly as

$$s'_i = \sum_j P_{ij}^s s_j, \quad b'_i = \sum_j P_{ij}^b b_j. \quad (9.86)$$

These representations are clearly reducible and may be decomposed into irreducible representations using the character table of the symmetry group. For site order we obtain the following decomposition

$$\mathcal{P}_s = A_1 \oplus B'_2 \oplus E_5. \quad (9.87)$$

The only representation also appearing in the point group  $C_{4v}$  is  $A_1$ , while the others are representations specific to the group  $C_{4v}'''$ . Hence, the translationally invariant content of this decomposition is  $A_1$ , which is not surprising as the only possible translationally invariant charge order on the square lattice is a uniform excess or defect charge. The other two representations correspond to translational symmetry broken charge order. It is not hard to convince oneself that the  $s$ -wave charge order at  $\vec{Q}_1$  transforms as  $B'_2$ .

For bond order we find that the representation  $\mathcal{P}_b$  has the following decomposition

$$\mathcal{P}_b = A_1 \oplus B_1 \oplus E'_1 \oplus E_3 \oplus E_5, \quad (9.88)$$

where we find the translationally invariant content to be  $A_1 \oplus B_1$ , as expected. We will come back to the translationally variant part when we discuss the specific condensates corresponding to these representations.

We move on to flux states on the square lattice. In order to find the distinct flux states transforming according to irreducible representations of the symmetry group we associate a flux  $\phi_i$  to each square plaquette of the lattice. Then the problem of finding the permutation corresponding to a given group member is similar to the problem of site order square lattice, since we have four fluxes as well as four sites. The crucial difference is that in case of fluxes reflections invert the sign of the fluxes and give rise to a minus sign in  $\phi'_i = \sum_j P_{ij}^\phi \phi_j$ . In addition, we must enforce the constraint

that the sum of fluxes in the (enlarged) unit cell is zero, up to integer multiples of the elementary flux quantum  $2\pi$ . This originates from the fact that density-wave states coming from interactions cannot cause magnetic field configurations with nonzero average. Decomposing the square lattice flux representation  $\mathcal{P}_\phi$  we obtain

$$\mathcal{P}_\phi = A_2 \oplus A'_2 \oplus E_2, \quad (9.89)$$

The translationally invariant content is simply given by  $A_2$ , which by definition corresponds to a state with the same flux  $\phi$  pierced through each hexagonal plaquette. Given the constraint that the flux through the unit cell must be zero up to integer multiples of  $2\pi$ , we have  $\phi/(2\pi) \in \mathbb{Z}$ . There is one other state fulfilling the constraints, which is a  $\pi$ -flux state given by  $\phi = \pi$ . This is a consequence of the compact nature of the (electromagnetic) gauge field on the lattice, meaning that  $\pi = -\pi \bmod 2\pi$ . The  $\pi$ -flux state [92, 187] has become a ubiquitous state in condensed matter with relevance to many seemingly disparate fields. It preserves time-reversal invariance and transforms as  $A_1$ , as any point group operation leaves the state invariant up to a gauge transformation. We will come back to it in more detail below. As will be shown below, the representation  $A'_2$  corresponds to a staggered flux state, of which the  $\pi$ -flux state may also be thought of as a particular case (since  $\pi = -\pi$  on a lattice).

Insofar as bond ordered states are concerned, to this point we have limited ourselves to the bonds connecting nearest neighbors of the square lattice. We will find this too restrictive as it excludes interesting density waves representing diagonal bond modulations. Including the diagonal bonds in the bond vector  $b_i$  adds another 8 bonds and yields the decomposition

$$\mathcal{P}_b = 2A_1 \oplus B_1 \oplus B_2 \oplus A'_1 \oplus B'_2 \oplus E'_1 \oplus E_2 \oplus 2E_3 \oplus E_5. \quad (9.90)$$

The double appearance of  $A_1$  comes from the fact that next-nearest neighbor (diagonal) and nearest neighbor bonds are never mixed by point group operations, and so we might have different bond strengths for both without lowering the symmetry. We will find the state corresponding to the  $A'_1$  representation to be particularly interesting. It corresponds to the square lattice  $d_{xy}$  state, and as such is closely related to the  $d_{x^2-y^2}$  state, which is the  $A'_2$  state of the flux order decomposition (9.89).

To conclude these more general considerations using just group theory, and before we come to the explicit expression for quite a number of the density wave states listed here, we demonstrate based on the elementary example of the square lattice case how the symmetry organization serves the purpose of identifying states with topological quantum numbers. In section 9.1.4 we presented two distinct possibilities for topological quantum numbers, the Chern number (connected to quantized off-diagonal conductivity) and electric polarization. Prerequisites for nonzero Chern number are time-reversal symmetry breaking and the absence of any reflection symmetries, which means we must consider the flux states given in equation (9.89). The

state corresponding to  $A'_2$  certainly breaks all reflections, but as can be seen from the character table of  $C_{4v}'''$ , it is even under any reflection followed by  $T(\vec{x}_i)$ . The translation may be thought of as a form of gauge transformation, leaving the Hamiltonian unitarily equivalent to itself under reflections, which mandates zero Chern numbers in the same way as pure reflection do. Hence, this state by itself cannot have nonzero Chern number. The same is true for the states belonging to  $E_2$ , which are even under  $T(\vec{x}_1 + \vec{x}_2)\sigma_v$ .

Concerning electric polarization, we see that we may restrict the attention to states which transform as  $1D$  representations of  $C_{4v}$ , as these are the only ones which have at least  $C_2$  symmetry. This considerably limits the possibilities, as for site order we only have the state  $B'_2$  and for bond order the states  $A_1$  and  $B_1$  contained in  $E_3$  which have the potential to acquire nontrivial quantum numbers, should they be insulating. We will investigate these possibilities below.

### 9.3.1 The density waves of the square lattice

It is now time to look at the explicit form density-wave orders transforming according to the representations just presented. We note once again that we mainly focus on spin singlet states, but we comment briefly on triplet states at the end of this section. We have stated that we are interested in density-waves at modulation vectors  $\vec{Q}_\mu$ , with  $\vec{Q}_\mu$  defined above. A general density-wave state is then specified by

$$\langle \hat{\psi}_\sigma^\dagger(\vec{k} + \vec{Q}_\mu) \hat{\psi}_{\sigma'}(\vec{k}) \rangle = \Delta_\mu(\vec{k}) \delta_{\sigma\sigma'} \quad (9.91)$$

Above we have commented on the special commensurability conditions of the ordering vectors  $\vec{Q}_\mu$ , which are summed up as  $2\vec{Q}_\mu = 0$  and  $\pm\vec{Q}_1 \pm \vec{Q}_2 \pm \vec{Q}_3 = 0$ . From these properties one can easily obtain compatibility conditions of density-wave states. In particular, the fact that  $2\vec{Q}_\mu = 0$  leads to (see also [166])

$$\frac{\Delta_\mu(\vec{k} + \vec{Q}_\mu)}{\Delta_\mu^*(\vec{k})} = 1, \quad (9.92)$$

or, to put it in a different form, writing  $\Delta_\mu(\vec{k}) = \Delta_\mu f_\mu(\vec{k})$  explicitly,  $f_\mu(\vec{k} + \vec{Q}_\mu)/f_\mu^*(\vec{k}) = \Delta_\mu^*/\Delta_\mu$ . In addition there are relations between the different  $\vec{Q}_\mu$ , due to  $\pm\vec{Q}_1 \pm \vec{Q}_2 \pm \vec{Q}_3 = 0$ . We have for instance

$$\begin{aligned} \langle \hat{\psi}_\sigma^\dagger(\vec{k} + \vec{Q}_1) \hat{\psi}_{\sigma'}(\vec{k}) \rangle &= \Delta_1(\vec{k}) = \langle \hat{\psi}_\sigma^\dagger(\vec{k} + \vec{Q}_2 + \vec{Q}_3) \hat{\psi}_{\sigma'}(\vec{k} + \vec{Q}_2 + \vec{Q}_2) \rangle = \\ &= \langle \hat{\psi}_\sigma^\dagger(\vec{k} + \vec{Q}_2 + \vec{Q}_3) \hat{\psi}_{\sigma'}(\vec{k} + \vec{Q}_3 + \vec{Q}_3) \rangle \end{aligned} \quad (9.93)$$

from which it easily follows that

$$\begin{aligned}\langle \hat{\psi}_\sigma^\dagger(\vec{k} + \vec{Q}_3) \hat{\psi}_{\sigma'}(\vec{k} + \vec{Q}_2) \rangle &= \Delta_1(\vec{k} - \vec{Q}_2) = \\ \langle \hat{\psi}_\sigma^\dagger(\vec{k} + \vec{Q}_2) \hat{\psi}_{\sigma'}(\vec{k} + \vec{Q}_3) \rangle^* &= \Delta_1^*(\vec{k} - \vec{Q}_3)\end{aligned}\quad (9.94)$$

Similar relations obviously hold for the other combinations of ordering momenta and thus we obtain the additional relation

$$\Delta_{\mu_1}(\vec{k} - \vec{Q}_{\mu_2}) = \Delta_{\mu_1}^*(\vec{k} - \vec{Q}_{\mu_3}), \quad \mu_1 \neq \mu_2 \neq \mu_3 \quad (9.95)$$

Armed with these general relations we proceed to explicit expression of density-wave states on the square lattice.

The simplest and almost trivial example of an  $s$ -wave state at momentum  $\vec{Q}_1$  is given by

$$\langle \hat{\psi}_\sigma^\dagger(\vec{k} + \vec{Q}_1) \hat{\psi}_{\sigma'}(\vec{k}) \rangle = \Delta_{\text{CDW}} \delta_{\sigma\sigma'}. \quad (9.96)$$

This state is a site ordered state with no momentum dependence, hence the commonly used label  $s$ -wave, and represents the staggered charge-ordering as is shown graphically in Fig. 9.2(a). In the decomposition of equation (9.87) it belongs to the representation  $B'_2$ . Substituting the ordering momentum  $\vec{Q}_2$  or  $\vec{Q}_3$  for  $\vec{Q}_1$  yields the remaining two charge-density waves, which are partners belonging to the representation  $E_5$ .

There are a number of  $p$ -wave type bond orders contained in the decomposition of equation (9.88). Two of them are associated to the ordering vector  $\vec{Q}_1$  and are given by

$$\begin{aligned}\langle \hat{\psi}_\sigma^\dagger(\vec{k} + \vec{Q}_1) \hat{\psi}_{\sigma'}(\vec{k}) \rangle &= i\Delta_{p_x}^{E'_1} \sin k_x \delta_{\sigma\sigma'}, \\ \langle \hat{\psi}_\sigma^\dagger(\vec{k} + \vec{Q}_1) \hat{\psi}_{\sigma'}(\vec{k}) \rangle &= i\Delta_{p_y}^{E'_1} \sin k_y \delta_{\sigma\sigma'}.\end{aligned}\quad (9.97)$$

Here we have chosen  $\Delta^{E'_1}$  real and therefore a factor of  $i$  is necessary due to equation (9.92). We give these states the label  $E'_1$  as they belong to this representation, and the fact that these are imaginary  $p$  waves underlines the time-reversal invariance of these bond orders. Figures 9.2(c)-(d) show these two  $p$  waves graphically. The  $p_x$  state of this doublet is seen to correspond to alternating weaker and stronger bonds in the  $x$  direction, like a Peierls distorted state, only modulated in the  $y$  direction as well. Another time-reversal invariant bond order contained in equation (9.88) is the doublet

$$\begin{aligned}\langle \hat{\psi}_\sigma^\dagger(\vec{k} + \vec{Q}_2) \hat{\psi}_{\sigma'}(\vec{k}) \rangle &= i\Delta_1^{E_3} \sin k_x \delta_{\sigma\sigma'}, \\ \langle \hat{\psi}_\sigma^\dagger(\vec{k} + \vec{Q}_3) \hat{\psi}_{\sigma'}(\vec{k}) \rangle &= -i\Delta_2^{E_3} \sin k_y \delta_{\sigma\sigma'}.\end{aligned}\quad (9.98)$$

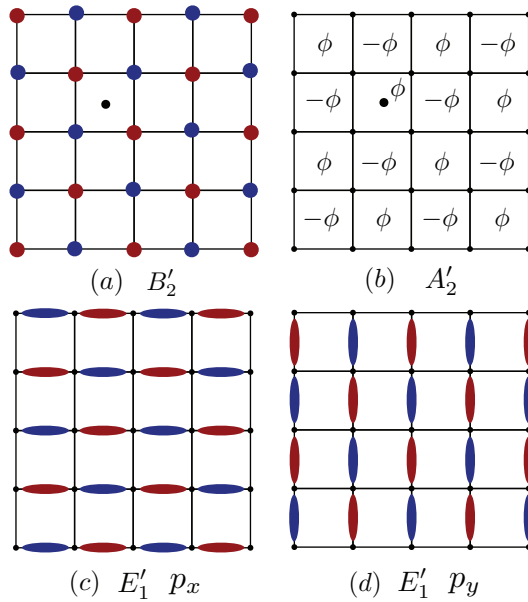


**Figure 9.2:** Graphical representation of some of the density wave states discussed in the main text, labeled by their irreducible representations. Red (blue) bonds represent stronger (weaker) bonds. All states have ordering vector  $\vec{Q}_1$  and black dots in the center of the squares denote the origin. (a) Site ordered, or charge-density wave state, (b)  $d_{x^2-y^2}$  state (which is a flux state), (c)-(d) Two partners of the bond ordered doublet  $E'_1$ .

It can be easily checked that these density-wave states transform as partners of  $E_3$ , which means that under twofold rotations  $C_2$  they transform into themselves instead of acquiring a minus sign as strict  $p$ -wave states would. We choose not to label them explicitly as  $p_x$  and  $p_y$  waves as the decomposition of  $E_3$  in terms of irreducible representations of  $C_{4v}$  is  $E_3 = A_1 \oplus B_1$ . The  $E_3$  doublet is shown in Fig. 9.3(a)-(b).

Exchanging  $\vec{Q}_2$  and  $\vec{Q}_3$  in equation (9.98) yields a time-reversal symmetry breaking doublet given by

$$\begin{aligned}\langle \hat{\psi}_\sigma^\dagger(\vec{k} + \vec{Q}_3) \hat{\psi}_{\sigma'}(\vec{k}) \rangle &= -\Delta_{p_x}^{E_2} \sin k_x \delta_{\sigma\sigma'}, \\ \langle \hat{\psi}_\sigma^\dagger(\vec{k} + \vec{Q}_2) \hat{\psi}_{\sigma'}(\vec{k}) \rangle &= \Delta_{p_y}^{E_2} \sin k_y \delta_{\sigma\sigma'}.\end{aligned}\quad (9.99)$$

These are real  $p$  waves and we must therefore look at equation (9.89) in order to identify the irreducible representation corresponding to this doublet and we find that it is  $E_2$ , a doublet of flux states, which we show in Fig. 9.3(c)-(d) in the  $A_2 \oplus B_2$  basis. To complete the identification of flux states in the decomposition (9.89), we have the  $d$ -wave staggered flux given by

$$\langle \hat{\psi}_\sigma^\dagger(\vec{k} + \vec{Q}_1) \hat{\psi}_{\sigma'}(\vec{k}) \rangle = \Delta_{d_{x^2-y^2}} i(\cos k_x - \cos k_y) \delta_{\sigma\sigma'}.\quad (9.100)$$

The  $d_{x^2-y^2}$  state is well-known in the context of high temperature superconductivity, as it has been discussed in connection to pseudogap physics in cuprates [188] and was found much earlier to be a mean-field solution of the Hubbard model [92, 189]. As we have already assigned the  $E_2$  doublet and this state clearly breaks translational symmetry, it must be the  $A'_2$  state, the staggered flux as shown in Fig. 9.2(b). Direct evaluation of the relevant point group operations confirms this. Its time-reversal invariant  $d$ -wave cousin which was also mentioned earlier already is

$$\langle \hat{\psi}_\sigma^\dagger(\vec{k} + \vec{Q}_1) \hat{\psi}_{\sigma'}(\vec{k}) \rangle = \Delta_{d_{xy}} \sin k_x \sin k_y \delta_{\sigma\sigma'}.\quad (9.101)$$

Note that they are just cousins and not partners of a two-dimensional representation in the context of square symmetry. The  $d_{xy}$  state transforms as  $A'_1$  as contained in the decomposition (9.90) since it is a next-nearest neighbor bond density-wave state. To complete the square lattice nearest-neighbor bond density-wave states we give an expression for the doublet states corresponding to  $E_5$ . These are

$$\begin{aligned}\langle \hat{\psi}_\sigma^\dagger(\vec{k} + \vec{Q}_3) \hat{\psi}_{\sigma'}(\vec{k}) \rangle &= \Delta_{p_x}^{E_5} \cos k_x \delta_{\sigma\sigma'}, \\ \langle \hat{\psi}_\sigma^\dagger(\vec{k} + \vec{Q}_2) \hat{\psi}_{\sigma'}(\vec{k}) \rangle &= \Delta_{p_y}^{E_5} \cos k_y \delta_{\sigma\sigma'}.\end{aligned}\quad (9.102)$$

Despite its appearance it makes sense to label them as  $p$ -waves, as they are odd under  $C_2$ , which is a consequence of the fact that  $E_5 = E_1$  when decomposed in terms of  $C_{4v}$ .

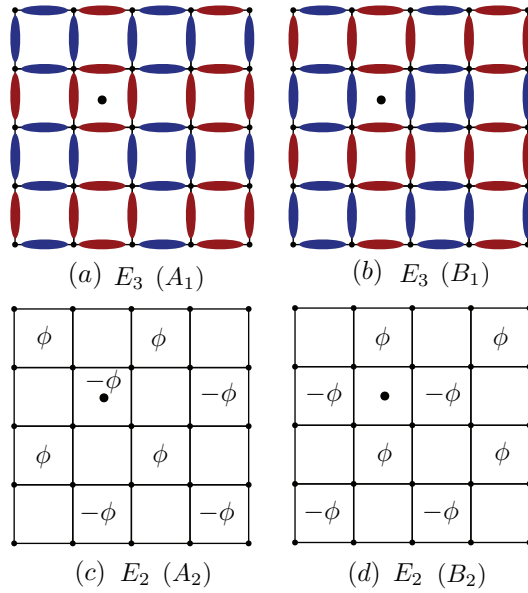


**Figure 9.3:** Graphical representation of square lattice density wave states at ordering vectors  $\vec{Q}_2$  and  $\vec{Q}_3$ . (a) and (b) show the bond ordered doublet states belonging to  $E_3$ , expressed so as to transform as  $A_1$  and  $B_1$  of the bare point group. (c) and (d) show the flux states belonging to  $E_2$ , expressed in the  $A_2$  and  $B_2$  basis.

This completes the listing of density-wave states transforming as the representations in the decompositions of equations (9.87) and (9.88). In addition we have mentioned one state coming from equation (9.90), i.e. the  $d_{xy}$  state, as there is a natural connection to the  $d_{x^2-y^2}$  state. Not only are they both  $d$ -wave states, their mere symmetry properties indicate that for a combined  $id_{x^2-y^2} + d_{xy}$  a topological quantum number can be defined. Indeed, we had noted in the beginning of this section that the state  $id_{x^2-y^2}$  transforms as  $A'_2$  and is thus even under reflections followed by translations. The combination  $id_{x^2-y^2} + d_{xy}$  changes this because  $d_{xy}$  transforms as  $A'_1$ . The difference is entirely due to reflections. The  $d_{xy}$  state is even under reflections but odd under translations by a primitive lattice vector ( $T(\vec{x}_1)$  or  $T(\vec{x}_2)$ ). Hence, reflections are manifestly broken in an  $id_{x^2-y^2} + d_{xy}$  state. The same is true for time-reversal symmetry, i.e. the time-reversal operation cannot be compensated by a translation, which is the case for a pure  $id_{x^2-y^2}$  state. This allows for the Chern number, the topological quantum number of the state, to be nonzero and it was indeed found that the chiral  $id_{x^2-y^2} + d_{xy}$  density-wave is a gapped Chern insulator state [190, 191]. We thus see how the organization of density waves in terms of symmetry serves one of the purposes laid out in the introduction. It leads in a direct way to the identification of states that can acquire additional quantum numbers of topological nature. In this case it leads us to known result, but in what follows we hope to demonstrate the general usefulness of the approach. A second intent of the symmetry perspective is to extract information on the low-energy properties of the symmetric parent state for a given filling. How the organization above serves this purpose we discuss in the next section.

As we have mentioned the Chern insulating chiral  $id + d$  density wave state, we briefly comment on possible nontrivial spinful triplet states of the square lattice. Even though these are known results, they however will set the stage for similar observations in case of other lattices. Just to ease ourselves into the possible triplet states, we recall the simplest and most obvious triplet state, i.e. the antiferromagnetic spin-density wave at  $\vec{Q}_1$ , which is the triplet version of  $s$ -wave site order,

$$\langle \hat{\psi}_\sigma^\dagger(\vec{k} + \vec{Q}_1) \hat{\psi}_{\sigma'}(\vec{k}) \rangle = \Delta_{\text{SDW}} \sigma_{\sigma\sigma'}^3. \quad (9.103)$$

We might have chosen a generic spin direction  $\vec{s} \cdot \vec{\sigma}_{\sigma\sigma'}$ , but we shall not be concerned with global spin rotation equivalence of spin density wave states. A time-reversal invariant version of the  $d_{x^2-y^2}$  state is given by

$$\langle \hat{\psi}_\sigma^\dagger(\vec{k} + \vec{Q}_1) \hat{\psi}_{\sigma'}(\vec{k}) \rangle = \Delta_{\sigma d_{x^2-y^2}} i(\cos k_x - \cos k_y) \sigma_{\sigma\sigma'}^3. \quad (9.104)$$

This  $\sigma id_{x^2-y^2}$  state may be thought of as two copies of the spinless  $d_{x^2-y^2}$  state, with inverted fluxes for the two spin species. Time-reversal invariance follows from the inversion of both spin and flux under time-reversal. The  $\sigma id_{x^2-y^2}$  is a semimetallic

state with isolated Dirac nodes, the spinless version of which will be discussed in more detail in the next section. For now it suffices to note that the combination  $\sigma i d_{x^2-y^2} + d_{xy}$ , in the same way as its spinless counterpart, is a gapped state with nontrivial topological character [191]. Its explicit expression reads

$$\langle \hat{\psi}_\alpha^\dagger(\vec{k} + \vec{Q}) \hat{\psi}_\beta(\vec{k}) \rangle = \Delta_{\text{QSH}} [i(\cos k_x - \cos k_y) \sigma_{\sigma\sigma'}^3 + \sin k_x \sin k_y \delta_{\sigma\sigma'}], \quad (9.105)$$

Its topological character follows from a simple and well-established argument, which uses the spin-projected Chern numbers  $C_\uparrow$  and  $C_\downarrow$ . The latter are well-defined since  $\sigma^3$  represents good quantum numbers. Time-reversal symmetry requires  $C_\uparrow + C_\downarrow = 0$ , but their difference is nonzero,  $C_\uparrow - C_\downarrow = \pm 2$ , indicating that the insulating density wave state is in the Quantum Spin Hall universality class [1, 23].

### 9.3.2 Spectral properties and low energy effects

As laid out in the introductory sections, one of purposes of studying the symmetry of condensates is to uncover any direct relation between the preserved or broken symmetries of condensates and their impact of the electronic spectrum. Now that we have discussed quite a number of specific density wave orders in the previous section, we can turn to the question of spectral properties. Naturally, the starting point is the spectrum of electrons on the square lattice, which is trivially given by  $E(\vec{k}) = -2t \sum_i \cos k_i$  where  $i = x, y$ . We focus on half filling, a filling at which the Fermi surface is nested by the wave vector  $\vec{Q}_1 = (\pi, \pi)$ , a widely known property. This is graphically depicted in Fig. 9.1. As a consequence of this nesting property, it is reasonable to expect condensates at ordering vector  $\vec{Q}_1$  to have strongest impact on the Fermi surface, possibly creating a full energy gap, as the mean-field Hamiltonian will now contain terms coupling states at momenta  $\vec{k}$  and  $\vec{k} + \vec{Q}_1$ , i.e. terms such as  $\hat{\psi}^\dagger(\vec{k}) \hat{\psi}(\vec{k} + \vec{Q}_1)$ . Let us therefore look into these states in particular. Indeed, a textbook example of a square lattice density wave state leading to insulating behaviour is the staggered charge ordered state, given in 9.96 and its spinful cousin in the (weak-coupling) antiferromagnet. The condensate functions are of  $s$ -wave type, i.e.  $\Delta_{\text{CDW}}$  for the charge density wave and  $\Delta_{\text{SDW}} \sigma^3$  for the (triplet) spin density wave, and therefore nodeless.

States which do have nodes in momentum space are the  $d$ -wave states given by condensate functions  $\Delta_{d_{x^2-y^2}}(\vec{k}) = \Delta_{d_{x^2-y^2}} i(\cos k_x - \cos k_y)$  and  $\Delta_{d_{xy}}(\vec{k}) = \Delta_{d_{xy}} \sin k_x \sin k_y$  [see the equations (9.100) and (9.101)], and these nodes coincide with the Fermi surface. The spectral consequence of this is the presence of remaining degeneracies at isolated points on the Fermi surface. Except for the isolated nodes, the spectrum is gapped out. For both of these  $d$ -wave states the degeneracies occur

at high symmetry points, which is connected to the symmetric nature of the condensate functions. We will now show explicitly that these degeneracies are protected by lattice symmetries. Based on the classification of these states in terms irreducible representations of the extended point group  $C_{4v}'''$  it is not all too difficult to establish which symmetries mandate the presence of degeneracies.

We recall the expression for the  $d_{x^2-y^2}$  state, which is

$$\langle \hat{\psi}^\dagger(\vec{k} + \vec{Q}_1) \hat{\psi}(\vec{k}) \rangle = \Delta_{d_{x^2-y^2}} i(\cos k_x - \cos k_y), \quad (9.106)$$

The nodes of this condensate function are located at the two inequivalent moment  $\vec{q}_0 = (\pi, \pi)/2$  and  $\vec{q}_0 = (-\pi, \pi)/2$ . The node at  $\vec{q}_0$  is shown in Fig. 9.1. The mean field fermion operators are given generically in equation (9.17) and for ordering at  $\vec{Q}_1$  we simply have

$$\hat{\chi}(\vec{k}) = \begin{bmatrix} \hat{\chi}_0(\vec{k}) \\ \hat{\chi}_1(\vec{k}) \end{bmatrix} = \begin{bmatrix} \hat{\psi}(\vec{k}) \\ \hat{\psi}(\vec{k} + \vec{Q}_1) \end{bmatrix}. \quad (9.107)$$

In order to study the robust symmetry protection of the degeneracies, we take  $\vec{q}_0$  as an example and abbreviate the fermion operator at this point as  $\hat{\Phi} = \hat{\chi}(\vec{q}_0)$ . The density wave state  $d_{x^2-y^2}$  preserves a number of symmetries and one can simply look up the representation  $A_2'$  in the character table to see what operations, or what combination of operations, constitutes a symmetry. A subset of these symmetries leave the point  $\vec{q}_0$  invariant and can therefore be used to derive constraints on the coupling between the two degenerate states at  $\vec{q}_0$ . Two of such symmetries are the inversion  $C_2$ , and the combination of the reflection  $\sigma_{1d} = C_4\sigma_v$  and  $T(\vec{x}_1)$ , where  $\sigma_v$  is the reflection sending  $(x, y) \rightarrow (x, -y)$  (for the precise and more detailed definition of the point group operations see Appendix A and C). Separately the reflection and the translation are broken, but the combination is preserved. Equation (9.18) can now simply be applied to obtain the effect of these symmetries on  $\hat{\Phi}$  and we find

$$\begin{aligned} C_2 &\rightarrow \hat{\chi}(-\vec{q}_0) = \hat{\chi}(\vec{q}_0 - \vec{Q}_1) = \tau^1 \hat{\Phi} \\ T(\vec{x}_1)\sigma_{1d} &\rightarrow \tau^3 \hat{\Phi}. \end{aligned} \quad (9.108)$$

Here  $\tau^i$  is a set of Pauli matrices acting on the two-component state  $\hat{\Phi}$ . From these relations it straightforwardly follows that the presence of these symmetries protects the degeneracy at  $\vec{q}_0$ . At  $\vec{q}_0$  the mean-field Hamiltonian must commute with both  $\tau^1$  and  $\tau^3$  and the only matrix which has this property is the unit matrix. This is fully analogous to the protection of the degeneracy at the Dirac point of the honeycob lattice, which is explicitly demonstrated in Appendix A. In the present example of the  $d_{x^2-y^2}$  density wave, it is possible to show the protection of the degeneracy at  $\vec{q}_0$  by a

single symmetry. Time-reversal symmetry  $\mathcal{T}$  is broken for the  $d_{x^2-y^2}$  density wave, but as Fig. 9.2(b) shows, the combination of  $\mathcal{T}$  and  $T(\vec{x}_1)$  is preserved, and maps  $\vec{q}_0$  to itself. The action of  $\mathcal{T}T(\vec{x}_1)$  on  $\Phi$  is

$$\mathcal{T}T(\vec{x}_1) \rightarrow \mathcal{K}\tau^3\tau^1\hat{\Phi}, \quad (9.109)$$

with  $\mathcal{K}$  complex conjugation, from which one obtains the condition  $\tau^3\tau^1\mathcal{H}^*(\vec{q}_0)\tau^1\tau^3 = \mathcal{H}(\vec{q}_0)$ . This requires  $\mathcal{H}(\vec{q}_0)$  to be proportional to the identity, proving that the degeneracy is symmetry protected.

In a very similar way one can show the symmetry protection of the degeneracy at  $\vec{q}_1 = (\pi, 0)$  existing in the  $d_{xy}$  state. Both time-reversal and the fourfold rotation  $C_4$  are symmetries and it is straightforward to deduce that these act on  $\hat{\chi}(\vec{q}_1)$  as  $\mathcal{K}\tau^3\tau^1\hat{\chi}(\vec{q}_1)$ , precluding a coupling between the two degenerate states at  $\vec{q}_1$ . Below we comment in more detail on the special role of the fourfold rotation  $C_4$  [86].

In the vicinity of the degeneracies present in the two examples of  $d$  wave states, the mean-field dispersion resembles that of Dirac fermions in case of the  $d_{x^2-y^2}$ , and a quadratic band crossing in case of  $d_{xy}$ . Hence we may reformulate the symmetry protection by stating that both the massless Dirac fermions in one case, and the quadratic band crossing are point group symmetry protected. Because of this, it is a natural and certainly interesting question to ask how additional symmetry breaking affects these low-energy descriptions. In accordance with the general theme of this work, that is the question we will address in the next two sections. We assume that we are deep inside the  $d$  wave states and will study in which way various symmetry broken density wave orders change the low energy properties of these “root” or “parent” states. This approach is similar to a recent study of band structure effects on superconducting states [192], where different “parent states” in principle competing with superconductivity were considered in order to study their impact on superconducting instabilities.

### Dirac fermions of the $\pi$ -flux state

A particularly interesting parent density-wave is the  $d_{x^2-y^2}$  density-wave state giving rise to Dirac nodes in the low-energy spectrum. Let us abbreviate the strength of the density wave, i.e. the order parameter  $\Delta_{d_{x^2-y^2}}$ , as  $\Delta$  for convenience. The nodes appear for arbitrary strength  $|\Delta|$  with different Fermi velocities for two orthogonal directions in momentum space, however, the specific value  $|\Delta| = 2t$  realizes the  $\pi$ -flux state on the square lattice. For illustrative purposes we take this value to correspond to the parent state and study the low-energy physics which is governed by a Dirac Lagrangian from a symmetry perspective. Suppressing spin indices we recall

the expression for the  $d$  wave state

$$\langle \hat{\psi}^\dagger(\vec{k} + \vec{Q}_1) \hat{\psi}(\vec{k}) \rangle = \Delta i(\cos k_x - \cos k_y), \quad (9.110)$$

and as we are interested in the low-energy Dirac physics we must include  $\hat{\psi}(\vec{k} + \vec{Q}_2)$  and  $\hat{\psi}(\vec{k} + \vec{Q}_3)$ , which are coupled as

$$\langle \hat{\psi}^\dagger(\vec{k} + \vec{Q}_2) \hat{\psi}(\vec{k} + \vec{Q}_3) \rangle = \Delta i(\cos k_x + \cos k_y). \quad (9.111)$$

The fermions field in terms of which we write the Hamiltonian is now properly four-dimensional and reads explicitly

$$\hat{\chi}(\vec{k}) = \begin{bmatrix} \hat{\chi}_0(\vec{k}) \\ \hat{\chi}_1(\vec{k}) \\ \hat{\chi}_2(\vec{k}) \\ \hat{\chi}_3(\vec{k}) \end{bmatrix} = \begin{bmatrix} \hat{\psi}(\vec{k}) \\ \hat{\psi}(\vec{k} + \vec{Q}_1) \\ \hat{\psi}(\vec{k} + \vec{Q}_2) \\ \hat{\psi}(\vec{k} + \vec{Q}_3) \end{bmatrix}. \quad (9.112)$$

For convenience we abbreviate the cosine functions as  $c_+(\vec{k}) \equiv \cos k_x + \cos k_y$  and  $c_-(\vec{k}) \equiv \cos k_x - \cos k_y$ . The Hamiltonian is block diagonal as  $\hat{\chi}_0$  and  $\hat{\chi}_1$  are decoupled from  $\hat{\chi}_2$  and  $\hat{\chi}_3$ , i.e.

$$\mathcal{H}(\vec{k}) = \begin{bmatrix} \mathcal{M}_1(\vec{k}) & \\ & \mathcal{M}_2(\vec{k}) \end{bmatrix}, \quad (9.113)$$

with the blocks given by

$$\begin{aligned} \mathcal{M}_1(\vec{k}) &= -2tc_+(\vec{k})\tau^3 - 2tc_-(\vec{k})\tau^2 \\ \mathcal{M}_2(\vec{k}) &= 2tc_-(\vec{k})\tau^3 + 2tc_+(\vec{k})\tau^2 \end{aligned} \quad (9.114)$$

where  $\tau^i$  is a set of Pauli matrices. As is well-known, the spectrum corresponding to this Hamiltonian has a doubly-degenerate Dirac node at  $\vec{q}_0 = (\pi/2, \pi/2)$ , analogous to the case of graphene. Expanding the Hamiltonian around this point yields the linear block diagonal structure

$$\begin{aligned} \mathcal{M}_1(\vec{q}_0 + \vec{q}) &= v_F(q_x\tau^3 + q_y\tau^2) \\ \mathcal{M}_2(\vec{q}_0 + \vec{q}) &= -v_F(q_y\tau^3 + q_x\tau^2), \end{aligned} \quad (9.115)$$

where we have rotated  $\vec{q}$  with respect to  $\vec{k}$  by  $\pi/4$ . The linearized Dirac Hamiltonian corresponds to the Dirac spinor defined as  $\hat{\Phi}(\vec{q}) = \hat{\chi}(\vec{q}_0 + \vec{q})$ . It is convenient to

employ a basis transformation in order to express the Hamiltonian in a simple form. Making the substitution

$$\hat{\Phi}(\vec{q}) \rightarrow \begin{bmatrix} 1 & \\ & e^{-i\pi\tau^1/4} \end{bmatrix} \hat{\Phi}(\vec{q}) \equiv \begin{bmatrix} 1 & \\ & g \end{bmatrix} \hat{\Phi}(\vec{q}), \quad (9.116)$$

achieves this and the transformed Hamiltonian reads

$$\mathcal{H}(\vec{q}) = v_F(q_x\tau^3 + q_y\nu^3\tau^2), \quad (9.117)$$

where  $\nu^i$  denotes another set of Pauli matrices acting on an effective valley space. More specifically, the  $\tau^i$  mix the states  $\hat{\chi}_{0,1}$  and  $\hat{\chi}_{2,3}$  between themselves, and the  $\nu^i$  mix the two sets. The Hamiltonian of equation (9.117) has the familiar Dirac form and one question we may ask is what are the possible Dirac masses and what do they correspond to physically. It is straightforward to determine the possible masses by finding combinations  $\nu^i\tau^j$  which anticommute with both  $\tau^3$  and  $\nu^3\tau^2$  [102]. All of the matrices  $\tau^1$ ,  $\nu^1\tau^2$  and  $\nu^2\tau^2$  have this property and, in addition, anti-commute between themselves. They constitute compatible masses which add in quadrature. There is another mass matrix,  $\nu^3\tau^1$ , which anti-commutes with  $\tau^3$  and  $\nu^3\tau^2$  but not with the other masses. Hence, this is a competing mass.

In order to establish a connection between the density-wave states discussed earlier and the present low-energy description of the  $\pi$ -flux state, we analyze the symmetry properties of the mass matrices and other fermion bilinears. The recipe for this analysis follows directly from the general considerations of Section 9.1 as we will now demonstrate. As such, it is similar to the approach described in [186]. Using the results of Section 9.1 we evaluate the effect of operations in  $C_{4v}'''$  on  $\hat{\chi}(\vec{q}_0)$ . As this is a point of high symmetry in the reduced Brillouin zone, we obtain a representation of the group, which can be fully specified by the action of the generators of the group. These are the translation  $T(\vec{x}_1)$ , the rotation  $C_4$  and the reflection  $\sigma_v$ . The only yet crucial difference with respect to general discussion of Section 9.1 is the fact that in case of the  $\pi$ -flux state symmetry operations may need to be supplemented by a gauge transformation, the combination of which leaves the Hamiltonian invariant. Taking this into account and using equation (9.18) we find

$$\begin{aligned} T(\vec{x}_1) &\rightarrow -iG\nu^3\tau^3\hat{\chi}(\vec{q}_0) \\ C_4 &\rightarrow i\nu^3\tau^3V\hat{\chi}(C_4\vec{q}_0) \\ \sigma_v &\rightarrow -iG\tau^3\hat{\chi}(\sigma_v\vec{q}_0) \end{aligned} \quad (9.118)$$

where  $V$  originates from the interchange of  $\hat{\chi}_2$  and  $\hat{\chi}_3$  and  $G$  is the necessary gauge transformation. They are given by

$$V = \begin{bmatrix} 1 & \\ & \tau^1 \end{bmatrix}, \quad G = \nu^1g = \nu^1e^{-i\pi\tau^1/4}. \quad (9.119)$$

As discussed earlier, even though  $\vec{q}_0$  is invariant under all operations in the reduced BZ, it is not so in the original BZ, and we must therefore bring it back to itself by adding proper reciprocal lattice vector of the reduced BZ. Consequently, we find

$$\begin{aligned}\hat{\chi}(C_4\vec{q}_0) &= \hat{\chi}(\vec{q}_0 + \vec{Q}_2) = \nu^1 \hat{\chi}(\vec{q}_0) \\ \hat{\chi}(\sigma_v\vec{q}_0) &= \hat{\chi}(\vec{q}_0 + \vec{Q}_3) = \nu^1 \tau^1 \hat{\chi}(\vec{q}_0).\end{aligned}\quad (9.120)$$

In a similar manner we can obtain the representation of time-reversal, which also should be supplemented by a gauge transformation in the present case. One finds

$$\mathcal{T} \rightarrow GK\hat{\chi}(-\vec{q}_0) = GK\tau^1\hat{\chi}(\vec{q}_0), \quad (9.121)$$

where  $\mathcal{K}$  is complex conjugation. As these expressions determine the action of the group generators, the action of the group is fully specified. Simplifying the combinations of Pauli matrices somewhat we obtain the following set of operators acting on  $\hat{\Phi}$ , where we stress that is not the transformed  $\hat{\Phi}$  defined by equation (9.116),

$$\begin{aligned}T(\vec{x}_1) &\rightarrow -ig\nu^2\tau^3\hat{\Phi} \\ C_4 &\rightarrow -i\nu^2\tau^2V\hat{\Phi} \\ \sigma_v &\rightarrow g\tau^2\hat{\Phi} \\ \mathcal{T} &\rightarrow g\mathcal{K}\nu^1\tau^1\hat{\Phi}.\end{aligned}\quad (9.122)$$

Then, using the unitary transformation expressed in equation (9.116), we obtain a representation of the group that can be used to classify all fermion bilinears  $\hat{\Phi}_i^\dagger M_{ij} \hat{\Phi}_j$  with  $M$  some tensor product of Pauli matrices, i.e.  $M_{ij} = (\nu^k \tau^l)_{ij}$ . Let us first take a look at the mass matrices, which are of particular interest. The mass term  $\tau^1$  is found to transform according to  $B'_2$ . In addition, we find that the masses  $\nu^1\tau^2$  and  $\nu^2\tau^2$  transform as partners of the two-dimensional representation  $E_3$ . From this it immediately follows which density-wave states presented in Section 9.3.1 correspond to these mass terms and will therefore gap out the parent  $\pi$ -flux state. These are, respectively, the site ordered state at ordering vector  $\vec{Q}_1$  given in equation (??) and the bond order doublet transforming as  $E_3$ , which is the real bond order doublet contained in the decomposition (9.88) and which we will see below is a flux-preserving generalization of equation (9.98). Here we observe how the symmetry of interaction-induced density wave orders allows for a direct identification of the impact of such density wave states at low energies. The three masses just identified are full analogs of masses (insulating states) in graphene [193–195]. We will analyze this connection in more detail below when we come to the honeycomb lattice itself, but for completeness we already mention what they correspond to in graphene. The site ordered state is trivially seen to correspond to a site ordered state on the honeycomb lattice, with

Irreps of $C_{4v}'''$	$B_2'$	$E_3$	$E_2$	$E_1'$	$E_5$
Irreps of $C_{4v}$	$B_2$	$A_1 \oplus B_1$	$A_2 \oplus B_2$	$E_1$	$E_1$
Basis functions	$\tau^1$	$\nu^1 \tau^2,$ $\nu^2 \tau^2$	$\nu^1,$ $\nu^2$	$\tau^2,$ $\nu^3 \tau^3$	$\frac{1}{\sqrt{2}}(\nu^1 - \nu^2 \tau^1),$ $\frac{1}{\sqrt{2}}(\nu^2 - \nu^1 \tau^1)$

**Table 9.1:** This table summarizes the identification of low-energy fermion bilinears as basis functions of irreducible representations of  $C_{4v}'''$ . In addition we present the irreducible representations of  $C_{4v}$  contained in those of  $C_{4v}'''$ .

a charge imbalance between the two sublattices (hence sometimes referred to as sublattice potential). The other two masses can be mapped onto the Kekule bond order in graphene.

Before we move on to establish a connection between other density-wave states listed in Section 9.3.1 and the Dirac matrices, we comment on the explicit expressions for mass generating density-wave states. The nature of the parent state we are considering here, i.e. the  $\pi$ -flux state, prevents us from directly associating the expressions written down in Section 9.3.1 with the mass matrices presented here. This is a consequence of the  $\pi$ -flux threading each square and the fact that some symmetry operations must be dressed with gauge transformation in order to leave the Hamiltonian invariant. The mass matrices  $\nu^1 \tau^2$  and  $\nu^2 \tau^2$  are time-reversal invariant and must therefore correspond to a flux-preserving density wave state. The doublet of equations (9.98) and (9.99) by themselves are not  $\pi$ -flux-preserving (even though the doublet (9.98) clearly preserves zero flux, the parent). We must therefore form appropriate linear combinations in order to form states that transform as  $E_3$  under the symmetry operations of the parent state. We find that the following linear combinations have this property

$$\begin{aligned}
 \langle \hat{\psi}_\sigma^\dagger(\vec{k} + \vec{Q}_2) \hat{\psi}_{\sigma'}(\vec{k}) \rangle &= -i\eta_1 \Delta_{\eta_1 \eta_2} (\sin k_x + i\eta_2 \sin k_y) \delta_{\sigma\sigma'}, \\
 \langle \hat{\psi}_\sigma^\dagger(\vec{k} + \vec{Q}_3) \hat{\psi}_{\sigma'}(\vec{k}) \rangle &= \Delta_{\eta_1 \eta_2} (\sin k_x + i\eta_2 \sin k_y) \delta_{\sigma\sigma'}.
 \end{aligned}
 \tag{9.123}$$

Here  $\eta_i = \pm$  and we have not only formed combinations of the  $E_2$  and  $E_3$  doublets as specified by (9.98) and (9.99), we have also constructed the condensates so as to form basis functions of the two  $A_1$  representations of  $C_{4v}$  contained in  $E_3$ . This is reflected in the appearance of  $p_x + ip_y$  functions. As there are two indices  $\eta_i$  both taking two values, they represent four distinct condensates. Let's first take  $\eta_1 = +$ . Then we find that the two density-wave states  $\eta_2 = \pm$  are precisely the flux-preserving mass terms transforming as  $E_3 = A_1 \oplus B_1$ . Hence, these are the condensate functions which

directly correspond to the Dirac masses  $\nu^1\tau^2$  and  $\nu^2\tau^2$ . Since they were obtained by taking linear combinations of  $E_1$  and  $E_2$  functions of the zero flux root state, it is natural to expect that we may form very similar linear combinations to obtain expressions for doublet functions belonging to  $E_2$  of the  $\pi$ -flux state. Indeed, taking  $\eta_1 = -$  yields the two ( $\eta_2 = \pm$ ) partners of the  $E_2$  representation, which do change the flux away from  $\pi$ . The Dirac matrices  $\nu^1$  and  $\nu^2$  provide the low-energy fermion bilinears belonging to these states. They are not masses which gap out each of two Dirac cones, but instead split the two Dirac cones in energy. One may call them masses in “valley space”.

Now that we have seen how density wave states, based on symmetry arguments, have the interpretation of Dirac masses at low energies, we proceed to establish a connection between some other density-wave states and Dirac matrices. In particular the doublets  $E'_1$  and  $E_5$ , which are part of (9.88) and were defined in the previous section, have an interesting low-energy structure. Taking the  $E'_1$  as an example, we may find Dirac matrices which transform as partners of this representation, by requiring that they are odd under the translations  $T(\vec{x}_1)$  and  $T(\vec{x}_2)$ , while being odd under  $C_2$  as well. Two matrices satisfying these constraints are  $\tau^2$  and  $\nu^3\tau^3$ , which are indeed the partners of  $E'_1$ . Similar reasoning leads to the combinations of Dirac matrices  $(\nu^1 - \nu^2\tau^1)/\sqrt{2}$  and  $(\nu^2 - \nu^1\tau^1)/\sqrt{2}$  belonging to  $E_5$ . As such, they correspond to the terms in the low-energy coming from the density waves transforming accordingly. What is the precise structure of these terms? To see this, we first define the three Dirac matrices  $\Omega^1 = \nu^1\tau^3$ ,  $\Omega^2 = \nu^1\tau^3$  and  $\Omega^3 = \nu^3$ . Note that these satisfy the  $su(2)$  algebra  $[\Omega^i, \Omega^j] = 2i\epsilon^{ijk}\Omega^k$ , and we can therefore use them as gauge charges of an  $SU(2)$  gauge field  $A_\alpha$  as  $A_\alpha = A_\alpha^i\Omega^i$  ( $\alpha = x, y$ ) and couple this gauge field to the low-energy Dirac fermions of the  $\pi$ -flux state as

$$\mathcal{H}(\vec{q}) = \hbar v_F [\tau^3(q_x - A_x^i\Omega^i) + \nu^3\tau^2(q_y - A_y^i\Omega^i)]. \quad (9.124)$$

Looking at what the products  $\tau^3\Omega^i$  and  $\nu^3\tau^2\Omega^i$  amount to, we see that one precisely obtains  $\nu^1$ ,  $\nu^2$  and  $\nu^3\tau^3$  in case of the former, and  $\nu^2\tau^1$ ,  $\nu^1\tau^1$  and  $\tau^2$  in case of the latter. This leads to the conclusion that density wave states transforming as  $E'_1$  and  $E_5$  enter to lowest order as gauge-fields in the low-energy Dirac theory of the parent  $\pi$ -flux state. As such they do not gap out the linear Dirac nodes, but shift them away from  $\vec{q}_0$  in the Brillouin zone. Non-Abelian gauge fields appearing in a low-energy Dirac theory of a condensed matter system have been discussed in the context of graphene [180] (to which we come back later) and we observe here that the translational symmetry broken density wave states belonging to the  $E'_1$  and  $E_5$  representation are direct square lattice analogs of these.

Table (9.1) summarizes the identification of Dirac matrices as basis functions of irreducible representations. In essence, as was demonstrated above, this table allows to directly interpret the effect of interaction induced site or bond ordered states

on the low-energy theory of the fully symmetric parent state, the  $\pi$ -flux state. Table (9.1) highlights an important conclusion which follows from the symmetry analysis presented here and which will reappear in the context of hexagonal lattices. All condensates which belong to representations that can be reduced in terms of “bare” point group representations ( $C_{4v}$  for the square lattice) as  $1D$  representations enter as masses in the low-energy description, either in valley space or providing a full spectral gap. This was demonstrated for  $E_3 = A_1 \oplus B_1$ , which lead to genuine masses and therefore spectral gaps, and  $E_2 = A_2 \oplus B_2$ , states of which have the effect of a valley-mass. In contrast, condensates transforming according to representations that contain only  $2D$  representations of the “bare” point group are found to correspond to gauge fields in the context of a low-energy Dirac description. These statements will be found to hold true for hexagonal lattices with symmetry protected Dirac points as well, such as the honeycomb and kagome lattice. In addition, we will find a more general connection between condensate functions transforming as  $1D$  representation and the presence of spectral gaps when looking at nested Fermi surfaces of the hexagonal lattice free dispersions.

### Quadratic band crossing

After this extensive exposition on the  $\pi$ -flux root state, we come now to the second parent state of interest. Whereas the  $\pi$ -flux state is essentially a  $d_{x^2-y^2}$  state, the other state we focus on is the  $d_{xy}$  state given in equation (9.101). Assuming we are very deep inside the  $d_{xy}$  state and writing the strength as  $\Delta = t_2$  we start from the following root state

$$\begin{aligned} \langle \hat{\psi}^\dagger(\vec{k} + \vec{Q}_1) \hat{\psi}(\vec{k}) \rangle &= t_2 \sin k_x \sin k_y, \\ \langle \hat{\psi}^\dagger(\vec{k} + \vec{Q}_2) \hat{\psi}(\vec{k} + \vec{Q}_3) \rangle &= -t_2 \sin k_x \sin k_y \end{aligned} \quad (9.125)$$

We choose to work again in the four-dimensional spinor basis specified in equation (9.112). As was the case for the  $\pi$ -flux state, the Hamiltonian is block diagonal, with the blocks defined as  $\mathcal{M}_i$ . The low-energy theory (at half filling) of the  $d_{xy}$  state is that of a quadratic band crossing (QBC) at  $\Gamma$ , i.e. an isolated degeneracy in the vicinity of which the dispersion is quadratic. The QBC exists in the  $\mathcal{M}_2$  block of the Hamiltonian, which reads

$$\mathcal{M}_2(\vec{k}) = 2t(\cos k_x - \cos k_y)\tau^3 - t_2 \sin k_x \sin k_y \tau^1, \quad (9.126)$$

while the  $\mathcal{M}_1$  block contains the high-energy modes at  $\Gamma$ . Hence, for the low-energy description we need to project into the subspace spanned by  $\hat{\chi}_2$  and  $\hat{\chi}_3$  and the low-

energy spinor is then given by

$$\hat{\Phi}(\vec{q}) = \begin{bmatrix} \hat{\chi}_2 \\ \hat{\chi}_3 \end{bmatrix} = \begin{bmatrix} \hat{\psi}(\vec{Q}_2) \\ \hat{\psi}(\vec{Q}_3) \end{bmatrix} \quad (9.127)$$

The low-energy Hamiltonian for small momenta  $\vec{q}$  takes the form

$$\mathcal{H}(\vec{q}) = 2t(q_x^2 - q_y^2)\tau^z - 2t_2q_xq_y\tau^1, \quad (9.128)$$

which directly follows from (9.126). We have seen above that the  $d_{xy}$  state transforms according to  $A'_1$ , which essentially means that it is odd under the translations  $T(\vec{x}_i)$ . The action of the generators of the group  $C_{4v}'''$  on the low-energy degrees of freedom is derived in the same way as before [see again equation (9.116)], and after projecting onto the low-energy subspace

$$\begin{aligned} T(\vec{x}_1) &\rightarrow -\tau^3\hat{\Phi} \\ C_4 &\rightarrow -i\tau^2\hat{\Phi} \\ \sigma_v &\rightarrow \tau^3\hat{\Phi} \\ \mathcal{T} &\rightarrow \mathcal{K}\hat{\Phi}. \end{aligned} \quad (9.129)$$

Based on the action of these operators we can deduce the effect on the  $d_{xy}$  root state, of density waves which lower the symmetry. Two well-known properties of QBC points [86] follow immediately from them. The first is that an energy gap is forbidden by time-reversal invariance. The opening of a gap would come from a constant term in (9.128) proportional to  $\tau^2$ , which is odd under time-reversal. The second is the protection of the QBC by  $C_4$  symmetry. In general a perturbation may split the QBC into two Dirac points, which is not possible however in the presence of  $C_4$  symmetry [86]. Intuitively this is obvious, as the splitting in two nodes away from  $\Gamma$  clearly violates fourfold rotational symmetry. From the above relations we see that  $C_4$  is the only operation acting as  $\tau^2$ , which anticommutes with both  $\tau^1$  and  $\tau^3$ , making them both odd under a fourfold rotation, precluding a constant term proportional to these matrices. Hence, the combined operation of time-reversal and fourfold rotation robustly protects the QBC at  $\Gamma$  in the RBZ.

We observe that the matrix  $\tau^1$  is odd under the vertical reflection  $\sigma_v$  and would therefore transform as  $B'_2$ . Indeed the CDW at ordering vector  $\vec{Q}_1$  couples to such a term. This would correspond to a splitting of the QBC point into two Dirac points. The time-reversal odd matrix  $\tau^2$ , the only matrix available to open up a spectral gap, couples to the density staggered flux state of equation (9.100). For any generic QBC point a spectral gap can only be opened by breaking time-reversal symmetry. This is due to the fact that a gapped QBC intrinsically carries a nonzero Chern number [86],

which is not compatible with time-reversal invariance. These two density waves, i.e. the  $B'_2$  and the  $A'_2$  state, are both modulated by  $\vec{Q}_1$  and therefore directly affect the QBC point due to the relation  $\langle \hat{\psi}^\dagger(\vec{k} + \vec{Q}_1) \hat{\psi}(\vec{k}) \rangle = \langle \hat{\psi}^\dagger(\vec{k} + \vec{Q}_2) \hat{\psi}(\vec{k} + \vec{Q}_3) \rangle$ . The same is true for the time-reversal invariant bond order doublet of equation (9.97). As these are  $p$ -wave states they enter in the low-energy description as  $q_x \tau^2$  and  $q_y \tau^2$ , where the momentum dependence ensures time-reversal invariance.

## 9.4 Condensates of hexagonal lattices

The second class of lattices for which we present an extensive and detailed discussion of the symmetry organization of particle-hole condensation are the hexagonal lattices. Two-dimensional lattices with hexagonal symmetry play a ubiquitous role in condensed matter physics, the honeycomb lattice realized in graphene being the highlight example. The kagome lattice, to name another well-known example, has attracted much attention since materials which have this basic lattice structure are considered to be prime candidates for intriguing physics such as spin liquid behaviour. At the same time, recent studies of hexagonal lattice fermion models with strong electronic interactions point towards new and unconventional correlated electronic phases, which are believed to originate from the hexagonal symmetry of such systems. With this in mind, in this section we will apply the method outlined in Section 9.1, and applied to the square lattice in 9.3, to three specific lattices, the honeycomb lattice, the kagome lattice and the triangular lattice.

The hexagonal lattices all have a triangular Bravais lattice and their first Brillouin zone takes the shape of a hexagon, which is shown in Fig. 9.4. In the following we will focus on translational symmetry breaking at two different sets of commensurate wave vectors. The first set consists of the corners of the Brillouin zone hexagon, a set which contains two inequivalent wave vectors  $\vec{K}_+$  and  $\vec{K}_-$ , the so-called  $K$ -points, see Fig. 9.4. The second set consists of the centers of the hexagon faces, the so-called  $M$ -points, also shown in Fig. 9.4. There are three inequivalent  $M$ -points and we will write them as  $\vec{Q}_\mu$ , with  $\mu = 1, 2, 3$ . The algebraic properties under addition are distinct for these two sets of ordering momenta. The  $K$ -points are related by  $\vec{K}_- = 2\vec{K}_+$  and  $3\vec{K}_+ = 0$ , from which it follows that  $\vec{K}_- = -\vec{K}_+$ . Observe that the  $K$ -points are generated by a single vector  $\vec{K}_+$  (or  $\vec{K}_-$  obviously). The  $M$ -points in the hexagonal Brillouin have the property  $2\vec{Q}_\mu = 0$ , which is equivalent to  $\vec{Q}_\mu$  defined for square symmetry systems. Indeed, the  $M$ -points satisfy  $\pm\vec{Q}_1 \pm \vec{Q}_2 \pm \vec{Q}_3 = 0$ . The difference with respect to the square lattice  $\vec{Q}_\mu$  is that all  $M$ -points are mixed by point group operations, while  $\vec{Q}_1 (= (\pi, \pi))$  is always mapped to itself for systems with square symmetry. Translational symmetry breaking at the  $K$ -points amounts a

tripling of the unit cell and is expected in case of the honeycomb and kagome lattices when these systems are doped to the Diracpoints of band structure, as  $K$  connects the Dirac nodes in momentum space. In contrast, translational symmetry breaking at the  $M$ -points leads to a quadrupled unit cell, and is expected to occur for all three hexagonal lattices when their band structure is filled to the van Hove points.

The rest of this section is divided into three parts, corresponding to the three lattices that will be discussed. The first part deals with the honeycomb lattice, while the second and third part focus on the kagome and triangular lattice, respectively. The most detailed treatment will be presented for the honeycomb lattice, as it will serve to highlight the features common to all three lattices. All three parts start with a group theoretical analysis of all the possible site, bond and flux density waves and then proceed to finding the explicit forms of these density waves in order to characterize their electronic properties. The honeycomb lattice part is subdivided into five distinct parts, the first three of which discuss the density waves of translationally invariant,  $K$ -point, and  $M$ -point density waves, respectively. In particular  $M$ -point ordering on the honeycomb lattice will be treated in great detail as we will introduce a formalism for obtaining density waves of definite symmetry that will find more general application in the context of the other hexagonal lattices. The last two parts focus on the spectral characterization of these density waves and its connection to the representations to which they belong. For  $K$ -point order the relevant low-energy description of the electronic systems is a Dirac theory located at those  $K$ -points and we will carefully study how the various density waves enter in such a Dirac theory, in a similar fashion as for the square lattice. For  $M$ -point order the relevant starting point for describing low-energy electrons is a hexagonal Fermi surface, energetically located at the van Hove points of band structure, and nested by the  $M$ -points. We will derive and present an effective low-energy theory around those  $M$ -points and show, using only symmetry arguments, how density wave states enter in such an effective description. Both of these parts are based on the honeycomb lattice, but the results and conclusions presented there apply to all hexagonal lattices. For this reason, the discussion of the kagome and triangular lattices will be more brief as we can draw from insight gained in the context of the honeycomb lattice. Specifically, in case of the kagome lattice we will combine the explicit construction of symmetric density waves and their impact on the mean field spectrum for the purpose of illustrating the power and utility of the lattice symmetry organization of the density waves. We will do the same for the triangular lattice, in which case we content ourselves with  $M$ -point ordered states, for the most part because we use the triangular lattice as the prime example illustrating spinful  $M$ -point condensates in Chapter 10.

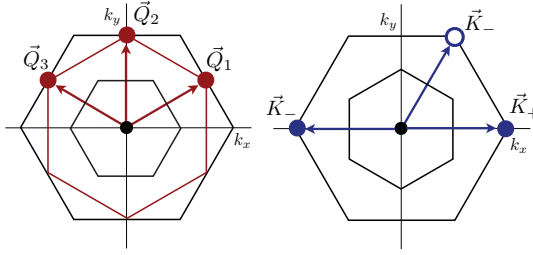


**Figure 9.4:** (Left) Outer black lined hexagon denotes the first Brillouin zone of hexagonal lattices (for instance honeycomb, kagome, but also triangular lattices). Bold red dots mark the  $M$ -point ordering vectors  $\vec{Q}_\mu$  (for the definition see Appendix A) and the red hexagon connecting these  $M$ -points denotes the Fermi surface at a specific lattice dependent filling fraction, which in case of the honeycomb lattice would be  $3/8$ . Inner black hexagon denotes the reduced Brillouin zone corresponding to  $M$ -point order (b) First Brillouin zone of the hexagonal lattices, with bold blue dots denoting the hexagon vertices  $\vec{K}_\pm$ . Inner black rotated hexagon denotes the reduced Brillouin zone corresponding to ordering at  $\vec{K}_\pm$ .

### 9.4.1 Honeycomb lattice

The honeycomb lattice is a lattice structure which has acquired fame since the isolation of single-atom graphite layers now known as graphene [98, 196]. The honeycomb lattice has a triangular Bravais lattice with a two-atom unit cell, and we follow the convention of labeling the atoms  $A$  and  $B$ . Details of Bravais and reciprocal vectors in addition to the real space positions of the unit cell atoms, definition of real space origin and lattice symmetries are given in Appendix A. We will first look at translationally invariant density-wave states, and then proceed to discuss translational symmetry broken states, at  $K$ -points and  $M$ -points respectively. Before we go into the details of these classes of condensates we employ straightforward group theory methods to derive which irreducible representations are expected for a given choice of translational symmetry breaking. As was the case for the square symmetry groups, translational symmetry breaking removes a certain set of translations from the translational symmetry group corresponding to the Bravais lattice. Adding these translations to the point group of the original Bravais lattice gives the extended point groups. In case of the hexagonal space group lattices, these extended groups are  $C_{6v}'''$  and  $C_{6v}''''$  for  $K$ -point ordering and  $M$ -point ordering, respectively. The number of primes pertain to the number of translations added to the point group  $C_{6v}$ . For more details we refer to Appendix C.

For density wave states at both  $K$ - and  $M$ -points we distinguish site order, bond order and flux states. Let us defer flux states for the moment and focus attention on site and bond order first. The general procedure is to label all sites and bonds within the unit cell by  $s_i$  and  $b_i$ , respectively. The index  $i$  runs over the number of sites or bonds in the unit cell, which depends on the modulation (ordering) vectors under consideration. For instance, for  $K$ -point ordering, we have 6 sites in the unit and 9 bonds. We then construct a representation of the extended point groups by associating each element of the group with a permutation  $P_{ij}^{s,b}$ , which follows from the way the group element permutes the sets  $\{s_i\}_{i=1}^6$  and  $\{b_i\}_{i=1}^9$ , i.e.

$$s'_i = \sum_j P_{ij}^s s_j, \quad b'_i = \sum_j P_{ij}^b b_j. \quad (9.130)$$

These representations, denoted as  $\mathcal{P}_{s,b}$ , may be decomposed into irreducible representations using the character table of the symmetry group. The decomposition then tells us how all possible condensates may be organized according to their transformation properties under symmetry group elements.

In case of site order at the  $K$ -points we find the following decomposition in terms of irreducible representations of  $C''_{6v}$

$$\mathcal{P}_s^K = A_1 \oplus B_2 \oplus G', \quad (9.131)$$

whereas we find for  $M$ -point ordering

$$\mathcal{P}_s^M = A_1 \oplus B_2 \oplus F_1 \oplus F_4, \quad (9.132)$$

which in this case is a decomposition in terms of irreducible representations of  $C'''_{6v}$ . These two decompositions share the combination  $A_1 \oplus B_2$  which is the translationally invariant content of the decomposition. It is not surprising that this is also contained in the decomposition of larger reducible representations of translational symmetry broken states. The combination  $A_1 \oplus B_2$  may also be obtained in a direct manner by focusing exclusively on the translationally invariant unit cell structures. The two sublattices corresponding to the  $A$  and  $B$  are either left invariant or interchanged by an element of  $C_{6v}$ , yielding a two-dimensional reducible representation of the symmetry group. Decomposing it in terms of irreducible representations simply gives  $A_1 \oplus B_2$ . As a spoiler of what follows, we note that  $B_2$  corresponds to a charge-density wave that corresponds to the sublattice potential often discussed in the context of graphene.

Repeating the same procedure for bond ordering we obtain for  $K$ -point ordering

$$\mathcal{P}_b^K = A_1 \oplus E_2 \oplus E'_1 \oplus G', \quad (9.133)$$

and for ordering at the  $M$ -points we find

$$\mathcal{P}_6^M = A_1 \oplus E_2 \oplus F_1 \oplus F_3 \oplus F_4. \quad (9.134)$$

Here we observe that the translationally invariant content is  $A_1 \oplus E_2$ . At this stage we leave these results for what they are, but will come back to them extensively when we discuss the explicit expressions of the density-wave states transforming according to the representations featuring in the decompositions derived here.

We now go into the details of flux states on the honeycomb lattice. In order to find the various flux states transforming according to irreducible representations of the relevant symmetry group we associate a flux  $\phi_i$  to each hexagonal plaquette of the honeycomb lattice. As such, the problem of finding the permutation corresponding to a given is similar to the problem of site order on the triangular lattice, with the crucial difference that reflections invert the flux and give rise to a minus sign. In addition, we must again enforce the constraint that the sum of fluxes in the unit cell is zero up to integer multiples of the elementary flux quantum  $2\pi$ . Working out the permutation representation and decomposing it into irreducible representations of  $C_{6v}''$  we find

$$\mathcal{P}_\phi^K = A_2 \oplus E_2'. \quad (9.135)$$

The translationally invariant content is simply given by  $A_2$ , which by definition corresponds to a state with the same flux  $\phi$  pierced through each hexagonal plaquette. To find the flux patterns contained in  $E_2'$  we first decompose it in irreducible representations of  $C_{6v}$  and find  $E_2' = A_2 \oplus B_2$ .

An analogous calculation for flux patterns coming from  $M$ -point ordering yields the decomposition

$$\mathcal{P}_\phi^M = A_2 \oplus F_2, \quad (9.136)$$

where the  $F_2$  representation can be further decomposed into  $A_2 \oplus E_2$ .

In the same way as for the square lattice, we can use the obtained representations for the different types of ordered states to analyse whether or not additional quantum numbers connected to topological characteristics can in principle be acquired by the condensates. The simplest task to identify orderings that are compatible with nonzero Chern number. We stress that we do not assume anything with regard to the spectral properties such as the existence of an energy gap, which is a necessary condition of a well-defined integer Chern number. Based on symmetry alone it is possible to narrow the possibilities down considerably. In particular, as was noted in Section 9.1.4, time-reversal symmetry mandates vanishing Chern number and therefore we are forced to consider the flux states. The translationally invariant state we already excluded, which leaves us with  $E_2'$  in case of  $K$ -point ordering, and  $F_2$  in case of  $M$ -point ordering.

We had already taken the effort of decomposing them further in terms of  $C_{6v}$  and found that both in case of  $K$ -point and  $M$ -point ordering there is a state  $A_2$  which breaks all reflections. Both are contained in larger dimensional representations of  $C_{6v}''$  and  $C_{6v}'''$ , the partners of which are mixed by the point group translations  $T(\vec{x}_i)$ . Hence, translations cannot compensate the odd reflections as was the case for the square lattice. These states are therefore genuine candidates for nontrivial topology and we will investigate this specifically once we have obtained explicit expression for them.

Insofar as quantized electric polarization is concerned, hexagonal symmetry restricts the possibilities. We iterate that hexagonal symmetry here refers strictly to the rotations and reflections, the bare point group elements. As stated in section 9.1.4, when  $C_6$  rotational symmetry is present, no nontrivial electric polarization is possible. The threefold rotational symmetry  $C_3$  restricts the polarization  $p_1 = p_2$  to be multiples of  $1/3$ . If, in addition, there exists a reflection (or two-fold rotation from  $D_3$ ) then it precludes nontrivial polarization if one of the lattice vectors  $\vec{x}_i$  is in the reflection plane (or one of its  $C_3$  equivalents). The point group  $C_{6v}$  has four representations which have  $C_3$  symmetry, which are all the  $1D$  representations. Two must be excluded as they have  $C_6$  in addition. Two other are  $B_1$  and  $B_2$ , only one of which admits nontrivial polarization due to the reflection. Which one depends on the translational symmetry breaking, in the sense that for  $K$ -point ordering the unit lattice vectors are  $2\vec{x}_1 + \vec{x}_2$  and  $\vec{x}_1 + 2\vec{x}_2$ . For  $M$ -point ordering they are  $2\vec{x}_1$  and  $2\vec{x}_2$ , which has the consequence that for translationally invariant order and order at  $M$ -points  $B_2$  states admit nontrivial polarization, while  $B_1$  states admit nontrivial polarization for  $K$ -point order. Based on these considerations we conclude that for site order the  $C_3$  symmetric state contained in the  $M$ -point triplet  $F_4$ , which is a  $B_2$  state may have nontrivial polarization. For bond order we have the  $K$ -point candidate  $B_1$  contained in  $E_1'$  and the  $M$ -point candidate  $B_2$  contained in  $F_4$ .

Before we start building the general particle-hole condensates on the honeycomb lattice, we note that we will use the matrix functions  $\tau^i$  (Pauli matrices), which operate on the sublattice degree of freedom.

### Translationally invariant singlet states at $\Gamma$

We start by considering translationally invariant states, some of which are nontrivial due to the sublattices of the honeycomb lattice. A general density-wave state with sublattice structure can then be written as

$$\langle \hat{\psi}_{i\sigma}^\dagger(\vec{k}) \hat{\psi}_{j\sigma'}(\vec{k}) \rangle = \vec{\Delta}(\vec{k}) \cdot \vec{\tau}_{ij} \delta_{\sigma\sigma'} \quad (9.137)$$

Here the  $\tau$ -matrices are Pauli matrices acting on the sublattice degree of freedom  $i, j = A, B$ . The simplest translationally invariant state we can write is the CDW

state which makes the two sublattices inequivalent and breaks inversion symmetry.

$$\langle \hat{\psi}_{i\sigma}^\dagger(\vec{k}) \hat{\psi}_{j\sigma'}(\vec{k}) \rangle = \Delta_{\text{CDW}} \tau_{ij}^3 \delta_{\sigma\sigma'} \quad (9.138)$$

The Pauli matrix  $\tau^3$  transforms according to  $B_2$  and this CDW state consequently transforms as  $B_2$ . Note that  $\Delta_{\text{CDW}} = \Delta_{\text{CDW}}^*$ . Intuitively this is immediately obvious, since the two sublattices are inequivalent and hence all operations that exchange  $A$  and  $B$  sites no longer constitute symmetries.

Next we look at translationally invariant bond-order states. There are three bonds in the unit cell which transform into each other under point group operations. In accordance with equation (9.133) we expect a one-dimensional representation  $A_1$ , which corresponds to the fully symmetric state, and a two-dimensional  $d$ -wave-like representation  $E_2$ . The state transforming as  $A_1$  is simply a uniform renormalization of the bond strength and therefore the overlap integral (hopping). The other two bond density-wave states transform according to  $d$ -wave functions ( $E_2$ ) and are given by

$$\begin{aligned} \langle \hat{\psi}_{i\sigma}^\dagger(\vec{k}) \hat{\psi}_{j\sigma'}(\vec{k}) \rangle &= \frac{\Delta_{x^2-y^2}}{3} \tau_{ij}^{x^2-y^2}(\vec{k}) \delta_{\sigma\sigma'} \\ \langle \hat{\psi}_{i\sigma}^\dagger(\vec{k}) \hat{\psi}_{j\sigma'}(\vec{k}) \rangle &= \frac{\Delta_{xy}}{\sqrt{3}} \tau_{ij}^{xy}(\vec{k}) \delta_{\sigma\sigma'} \end{aligned} \quad (9.139)$$

Here the matrix  $\tau^{x^2-y^2}(\vec{k})$  is defined as

$$\tau^{x^2-y^2}(\vec{k}) = \begin{bmatrix} f_{x^2-y^2}(\vec{k}) & \\ f_{x^2-y^2}^*(\vec{k}) & \end{bmatrix}, \quad (9.140)$$

and  $\tau^{xy}(\vec{k})$  is defined similarly. The functions  $f_{x^2-y^2}$  and  $f_{xy}$  are given by

$$\begin{aligned} f_{x^2-y^2}(\vec{k}) &= (-2e^{-i\vec{k}\cdot\vec{\delta}_1} + e^{-i\vec{k}\cdot\vec{\delta}_2} + e^{-i\vec{k}\cdot\vec{\delta}_3}) e^{i\varphi(\vec{k})} \\ f_{xy}(\vec{k}) &= (e^{-i\vec{k}\cdot\vec{\delta}_2} - e^{-i\vec{k}\cdot\vec{\delta}_3}) e^{i\varphi(\vec{k})}. \end{aligned} \quad (9.141)$$

which may be immediately recognized as real  $d$ -wave combinations of the three exponentials  $e^{i\vec{k}\cdot\vec{\delta}_i}$ , which transform into each other under the operations of the point group. The exponential  $e^{-i\varphi(\vec{k})} \equiv e^{-i\vec{k}\cdot\vec{\delta}_1}$  is included to enforce the gauge choice of equation (9.4). We adopt the convention of including the factor  $e^{-i\varphi(\vec{k})}$  explicitly so as not to risk obscuring the three nearest-neighbor exponentials.

What we have not discussed in the introduction to this honeycomb lattice section, are bond density waves which emerging on next-nearest neighbor bonds. All bond order decompositions, equations (9.133) and (9.134), pertain to nearest neighbor bonds connecting the two sublattices. Even though we have not derived the decompositions,

we nevertheless briefly discuss the next-nearest neighbor bond order since it plays an important role in the literature [84, 167, 168]. Intra-sublattice bond order instabilities have been at the heart of recent studies on topological particle-hole condensates on the honeycomb lattice.

We proceed to writing  $k_j = \vec{k} \cdot \vec{x}_j$  where  $\vec{x}_j$  are the Bravais lattice vectors (see also Appendix A.3 for more on these definitions). Using this, we can directly write orbital momentum basis functions which transform as 1D representations under all elements of the point group.

$$\begin{aligned} f_{A_1}(\vec{k}) &= \cos k_1 + \cos k_2 + \cos k_3 \\ f_{B_1}(\vec{k}) &= \sin k_1 + \sin k_2 + \sin k_3 \end{aligned} \quad (9.142)$$

These functions may be combined with sublattice functions (Pauli matrices) to construct states with specific symmetry. Let us start by considering the most famous example of a condensate functions that may be constructed in such a way. We can combine  $f_{B_1}$  with  $\tau^3$ , which transform as  $B_1$  and  $B_2$ , respectively, to obtain a density-wave state that transforms as  $A_2 = B_1 \otimes B_2$ , as expected from the character table. The expression for the condensate reads

$$\langle \hat{\psi}_{i\sigma}^\dagger(\vec{k}) \hat{\psi}_{j\sigma'}(\vec{k}) \rangle = \Delta_{A_2} f_{B_1}(\vec{k}) \tau_{ij}^3 \delta_{\sigma\sigma'} \quad (9.143)$$

Note that we need to have  $(\Delta_{A_2})^* = \Delta_{A_2}$  hence we have one real parameter. This state does not break any rotational symmetries, however, the point group reflections are all broken, together with time-reversal symmetry. The state described by this condensate function has a gapped mean-field spectrum and is in fact precisely the state introduced by Haldane [76] in order to demonstrate as a matter of principle that a Quantum Hall effect can occur in a lattice system in the absence of external magnetic fields. It has been argued in the literature that such a density wave state indeed emerges from next-nearest neighbor interactions in a mean field treatment [84].

Another example of a density wave state we can form simply by combining functions of specific symmetry, is a state which does not break any lattice symmetries, but does however break the particle-hole symmetry of the bare honeycomb lattice. It is obtained by combining the  $f_{A_1}$  function with the unit matrix  $\delta_{ij}$ . The condensate function reads

$$\langle \hat{\psi}_{i\sigma}^\dagger(\vec{k}) \hat{\psi}_{j\sigma'}(\vec{k}) \rangle = \Delta_{A_1} f_{A_1}(\vec{k}) \delta_{ij} \delta_{\sigma\sigma'} \quad (9.144)$$

Also in this case one has  $(\Delta_{A_1})^* = \Delta_{A_1}$ .

As we are considering intra-sublattice bond order, the two available sublattice functions are  $\delta_{ij}$  and  $\tau_{ij}^3$ . Combining them with the two orbital momentum functions  $f_{A_1}$  and  $f_{B_1}$  yields four different states, two of which we have just discussed. The

others must have symmetries  $B_1 = A_1 \otimes B_1$  and  $B_2 = B_2 \otimes A_1$ . The condensate functions are then give by

$$\begin{aligned}\langle \hat{\psi}_{i\sigma}^\dagger(\vec{k}) \hat{\psi}_{j\sigma'}(\vec{k}) \rangle &= \Delta_{B_1} f_{B_1}(\vec{k}) \delta_{ij} \delta_{\sigma\sigma'}, \\ \langle \hat{\psi}_{i\sigma}^\dagger(\vec{k}) \hat{\psi}_{j\sigma'}(\vec{k}) \rangle &= \Delta_{B_2} f_{A_1}(\vec{k}) \tau_{ij}^3 \delta_{\sigma\sigma'}\end{aligned}\quad (9.145)$$

Note that the second of these two transforms as  $B_2$ , which is the same as the site ordered state of equation (9.138). Hence, already anticipating the conclusion of Section 9.4.1, this density wave state opens up a gap in the mean-field spectrum.

### Translational symmetry breaking at $\vec{K}_\pm$

We move on to translational symmetry broken states at wave-vector  $\vec{K}_\pm = \pm(4\pi/3, 0)$ . We will start with site order and then discuss bond-density wave orders. For site order we expect states corresponding to representations contained in (9.131). As we already found the translationally symmetric  $A_1$  and  $B_2$  states, we are left to identify the  $G'$  ( $= E_1 \oplus E_2$ ) states.

In the case of site order the relevant sublattice functions are  $\tau^0 = \delta$  and  $\tau^3$ . We will look for condensates which transform as  $G'$  and are simultaneously organized as partners of  $E_1$  and  $E_2$  contained in  $G'$ . Such condensates are pedagogically derived in real space. We start from a properly modulated state on the  $A$ -sublattice (suppressing spin indices for the sake of brevity)

$$\langle \hat{\psi}_A^\dagger(\vec{x}) \hat{\psi}_A(\vec{y}) \rangle = \Delta \cos(\vec{K} \cdot \vec{x}) \delta_{\vec{x}, \vec{y}}. \quad (9.146)$$

Since the little group of  $\vec{K}_\pm$  is  $C_{3v}$  (see also above) it is sensible to first build a set of three objects which transform into each other under the threefold rotation. Doing this for the expectation value in equation (9.146) we find the two related states

$$\begin{aligned}C_3 &\rightarrow \langle \hat{\psi}_A^\dagger(\vec{x}) \hat{\psi}_A(\vec{y}) \rangle = \Delta \cos(\vec{K} \cdot \vec{x} + \vartheta) \delta_{\vec{x}, \vec{y}} \\ C_3^{-1} &\rightarrow \langle \hat{\psi}_A^\dagger(\vec{x}) \hat{\psi}_A(\vec{y}) \rangle = \Delta \cos(\vec{K} \cdot \vec{x} + 2\vartheta) \delta_{\vec{x}, \vec{y}}\end{aligned}\quad (9.147)$$

where  $\vartheta = 2\pi/3 = -i \ln \omega$ . In general, for three objects  $|a\rangle, |b\rangle, |c\rangle$  related by a three-fold rotation, one may form a fully symmetric combination, i.e.  $|a\rangle + |b\rangle + |c\rangle$  and a doublet of states transforming as partners of the two-dimensional representation of  $C_{3v}$ . The latter doublet is written as  $|E, 1\rangle = (-2|a\rangle + |b\rangle + |c\rangle)/3$  and  $|E, 2\rangle = (|b\rangle - |c\rangle)/\sqrt{3}$ . Now if we make the identification  $|a\rangle = \cos(\vec{K} \cdot \vec{x}) \equiv \cos a$ ,  $|b\rangle = \cos(\vec{K} \cdot \vec{x} + \vartheta) \equiv \cos b$  and  $|c\rangle = \cos(\vec{K} \cdot \vec{x} + 2\vartheta) \equiv \cos c$  an expression for the doublets of  $E_1$  and  $E_2$  is immediately obtained. We are left with finding expressions for the  $B$

sublattice. They are fixed by the character table of  $C_{6v}$  in the sense that the character table tells us that the partners of  $E_1$  are odd under  $C_2$ , while the partners of  $E_2$  are even. As the inversion  $C_2$  exchanges sublattices this uniquely fixes  $\langle \hat{\psi}_B^\dagger(\vec{x}) \hat{\psi}_B(\vec{y}) \rangle$ . It is important to realize that the threefold rotation  $C_3$  maps  $A$  and  $B$  atoms to different unit cells. This is reflected in the expression for the condensate expectation value on the  $B$ -sublattice, which read  $(-2 \cos c + \cos b + \cos a)/3$  and  $(\cos b - \cos a)/\sqrt{3}$ . Transforming to momentum space yields expressions for the four density wave states transforming as  $G' = E_1 \oplus E_2$ , i.e. for  $E_2$  (reinstating spin)

$$\begin{aligned} \langle \hat{\psi}_{i\sigma}^\dagger(\vec{k} + \vec{K}_+) \hat{\psi}_{j\sigma'}(\vec{k}) \rangle &= \frac{\Delta_{x^2-y^2}^1}{3} (-2 + \omega + \omega^2) \underline{\tau}_{ij} \delta_{\sigma\sigma'} \\ \langle \hat{\psi}_{i\sigma}^\dagger(\vec{k} + \vec{K}_+) \hat{\psi}_{j\sigma'}(\vec{k}) \rangle &= \frac{\Delta_{xy}^1}{\sqrt{3}} (\omega^2 - \omega) \underline{\tau}_{ij} \delta_{\sigma\sigma'}, \end{aligned} \quad (9.148)$$

and for the  $E_1$  doublet

$$\begin{aligned} \langle \hat{\psi}_{i\sigma}^\dagger(\vec{k} + \vec{K}_+) \hat{\psi}_{j\sigma'}(\vec{k}) \rangle &= \frac{\Delta_{xz}^2}{3} (-2 + \omega + \omega^2) [\underline{\tau}^3]_{ij} \delta_{\sigma\sigma'} \\ \langle \hat{\psi}_{i\sigma}^\dagger(\vec{k} + \vec{K}_+) \hat{\psi}_{j\sigma'}(\vec{k}) \rangle &= \frac{\Delta_{yz}^2}{\sqrt{3}} (\omega^2 - \omega) [\underline{\tau}^3]_{ij} \delta_{\sigma\sigma'}. \end{aligned} \quad (9.149)$$

Note that  $\langle \hat{\psi}_{i\sigma}^\dagger(\vec{k} + \vec{K}_+) \hat{\psi}_{j\sigma'}(\vec{k}) \rangle^* = \langle \hat{\psi}_{j\sigma'}^\dagger(\vec{k} + \vec{K}_-) \hat{\psi}_{i\sigma}(\vec{k}) \rangle$ . Here the matrix  $\underline{\tau}$  accounts for the fact that threefold rotations do not preserve the honeycomb unit cell and is given by

$$\underline{\tau} = \begin{bmatrix} 1 & \\ & \omega \end{bmatrix}. \quad (9.150)$$

One observes that in momentum space the  $d$ -wave nature of these doublets is reflected in the combinations of phases  $(-2 + \omega + \omega^2)/3$  and  $(\omega - \omega^2)/\sqrt{3}$ . They are easily seen to be equal to  $(-2 + \omega + \omega^2)/3 = -1$  and  $(\omega - \omega^2)/\sqrt{3} = i$ . Based on this it is also straightforward to see that the symmetric combination  $\cos a + \cos b + \cos c \rightarrow 1 + \omega + \omega^2$  vanishes. This is not surprising as the symmetric combination, combined with either  $\tau^0$  or  $\tau^3$  would transform as a  $1D$  representation and there are no such translational symmetry broken states, as we learned from (9.131). Before we proceed to bond order, we note that

$$\begin{aligned} (-2 \cos a + \cos b + \cos c)/3 &\sim \cos(\vec{K} \cdot \vec{x}) \\ (\cos b - \cos c)/\sqrt{3} &\sim \sin(\vec{K} \cdot \vec{x}), \end{aligned} \quad (9.151)$$

which relates the density wave states derived here purely on symmetry grounds to CDWs discussed in the context of graphene [180]. These CDWs were shown to

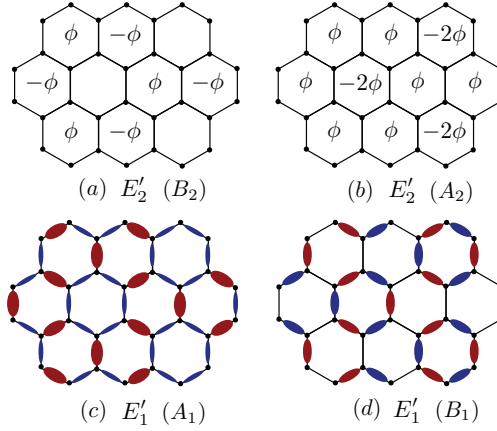


**Figure 9.5:** Graphical representation of some density wave orders on the honeycomb lattice. (a)-(b) denote the flux states which are partners of the  $E'_2$  doublet, while (c)-(d) denote the bond ordered states transforming as  $E'_1$ , which are nothing but the two linearly independent Kekule distortions known to gap out the honeycomb Dirac fermions.

correspond to non-Abelian gauge fields in the low-energy theory of graphene, which we will comment on more extensively below. In addition, this reduction shows that starting with a cosine in equation (9.146) did not constitute a loss of generality.

After having exhaustively discussed and classified site order based on symmetry, we move on to translational symmetry broken bond order. It makes sense to explicitly distinguish nearest-neighbor and next-nearest neighbor bond order and we choose to focus mainly on the former. In fact, the decomposition of bond order states in equation (9.133) refers to nearest neighbor bond order exclusively. The translational symmetry broken content of the decomposition is  $E'_1 \oplus G'$ , which may be decomposed further into  $A_1 \oplus B_1 \oplus E_1 \oplus E_2$  in terms of representations of  $C_{6v}$ . In the following we identify the states corresponding to these representations and we will see that they are actually very familiar states.

We start with some general relations which hold for any hexagonal symmetry system with sublattices. A general bond order state is specified by the expectation value

$$\langle \hat{\psi}_{i\sigma}^\dagger(\vec{k} + \vec{K}_\pm) \hat{\psi}_{j\sigma'}(\vec{k}) \rangle = [\hat{\Delta}_\pm(\vec{k})]_{ij}, \quad (9.152)$$

where  $\hat{\Delta}_\pm(\vec{k})$  is a matrix valued function in sublattice space. Using the properties of

the  $\vec{K}_\pm$  one can deduce the following relations

$$\begin{aligned}
\langle \hat{\psi}_{i\sigma}^\dagger(\vec{k}) \hat{\psi}_{j\sigma'}(\vec{k} + \vec{K}_\pm) \rangle &= [\hat{\Delta}_\pm(\vec{k})]_{ij}^\dagger \\
\langle \hat{\psi}_{i\sigma}^\dagger(\vec{k}) \hat{\psi}_{j\sigma'}(\vec{k} + \vec{K}_\mp) \rangle &= [\hat{\Delta}_\pm(\vec{k} + \vec{K}_\mp)]_{ij} \\
\langle \hat{\psi}_{i\sigma}^\dagger(\vec{k} + \vec{K}_\mp) \hat{\psi}_{j\sigma'}(\vec{k}) \rangle &= [\hat{\Delta}_\pm(\vec{k} + \vec{K}_\mp)]_{ij}^\dagger \\
\langle \hat{\psi}_{i\sigma}^\dagger(\vec{k} + \vec{K}_\mp) \hat{\psi}_{j\sigma'}(\vec{k} + \vec{K}_\pm) \rangle &= [\hat{\Delta}_\pm(\vec{k} + \vec{K}_\pm)]_{ij} \\
\langle \hat{\psi}_{i\sigma}^\dagger(\vec{k} + \vec{K}_\pm) \hat{\psi}_{j\sigma'}(\vec{k} + \vec{K}_\mp) \rangle &= [\hat{\Delta}_\pm(\vec{k} + \vec{K}_\mp)]_{ij}^\dagger
\end{aligned} \tag{9.153}$$

In particular, these constraints imply for the honeycomb lattice that bond order is fully determined by  $[\hat{\Delta}_\pm(\vec{k})]_{AB} = \Delta_\pm(\vec{k})$  and we only need to specify these two functions to distinguish different condensates. In addition, time-reversal invariance imposes the constraint  $\Delta_-(\vec{k}) = (\Delta_+(-\vec{k}))^*$  on the condensate functions. As long as this constraint is satisfied the density wave states will be part of the decomposition in (9.133).

We first look at the states corresponding to the  $E'_1$  doublet. The two partners of this doublet are contained in the functions

$$\begin{aligned}
\Delta_+(\vec{k}) &= \Delta_{E'_1} \omega^2 (e^{-i\vec{k}\cdot\vec{\delta}_1} + \omega^2 e^{-i\vec{k}\cdot\vec{\delta}_2} + \omega e^{-i\vec{k}\cdot\vec{\delta}_3}) e^{i\varphi(\vec{k})}, \\
\Delta_-(\vec{k}) &= \Delta_{E'_1}^* \omega (e^{-i\vec{k}\cdot\vec{\delta}_1} + \omega e^{-i\vec{k}\cdot\vec{\delta}_2} + \omega^2 e^{-i\vec{k}\cdot\vec{\delta}_3}) e^{i\varphi(\vec{k})}.
\end{aligned} \tag{9.154}$$

The order parameter  $\Delta_{E'_1}$  is complex and the two partners of the doublet are given by the real and imaginary parts of the order parameter  $\Delta_{E'_1}$ . We find in addition that the real and imaginary parts are precisely the states transforming as  $A_1$  and  $B_1$  of the group  $C_{6v}$ . What is the interpretation of these states? They are actually very familiar bond ordered states on the honeycomb lattice, as they are nothing else than the Kekule distortions of the hopping texture [197]. This is not very hard to believe, as the Kekule pattern is known to be tied to a tripling of the unit cell, and by inspecting a typical Kekule bond modulation it is easy to identify it as a state that is even under all rotations and reflections (for properly chosen origin), therefore transforming as  $A_1$ . In graphene, the hallmark condensed matter example of a honeycomb lattice, the Kekule modulations have been discussed as perturbations generating a mass for the low-energy Dirac fermions. We will come back to the low-energy description of this  $E'_1$  doublet from the perspective of symmetry.

Before we take a closer look at the precise structure of the  $E'_1$  doublet functions, we show that the time-reversal breaking doublet  $E'_2$  which is part of the flux state decomposition of equation (9.135), is easily obtained by using the time-reversal oddness condition  $\Delta_-(\vec{k}) = -(\Delta_+(-\vec{k}))^*$ . Indeed, the  $E'_2$  flux doublet is simply given

by

$$\begin{aligned}\Delta_+(\vec{k}) &= \Delta_{E'_2} \omega^2 (e^{-i\vec{k}\cdot\vec{\delta}_1} + \omega^2 e^{-i\vec{k}\cdot\vec{\delta}_2} + \omega e^{-i\vec{k}\cdot\vec{\delta}_3}) e^{i\varphi(\vec{k})}, \\ \Delta_-(\vec{k}) &= -\Delta_{E'_2}^* \omega (e^{-i\vec{k}\cdot\vec{\delta}_1} + \omega e^{-i\vec{k}\cdot\vec{\delta}_2} + \omega^2 e^{-i\vec{k}\cdot\vec{\delta}_3}) e^{i\varphi(\vec{k})}.\end{aligned}\quad (9.155)$$

While not as widely known as the Kekule distortion, these states have been discussed as time-reversal symmetry broken states with nontrivial topological characteristics emerging as mean-field solutions of an interacting honeycomb lattice model away from half filling [185, 198]. Based on the symmetry classification presented here it is now straightforward to see why one of these states permits additional topological quantum numbers. As we had noted in the beginning of this section, the flux doublet  $E'_2$  is further decomposed in terms of the rotational and reflection elements as  $E'_2 = A_2 \oplus B_2$ . Hence only one of these flux states breaks all reflections allowing for nontrivial topological Fermi surface properties [177]. In particular, if such a state would induce gaps in the spectrum, the Chern number may be nonzero. The spectral effects of all density waves constructed from  $K$ -point momenta will be discussed in more detail in Section 9.4.1, but here we already disclose that the  $A_2$  state is not gapped, making the Chern number a meaningless quantity. However, one may still calculate the off-diagonal (Hall) conductivity and find that it is nonzero in case of the  $A_2$  state [185], but not quantized. Any unbroken reflection would necessarily imply vanishing Hall conductivity.

In the introductory part of this section, where we showed which irreducible representations are contained in the site, bond and flux order representations for a given type of translational symmetry breaking, we had identified one state which may have quantized electric polarization. This is the  $B_1$  bond order state coming from the  $E'_1$  doublet. The mean field spectrum of this state is in fact gapped, as it is one of the Kekule partners. However, a simple argument shows that evaluating equation (9.40) must yield a trivial result for the appropriate filling (half filling). As the  $B_1$  state belongs to the doublet  $E'_1$  with the  $A_1$  state as its partner, it is possible to adiabatically deform one state into the other without closing the energy gap, indeed a known property of the two Kekule distortions. Hence, the  $B_1$  state must have the same topological characteristics as the  $A_1$  state.

Before we continue and look at density wave states at  $M$ -point wave vectors, we make three comments. The first comment concerns the bond order doublets. From the general decomposition of  $K$ -point bond order in equation (9.133), it is clear that in addition to the aforementioned translational symmetry broken doublet  $E'_1$ , there is a collection of states transforming as  $G' = E_1 \oplus E_2$ . These are easily constructed from the functions of the Kekule modulations, by just taking the usual  $d$ -wave and combinations,  $(x^2 - y^2, xy)$  and  $(xz, yz)$ . For instance, the  $E_2$  condensates are given

by

$$\begin{aligned}\Delta_{+}^{x^2-y^2}(\vec{k}) &= \Delta_{x^2-y^2} \frac{\omega^2}{\sqrt{3}} (-2e^{-i\vec{k}\cdot\vec{\delta}_1} + \omega^2 e^{-i\vec{k}\cdot\vec{\delta}_2} + \omega e^{-i\vec{k}\cdot\vec{\delta}_3}) e^{i\varphi(\vec{k})}, \\ \Delta_{+}^{xy}(\vec{k}) &= \Delta_{xy} \omega^2 (\omega^2 e^{-i\vec{k}\cdot\vec{\delta}_2} - \omega e^{-i\vec{k}\cdot\vec{\delta}_3}) e^{i\varphi(\vec{k})}\end{aligned}\quad (9.156)$$

where  $(\Delta_{x^2-y^2}, \Delta_{xy})$  are both real in this case, and  $\Delta_{-}(\vec{k})$  is given by the time-reversal invariance condition.  $d$ -wave doublets that break time-reversal invariance do not need to be considered as they cannot give any new state. This immediately follows from equation (9.135), which states that the only distinct flux states are  $A_2$  and  $E'_2$ , which we have already identified.

The second comment we wish to add concerns the precise structure of the translational symmetry broken condensate functions. Sticking to the Kekule bond order functions given in equation (9.154), and rearranging terms by working out the complex factors  $\omega$  and  $\omega^2$ , we can write  $\Delta_{\pm}(\vec{k})$  (for the  $\text{Re } \Delta_{E'_1}$  state) as

$$\begin{aligned}\Delta_{+}(\vec{k}) &\sim [-\lambda_1^{(1,E_2)*}(\vec{k}) - i\lambda_2^{(1,E_2)*}(\vec{k})], \\ \Delta_{-}(\vec{k}) &\sim [-\lambda_1^{(1,E_2)*}(\vec{k}) + i\lambda_2^{(1,E_2)*}(\vec{k})]\end{aligned}\quad (9.157)$$

This rearrangement shows that the  $E'_1$  condensates are specific linear combinations of the doublet orbital functions  $\vec{\lambda}^{(1,E_2)}$ , which are explicitly given in Appendix A. In light of the earlier discussion of charge order, we can go one step further and present the coefficients of the terms in a more suggestive form. It was shown that  $-1 = (-2 + \omega + \omega^2)/3$  and  $i = (\omega - \omega^2)/\sqrt{3}$ , which we may collect in a vector  $\vec{d}^{E_2}$ . In this way we can write the functions  $\Delta_{\pm}(\vec{k})$  as

$$\begin{aligned}\Delta_{+}(\vec{k}) &\sim [\vec{d}^{E_2} \cdot \vec{\lambda}^{(1,E_2)}(\vec{k})]^*, \\ \Delta_{-}(\vec{k}) &\sim \vec{d}^{E_2} \cdot \vec{\lambda}^{(1,E_2)}(-\vec{k}).\end{aligned}\quad (9.158)$$

Written in this way, the nature of these condensates as basis functions which transform as  $A_1$  and  $B_1$  under operations of the group  $C_{6v}$  is most apparent. For instance, simple inner products of vectors transforming as  $E_2$  will be functions transforming as  $A_1$ . In general, taking inner products as  $\vec{d}^{E_2} \cdot M \vec{\lambda}^{(1,E_2)}$  is expected to yield functions transforming as  $1D$  representations for  $M = \tau^0, \tau^2$ , while choosing  $M = \tau^1, \tau^3$  gives the two partners of a  $2D$  representation. This holds true for the case of the Kekule distortions, as  $[\vec{d}^{E_2} \cdot \vec{\lambda}^{(1,E_2)}]^*$  and  $[\vec{d}^{E_2} \cdot \tau^2 \vec{\lambda}^{(1,E_2)}]^*$  indeed correspond to  $\text{Re } \Delta_{E'_1}$  and  $\text{Im } \Delta_{E'_1}$ , respectively.

We therefore observe how the condensate functions are structured in terms of group theory.

### Translational symmetry breaking at $\vec{Q}_\mu$

This part deals with the second set of hexagonal lattice ordering vectors leading to translational symmetry broken density waves, the  $M$ -points of the hexagonal Brillouin zone. We have shown that in case of the honeycomb lattice there are six distinct translational symmetry broken site ordered states and nine distinct bond ordered states. For site order they transform as  $F_1 \oplus F_4$ , which is sensible as  $F_4 = B_2 \otimes F_1$ . The sublattice function relevant for site order is  $\tau^3$  and it indeed transforms as  $B_2$ . In what follows we systematically derive the density-wave states transforming as these representations, where we first focus on site order and then move on to bond order. More specifically, the aim will be to derive condensate functions that transform as the representations of the bare point group  $C_{6v}$  contained in the  $F_i$  representations of  $C_{6v}'''$ . We anticipate this to be the most convenient basis in which to express the density wave states so as to relate their symmetry properties to spectral properties at relevant densities. Before we start with site order however, it is helpful to go through some generalities of ordered states with modulation vectors  $\vec{Q}_\mu$ , i.e. the  $M$ -point vectors. This general setting will allow to derive the symmetric states in a straightforward way.

To express the most general real space modulations given a certain set of wave vectors  $\vec{Q}_\mu$  one needs the linearly independent functions  $\cos(\vec{Q}_\mu \cdot \vec{x})$  and  $\sin(\vec{Q}_\mu \cdot \vec{x})$ . In the case of  $M$ -point vectors the functions  $\sin(\vec{Q}_\mu \cdot \vec{x})$  are identically zero, as  $2\vec{Q}_\mu = 0$  which leaves only two possible values for the inner products  $\vec{Q}_\mu \cdot \vec{x} = 0, \pi$ . Hence one only requires the cosine functions, which incidentally is consistent with the unit cell quadrupling. The three functions  $\cos(\vec{Q}_\mu \cdot \vec{x})$  may be conveniently collected in a vector  $\vec{\xi}(\vec{x})$  as  $\xi_\mu = \xi_\mu(\vec{x}) = \cos(\vec{Q}_\mu \cdot \vec{x})$ . We stress here that this pertains to all lattices with hexagonal symmetry. Even more, one can now deduce the effect of space group operations on the vector  $\vec{\xi}$  and exploit this later. Translations for instance are given by  $\xi_\mu(\vec{x} + \vec{x}_j)$ , which is easily seen to reduce to  $\xi_\mu(\vec{x} + \vec{x}_j) = [G_j]_{\mu\nu} \xi_\nu(\vec{x})$ , where  $G_j$  is some matrix depending on  $j$  and summation over repeated indices is implied. We define and find that

$$\begin{aligned} \vec{\xi}(\vec{x} + \vec{x}_1) &= G_1 \vec{\xi}(\vec{x}) = \begin{bmatrix} -1 & & \\ & -1 & \\ & & 1 \end{bmatrix} \vec{\xi}, \\ \vec{\xi}(\vec{x} + \vec{x}_2) &= G_2 \vec{\xi}(\vec{x}) = \begin{bmatrix} 1 & & \\ & -1 & \\ & & -1 \end{bmatrix} \vec{\xi}, \\ \vec{\xi}(\vec{x} + \vec{x}_1 + \vec{x}_2) &= G_3 \vec{\xi}(\vec{x}) = G_1 G_2 \vec{\xi} \end{aligned} \quad (9.159)$$

All  $G_j$  commute, square to one, and multiplying two of them gives the third.

With regard to point group operations, any point group element may be uniquely written in terms of two generators, i.e.  $C_6^{m_2} \sigma_v^{m_1}$ . We thus need the action of the generators on  $\vec{\xi}$ . We first look at the rotational generator and define the matrix  $X$  to correspond to the permutation of  $\xi_\mu$  as a consequence of  $C_6$ , i.e.

$$\vec{\xi}(C_6 \vec{x}) = X \vec{\xi}(\vec{x}), \quad X = \begin{bmatrix} 0 & 0 & 1 \\ 1 & 0 & 0 \\ 0 & 1 & 0 \end{bmatrix} \quad (9.160)$$

Note that  $X$  has the property  $X^3 = 1$  and thus  $X^{-1} = X^2$ . In addition the relation  $X^{-1} = X^T$  holds, where  $X^T$  is the transpose. It thus follows that  $\vec{\xi}(C_3 \vec{x}) = X^T \vec{\xi}(\vec{x})$  and  $\vec{\xi}(C_2 \vec{x}) = \vec{\xi}(\vec{x})$ . For the reflection  $\sigma_v$  we have that

$$\vec{\xi}(\sigma_v \vec{x}) = Y \vec{\xi}(\vec{x}), \quad Y = \begin{bmatrix} 0 & 0 & 1 \\ 0 & 1 & 0 \\ 1 & 0 & 0 \end{bmatrix} \quad (9.161)$$

Some useful relations between the  $G_j$  and  $X$  and  $Y$  are collected in Appendix C.2.1.

As stated, the aim for both site and bond order is to derive condensate functions based on their transformation properties under point group operations alone. In the case of site order we may start with the most general real space  $M$ -point condensate

$$\langle \hat{\psi}_{i\sigma}^\dagger(\vec{x}) \hat{\psi}_{j\sigma'}(\vec{y}) \rangle = \Delta \vec{\zeta}_i \cdot \vec{\xi}(\vec{x}) \delta_{\vec{x}, \vec{y}} \delta_{ij} \delta_{\sigma\sigma'} \quad (9.162)$$

where the two real vectors  $\vec{\zeta}_A$  and  $\vec{\zeta}_B$  fully specify the site ordered state, each vector giving the linear combination of  $\xi_\mu$  functions on sublattice. The idea now is to derive constraints on the  $\vec{\zeta}_i$  given a set of symmetries the density wave state should preserve or break. The symmetry constraints we should impose follow directly from the decomposition of  $F_1$  and  $F_4$  in terms of representations of  $C_{6v}$  and we simply find that  $F_1 = A_1 \oplus E_2$ , while  $F_4 = B_2 \oplus E_1$ . It is best to start with the 1D representations  $A_1$  and  $B_2$ . A look at the character table of the group  $C_{6v}$ , which is given in Appendix ??, tells us that all functions transforming as any of the four 1D irreducible representations must be even under the threefold rotations. It seems therefore natural to first impose this condition. The effect of a point group operation  $R$  is to act on the vectors  $\vec{\zeta}_i$  with a matrix composed of the  $G_i$ ,  $X$  and  $Y$  elements. In case of the threefold rotation we found that they act as

$$\begin{aligned} C_3 &: \vec{\zeta}_A \rightarrow G_2 X^T \vec{\zeta}_A \\ C_3^{-1} &: \vec{\zeta}_A \rightarrow G_3 X \vec{\zeta}_A = (G_2 X^T)^2 \vec{\zeta}_A \end{aligned} \quad (9.163)$$

and similarly, the effect of the threefold rotations on  $\vec{\zeta}_B$  is given by

$$\begin{aligned} C_3 &: \vec{\zeta}_B \rightarrow G_3 X^T \vec{\zeta}_B \\ C_3^{-1} &: \vec{\zeta}_B \rightarrow G_1 X \vec{\zeta}_B = (G_3 X^T)^2 \vec{\zeta}_B \end{aligned} \quad (9.164)$$

From this, and the fact that  $(G_2 X^T)^3 = (G_3 X^T)^3 = 1$ , we conclude that the following choice will correspond to a density wave state symmetric under the threefold rotations

$$\begin{aligned} \vec{\zeta}_A &\rightarrow \frac{1}{3}(1 + G_2 X^T + G_2 X^T G_2 X^T) \vec{\zeta}_A \\ \vec{\zeta}_B &\rightarrow \frac{1}{3}(1 + G_3 X^T + G_3 X^T G_3 X^T) \vec{\zeta}_B \end{aligned} \quad (9.165)$$

The three diagonal reflections do not change the sublattices either and we can look at the constraints they impose on the newly defined  $\vec{\zeta}'_i$ . We derive that all three reflections lead to the same constraint on each of the  $\vec{\zeta}'_i$ , which are given by

$$\begin{aligned} X^T Y \vec{\zeta}'_A &= \vec{\zeta}'_A \\ G_3 Y \vec{\zeta}'_B &= \vec{\zeta}'_B \end{aligned} \quad (9.166)$$

Note that in principle we should have allowed states to be even or odd under reflections, but the two states we are after are both even under reflections and we therefore exclude the odd states. The constraints coming from these reflections already narrow the choices for  $\vec{\zeta}'_i$  down. Indeed, both  $X^T Y$  and  $G_3 Y$  should be interpreted as elements of  $SO(3)$  acting on the vectors  $\vec{\zeta}'_i$ , and it is certainly not surprising that both are reflections in  $SO(3)$ . Reflections leave a plane invariant and equation (9.166) consequently restricts the  $\vec{\zeta}'_i$  to lie in precisely the invariant plane. That still leaves two independent degrees of freedom and we need further constraints to find the unique solutions corresponding to states of symmetry  $A_1$  and  $B_2$ . Point group elements left to consider all exchange sublattice, and in case of for instance the inversion  $C_2$ , we obtain the relations

$$\begin{aligned} G_3 \vec{\zeta}'_A &= \pm \vec{\zeta}'_B \\ G_3 \vec{\zeta}'_B &= \pm \vec{\zeta}'_A, \end{aligned} \quad (9.167)$$

which may be combined to give the trivial relation  $(G_3)^2 \vec{\zeta}'_A = \vec{\zeta}'_A$ . Triviality follows from  $(G_3)^2 = 1$ . Also note that in case of inversion we need to distinguish  $A_1$  and  $B_2$ , as the latter is odd. We find that the definitive constraint can be derived from the

sixfold rotation, which leads to

$$\begin{aligned} X\vec{\zeta}_A &= \pm\vec{\zeta}_B \\ G_3\vec{\zeta}_B &= \pm\vec{\zeta}_A. \end{aligned} \quad (9.168)$$

These expressions can be combined to give  $G_3X\vec{\zeta}_A = \vec{\zeta}'_A$ . Again interpreting the matrix  $G_3X$  as an  $SO(3)$  element, we see that it describes a rotation of the vector it acts on. In particular the constraint  $G_3X\vec{\zeta}'_A = \vec{\zeta}'_A$  means that the vector  $\vec{\zeta}'_A$  is left invariant by the rotation  $G_3X$ , from which it directly follows that  $\vec{\zeta}'_A$  must be proportional to the axis of rotation and therefore is uniquely fixed up to a sign. The vector  $\vec{\zeta}'_B$  is then immediately determined by the constraints as well. We find that the solutions for  $\vec{\zeta}'_i$  are given by

$$\vec{\zeta}'_A = \frac{1}{\sqrt{3}} \begin{bmatrix} -1 \\ -1 \\ 1 \end{bmatrix}, \quad \vec{\zeta}'_B = \pm \frac{1}{\sqrt{3}} \begin{bmatrix} 1 \\ -1 \\ -1 \end{bmatrix} \quad (9.169)$$

where the overall sign (which is immaterial) has been fixed by fully specifying  $\vec{\zeta}'_A$ . The relative sign distinguishing between  $A_1$  and  $B_2$  is incorporated in  $\vec{\zeta}'_B$ , consistent with the sublattice function  $\tau^3$ . At this point we should remember that the condensate functions were formulated in terms of  $\vec{\zeta}_i$  and we should use equation (9.165) to obtain these vectors. We find that the  $\vec{\zeta}_i$  are exactly equal to the  $\vec{\zeta}'_i$ , i.e.  $\vec{\zeta}_i = \vec{\zeta}'_i$ . One way to explain this seemingly surprising fact is to note that the constraints coming from the sixfold rotation  $C_6$  are the same for both  $\vec{\zeta}_i$  and  $\vec{\zeta}'_i$ . Since these constraints, expressed in equation (9.168), are strong enough to uniquely fix both  $\vec{\zeta}_i$  and  $\vec{\zeta}'_i$ , we conclude that they must be the same. At the same time this raises the question why one would consider the constraints coming from  $C_3$ , or  $\sigma_d$ , in the first place. The reason is that considering the action of  $C_3$  yields the building blocks for constructing the doublets contained in  $F_1$  and  $F_4$ , as will be demonstrated just below.

First we write down the condensate functions in momentum space now that we have found the  $\vec{\zeta}_i$ . Based on the above they can simply be expressed as

$$\begin{aligned} \langle \hat{\psi}_{i\sigma}^\dagger(\vec{k} + \vec{Q}_\mu) \hat{\psi}_{j\sigma'}(\vec{k}) \rangle &= \frac{1}{\sqrt{3}} \Delta_{A_1}^{F_1} \zeta_i^\mu \delta_{ij} \delta_{\sigma\sigma'} \\ \langle \hat{\psi}_{i\sigma}^\dagger(\vec{k} + \vec{Q}_\mu) \hat{\psi}_{j\sigma'}(\vec{k}) \rangle &= \frac{1}{\sqrt{3}} \Delta_{B_2}^{F_4} \zeta_i^\mu \tau_{ij}^3 \delta_{\sigma\sigma'} \end{aligned} \quad (9.170)$$

Before we come to the specific expressions of the doublets, we take an alternative look at the way to derive the  $\vec{\zeta}'_i$  and in particular why it is helpful to define the  $\vec{\zeta}'_i$  with equation (9.165). By looking at the action of the threefold rotation we identified

three objects transforming into each other under threefold rotations. Forming the symmetric combination for each of the sublattices led to equation (9.165). Taking the  $A$  sublattice as an example we can define the matrix of the symmetric combination as  $P$ , i.e.  $P = (1 + G_2 X^T + G_2 X^T G_2 X^T)/3$ . Then we find that  $P^2 = P$  and therefore  $P$  is a projector having two possible eigenvalues, 0 and 1. It follows that a nontrivial (zero) solution for  $\vec{\zeta}_i$  must belong to the subspace mapped to 1, while it simultaneously shows that necessarily  $\vec{\zeta}_i = \vec{\zeta}_i'$ . This subspace is found to be spanned specisely by  $\vec{\zeta}_A'$  given in equation (9.169), while an exactly analogous calculations confirms that for the  $B$  sublattice the nontrivial subspace is spanned by  $\vec{\zeta}_B'$  given in equation (9.169). The kernel of  $P$  (for the  $A$ -sublattice), i.e. the subspace mapped to 0, is found to be spanned by

$$\left\{ \frac{1}{\sqrt{2}} \begin{bmatrix} 1 \\ -1 \\ 0 \end{bmatrix}, \frac{1}{\sqrt{6}} \begin{bmatrix} 1 \\ 1 \\ 2 \end{bmatrix} \right\}, \quad (9.171)$$

which corroborates that there are no more site ordered states corresponding to  $1D$  representations of  $C_{6v}$ .

The doublets contained in  $F_1$  and  $F_2$  can be simply obtained by first defining a triple of vectors for each sublattice which transform into each other under the threefold rotations. Per the above they are given by

$$\vec{\zeta}_{Aa} = \frac{1}{3}(G_2 X^T)^a \vec{\zeta}_A', \quad \vec{\zeta}_{Ba} = \frac{1}{3}(G_3 X^T)^a \vec{\zeta}_B', \quad (9.172)$$

where  $a = 1, 2, 3$ . It is crucial to note that the  $\vec{\zeta}_i'$  here are *different* from the ones just found for the  $1D$  representations. The task here is to find the proper  $\vec{\zeta}_i'$  consistent with  $d$ -wave and/or  $p$ -wave symmetry doublets  $E_2$  and  $E_1$ . For each sublattice we expect doublet functions of the form  $x^2 - y^2 \sim (\zeta_{i1}^a + \zeta_{i2}^a - 2\zeta_{i3}^a)/\sqrt{3}$  and  $xy \sim \zeta_{i1}^a - \zeta_{i2}^a$ . In order to find the proper  $\vec{\zeta}_i'$  we define the matrices

$$\begin{aligned} P_{x^2-y^2} &= \frac{1}{3}(-2 + G_2 X^T + G_2 X^T G_2 X^T) \\ P_{xy} &= \frac{1}{3}(G_2 X^T - G_2 X^T G_2 X^T) \end{aligned} \quad (9.173)$$

and similarly for  $B$  of course. For these objects we derive the relations  $P_{x^2-y^2}^2 = -P_{x^2-y^2}$  and  $P_{xy}^2 = P_{x^2-y^2}$ , where the latter leads additionally to  $P_{xy}^4 = -P_{x^2-y^2}$ . The property  $P_{x^2-y^2}^2 = -P_{x^2-y^2}$  implies that  $P_{x^2-y^2}$  is also a projector of some form, having eigenvalues  $-1$  and  $0$ . Examining the kernel of the linear mapping  $P_{x^2-y^2}$  and the subspace corresponding to eigenvalue  $-1$ , we find that the vector

$[-1, -1, 1]^T/\sqrt{3}$  now spans the kernel, while the subspace given in Eq. (9.171) is the eigenspace corresponding to eigenvalue  $-1$ . This provides two independent vectors that are valid choices for  $\vec{\zeta}_A$ . Repeating the same calculation for the  $B$ -sublattice we find that the vector  $[1, -1, -1]^T/\sqrt{3}$  is in the kernel of  $P_{x^2-y^2}$ , while the subspace

$$\left\{ \frac{1}{\sqrt{2}} \begin{bmatrix} 1 \\ 1 \\ 0 \end{bmatrix}, \frac{1}{\sqrt{6}} \begin{bmatrix} -1 \\ 1 \\ -2 \end{bmatrix} \right\}, \quad (9.174)$$

constitutes the  $-1$  eigenspace. The relation between  $\vec{\zeta}_A$  and  $\vec{\zeta}_B$  is then fixed by considering the inversion  $C_2$ . As found earlier we have  $G_3\vec{\zeta}_A = \pm\vec{\zeta}_B$ . Hence, if we fix

$$\vec{\zeta}_A = \frac{1}{\sqrt{2}} \begin{bmatrix} 1 \\ -1 \\ 0 \end{bmatrix}, \quad \vec{\zeta}_B = \frac{1}{\sqrt{2}} \begin{bmatrix} -1 \\ -1 \\ 0 \end{bmatrix} \quad (9.175)$$

we can incorporate the sublattice sign difference by using  $\tau^3$ . Note that we could have chosen the other vector, i.e.  $[1, 1, 2]^T/\sqrt{6}$  and correspondingly for  $B$ , but as it turns out this does not generate anything new.

We are now in a position to write down the expressions for two doublets, one of which transforms as  $E_2$  in  $F_1$  and the other as  $E_1$  in  $F_4$ . The former doublet reads

$$\begin{aligned} \langle \hat{\psi}_{i\sigma}^\dagger(\vec{k} + \vec{Q}_\mu) \hat{\psi}_{j\sigma'}(\vec{k}) \rangle &= \frac{1}{\sqrt{3}} \Delta_{x^2-y^2} (\zeta_{i1}^\mu + \zeta_{i2}^\mu - 2\zeta_{i3}^\mu) \delta_{ij} \delta_{\sigma\sigma'} \\ \langle \hat{\psi}_{i\sigma}^\dagger(\vec{k} + \vec{Q}_\mu) \hat{\psi}_{j\sigma'}(\vec{k}) \rangle &= \frac{1}{\sqrt{3}} \Delta_{xy} (\zeta_{i1}^\mu - \zeta_{i2}^\mu) \delta_{ij} \delta_{\sigma\sigma'}, \end{aligned} \quad (9.176)$$

whereas the latter takes the form

$$\begin{aligned} \langle \hat{\psi}_{i\sigma}^\dagger(\vec{k} + \vec{Q}_\mu) \hat{\psi}_{j\sigma'}(\vec{k}) \rangle &= \frac{1}{\sqrt{3}} \Delta_{xz} (2\zeta_{i3}^\mu - \zeta_{i1}^\mu - \zeta_{i2}^\mu) \tau_{ij}^3 \delta_{\sigma\sigma'} \\ \langle \hat{\psi}_{i\sigma}^\dagger(\vec{k} + \vec{Q}_\mu) \hat{\psi}_{j\sigma'}(\vec{k}) \rangle &= \frac{1}{\sqrt{3}} \Delta_{yz} (\zeta_{i1}^\mu - \zeta_{i2}^\mu) \tau_{ij}^3 \delta_{\sigma\sigma'} \end{aligned} \quad (9.177)$$

A similar approach leads to the construction of symmetric bond density wave order. Again the explicit derivation is most conveniently carried out in real space. We expect translational symmetry broken states transforming as  $F_1 \oplus F_3 \oplus F_4$ , and proceeding as before to express them in a basis consistent with the decompositions in terms of  $C_{6v}$ , we set out to find basis functions of  $A_1 \oplus B_1 \oplus B_2 \oplus 2E_1 \oplus E_2$ .

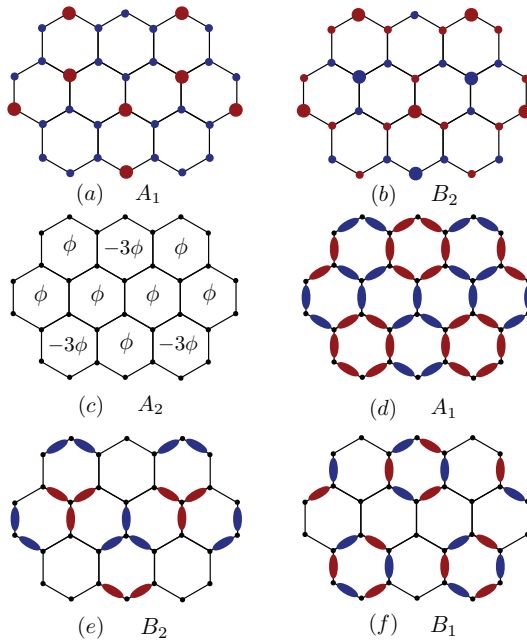


**Figure 9.6:** Site, bond and flux ordered density wave states on the honeycomb lattice with  $M$ -point vector modulations. (a), (b) Site ordered states with  $A_1$  and  $B_2$  symmetry. (c) Flux ordered state with  $A_2$  symmetry. (d)-(f) Bond ordered states with  $A_1$ ,  $B_2$  and  $B_1$  symmetry, coming from  $F_1$ ,  $F_4$  and  $F_3$ , respectively.

The starting point are bond order condensate functions parametrized by  $\vec{\zeta}_i$  with  $i = 1, 2, 3$ ,

$$\begin{aligned}\langle \hat{\psi}_{A\sigma}^\dagger(\vec{x}) \hat{\psi}_{B\sigma'}(\vec{y}) \rangle &= \Lambda + \Delta \vec{\zeta}_1 \cdot \vec{\xi}(\vec{x}) \delta_{\vec{x}, \vec{y}} \delta_{\sigma\sigma'} \\ \langle \hat{\psi}_{A\sigma}^\dagger(\vec{x}) \hat{\psi}_{B\sigma'}(\vec{y}) \rangle &= \Lambda + \Delta \vec{\zeta}_2 \cdot \vec{\xi}(\vec{x}) \delta_{\vec{x} - \vec{x}_1, \vec{y}} \delta_{\sigma\sigma'} \\ \langle \hat{\psi}_{A\sigma}^\dagger(\vec{x}) \hat{\psi}_{B\sigma'}(\vec{y}) \rangle &= \Lambda + \Delta \vec{\zeta}_3 \cdot \vec{\xi}(\vec{x}) \delta_{\vec{x} + \vec{x}_2, \vec{y}} \delta_{\sigma\sigma'}.\end{aligned}\quad (9.178)$$

The action of point group operations provides us with constraints on the  $\vec{\zeta}_i$ , which we summarize here more concisely than in the case of site order. The threefold rotations give relations  $\vec{\zeta}_2 = G_2 X^T \vec{\zeta}_1$  and  $\vec{\zeta}_3 = (G_2 X^T)^2 \vec{\zeta}_1$ . The sixfold rotations give the relations  $G_2 X \vec{\zeta}_1 = \pm \vec{\zeta}_3 = \pm (G_2 X^T)^2 \vec{\zeta}_1$  and  $X^T \vec{\zeta}_1 = \pm \vec{\zeta}_2 = \pm G_2 X^T \vec{\zeta}_1$ . Both lead to the same constraint  $G_3 \vec{\zeta}_1 = \pm \vec{\zeta}_1$ . The diagonal reflections all impose the constraint  $G_3 Y \vec{\zeta}_1 = \pm \vec{\zeta}_1$ , while the vertical reflections impose the constraint  $Y \vec{\zeta}_1 = \pm \vec{\zeta}_1$ . All these constraints can be solved to obtain solutions for  $\vec{\zeta}_1 = \vec{\zeta}$ , for which we may as well drop the index, since there is only one to consider. The equation  $G_3 \vec{\zeta} = \vec{\zeta}$  gives the immediate and unique solution

$$\vec{\zeta} = \begin{bmatrix} 0 \\ 1 \\ 0 \end{bmatrix}, \quad (9.179)$$

and it is a simple matter to check that this state transforms as  $A_1$  by evaluating the other constraints. The equation  $G_3 \vec{\zeta} = -\vec{\zeta}$  on the other hand, admits a solution of the form  $\vec{\zeta} = [\zeta_1, 0, \zeta_3]^T$ . The constraints of the reflections lead to the relations  $\zeta_1 = \pm \zeta_3$ , or in other words

$$\vec{\zeta} = \frac{1}{\sqrt{2}} \begin{bmatrix} 1 \\ 0 \\ \pm 1 \end{bmatrix}. \quad (9.180)$$

Evaluating the constraints it is straightforward to check that the solution with  $+1$  corresponds to the  $B_1$  representation, while the  $-1$  solution corresponds to the  $B_2$  representation.

In momentum space the condensate functions are generically expressed as

$$\langle \hat{\psi}_{i\sigma}^\dagger(\vec{k} + \vec{Q}_\mu) \hat{\psi}_{j\sigma'}(\vec{k}) \rangle = [\hat{\Delta}_\mu(\vec{k})]_{ij}, \quad (9.181)$$

where the  $\hat{\Delta}_\mu(\vec{k})$  should be read as a matrix in sublattice space. Using the properties of the ordering momenta  $\vec{Q}_\mu$  we establish the relations

$$\begin{aligned}\langle \hat{\psi}_{i\sigma}^\dagger(\vec{k}) \hat{\psi}_{j\sigma'}(\vec{k} + \vec{Q}_\mu) \rangle &= [\hat{\Delta}_\mu(\vec{k})]_{ij}^\dagger \\ \langle \hat{\psi}_{i\sigma}^\dagger(\vec{k}) \hat{\psi}_{j\sigma'}(\vec{k} + \vec{Q}_\mu) \rangle &= [\hat{\Delta}_\mu(\vec{k} + \vec{Q}_\mu)]_{ij},\end{aligned}\quad (9.182)$$

and, in addition we easily find that

$$\langle \hat{\psi}_{i\sigma}^\dagger(\vec{k} + \vec{Q}_\gamma) \hat{\psi}_{j\sigma'}(\vec{k} + \vec{Q}_\nu) \rangle = [\hat{\Delta}_\mu(\vec{k} + \vec{Q}_\nu)]_{ij}, \quad (9.183)$$

where  $\mu \neq \nu \neq \gamma$ . These relations fully fix the bond order density-wave state in terms of the four matrices  $\hat{\Delta}_\mu(\vec{k})$ . These matrices are however not independent, which follows directly from  $\langle \hat{\psi}_{i\sigma}^\dagger(\vec{k} + \vec{Q}_\mu) \hat{\psi}_{j\sigma'}(\vec{k}) \rangle = [\hat{\Delta}_\mu(\vec{k} + \vec{Q}_\mu)]_{ij}^\dagger$ . Bond ordered states on the honeycomb lattice are therefore specified completely by the four complex functions  $[\hat{\Delta}_\mu(\vec{k})]_{AB} = \Delta_\mu(\vec{k})$ .

In order to write down explicit condensate functions, we recall that we defined

$$\vec{\zeta}_a = (G_2 X^T)^a \vec{\zeta}, \quad (9.184)$$

where the label  $a$  corresponds to one of the three elementary bonds, and per the above we have three independent choices for  $\vec{\zeta}$ , one for each of the states transforming as  $1D$  representations. The bond density waves corresponding to  $A_1$ ,  $B_1$  and  $B_2$  are then simply obtained by substituting the appropriate  $\vec{\zeta}$  of equations (9.179)-(9.180) into (9.184) first and then write

$$\Delta_\mu(\vec{k}) = (\zeta_1^\mu e^{-i\delta_1 \cdot \vec{k}} + \zeta_2^\mu e^{-i\delta_2 \cdot \vec{k}} + \zeta_3^\mu e^{-i\delta_3 \cdot \vec{k}}) e^{i\varphi(\vec{k})}. \quad (9.185)$$

The doublets are simply obtained by forming  $d$ -wave type combinations  $\sim \zeta_1 + \zeta_2 - 2\zeta_3$  and  $\sim \zeta_1 - \zeta_2$ . This then completes the description of the condensate functions encoding bond order coming from the decomposition (9.134).

This brings us to the final case of honeycomb lattice  $M$ -point order we discuss here, which is the flux ordered state contained in the flux decomposition of equation (9.136) and transforming as  $A_2$ . The good news is that we already went through quite some effort when deriving symmetric bond ordered states and an explicit expression for the  $A_2$  flux ordered state is almost directly obtained by making the condensate function of equation (9.185) imaginary. We thus write

$$\Delta_\mu(\vec{k}) = i(\zeta_1^\mu e^{-i\delta_1 \cdot \vec{k}} + \zeta_2^\mu e^{-i\delta_2 \cdot \vec{k}} + \zeta_3^\mu e^{-i\delta_3 \cdot \vec{k}}) e^{i\varphi(\vec{k})}, \quad (9.186)$$

and the only task left is to check which one of the three choices for  $\vec{\zeta}$  given in equations (9.179)-(9.180) yields a state with nonzero flux. As there is no other flux ordered state transforming as a  $1D$  representation according to equation (9.136), we know that two of the three choices for  $\vec{\zeta}$  correspond to a state which is gauge-equivalent to a bond ordered state already obtained. Checking symmetries we find that  $\vec{\zeta} = (1, 0, 1)^T$  generates the  $A_2$  symmetric state when substituted into equation (9.184) and (9.186). In the introductory part of this honeycomb lattice section we have argued that the  $A_2$  flux ordered state is symmetry-compatible QAH effect. Now that we have an explicit expression of this density wave state, we can analyze the mean field spectrum

and find out whether it does indeed host a QAH effect. The first point to address is the insulating nature of the ground state. We find that the presence of the density wave does indeed open up a full spectral gap, thus making the ground state insulating. The second question is whether or not the Chern number, which characterizes the topological nature of the insulating state, is nonzero. To this end we simply employ formula (9.35) to conclude that the insulating ground state is indeed a Chern insulator. This is an interesting result, as it demonstrates that a Chern insulator on the honeycomb lattice can in principle be realized with purely nearest neighbor hoppings, modulated by  $M$ -point ordering vectors. On top of that, the exposition of  $M$ -point order on the kagome and triangular lattices following below will highlight that such a Chern insulating is not a peculiarity of the honeycomb lattice, but exists for all lattices with hexagonal symmetry. Finally, in Section 10 we will explain in detail how these flux ordered states on various lattices transforming as  $A_2$  have very interesting spinful generalizations, such as for instance QSH states.

As this flux ordered state is of wider interest than just the honeycomb lattice or its concomitant Quantum Anomalous Hall effect, we take a closer look at the functions  $\Delta_\mu(\vec{k})$  of equation (9.186). Substituting the  $\vec{\zeta}_a$  one finds

$$\begin{aligned}\Delta_1(\vec{k}) &= i(e^{-i\delta_1 \cdot \vec{k}} - e^{-i\delta_3 \cdot \vec{k}})e^{i\varphi(\vec{k})}/\sqrt{2}, \\ \Delta_2(\vec{k}) &= i(e^{-i\delta_3 \cdot \vec{k}} - e^{-i\delta_2 \cdot \vec{k}})e^{i\varphi(\vec{k})}/\sqrt{2}, \\ \Delta_3(\vec{k}) &= i(e^{-i\delta_1 \cdot \vec{k}} - e^{-i\delta_2 \cdot \vec{k}})e^{i\varphi(\vec{k})}/\sqrt{2}.\end{aligned}\tag{9.187}$$

Inspecting the structure of these condensate functions, we see that they have the form of a  $d$ -wave function. The two particular exponentials appearing for each of the  $\vec{Q}_\mu$  are the ones which get mapped onto each other by the reflections leaving the respective  $\vec{Q}_\mu$  invariant. The relative sign difference ensures reflection symmetry breaking. We therefore note for future reference, that for each  $\vec{Q}_\mu$ , the condensate functions ( $\Delta_\mu(\vec{k})$  in this case) should transform as representations of  $C_{2v}$ . This is the complementary momentum space view on constructing density wave states with specific symmetry, which we will come back to in Section 9.4.3 as well.

To conclude this section on the honeycomb lattice we address the remaining open question regarding topological quantum numbers associated to  $M$ -point ordered states. In the beginning of this honeycomb lattice section we had identified two candidate states with  $C_3$  symmetry to have quantized electric polarization. Both states have  $B_2$  symmetry and derive from  $F_4$  representations. One is the site order state of equation (9.170) and the other is a bond order state, which is obtained from equation (9.185) by substituting the proper  $\vec{\zeta}_i$ . The  $B_2$  site ordered state is found not to be gapped, but instead to have an isolated, albeit accidental, degeneracy. The  $B_2$  bond order state is gapped, however we find the ground state not to have quantized

fractional polarization according to an evaluation of equation (9.40). Hence, there are no  $M$ -point condensates with nontrivial polarization quantum numbers on the honeycomb lattice.

#### Low-energy description: Dirac points

One of the most famous and intriguing characteristics of the honeycomb lattice, is the conic degeneracy of the electronic spectrum at the Brillouin zone vertices [76, 98, 199, 200]. In the vicinity of these degeneracies, which are located at momenta  $\vec{K}_\pm = \pm(4\pi/3, 0)$  (see Fig. 9.4) and are often referred to as “valleys”, the low-energy electronic degrees of freedom can be described by a Dirac Hamiltonian of a massless particle. Indeed, expanding the unperturbed Hamiltonian of electrons hopping on a honeycomb lattice around  $\vec{K}_\pm$  in small momenta  $\vec{q}$  one finds the low-energy Hamiltonian [199]

$$\mathcal{H}(\vec{q}) = \hbar v_F (q_x \nu^3 \tau^1 + q_y \tau^2) \quad (9.188)$$

(where  $v_F = \sqrt{3}ta/(2\hbar)$ ) acting on the Dirac spinor  $\hat{\Phi}(\vec{q})$  which is defined by

$$\hat{\Phi}(\vec{q}) = \begin{bmatrix} \hat{\psi}_A(\vec{K}_+ + \vec{q}) \\ \hat{\psi}_B(\vec{K}_+ + \vec{q}) \\ \hat{\psi}_A(\vec{K}_- + \vec{q}) \\ \hat{\psi}_B(\vec{K}_- + \vec{q}) \end{bmatrix}. \quad (9.189)$$

Here we have chosen the Pauli matrices  $\tau^i$  to act on the sublattice degree of freedom, while the set of matrices  $\nu^i$  acts on the valley degree of freedom. One often finds it convenient to express the Dirac Hamiltonian in a different basis, a basis which corresponds to the chiral representation of the Dirac theory. This is achieved by exchanging the  $A$  and  $B$  sublattice in one of the valleys [the matrix  $V$  of equation (9.119) implements this transformation], such as  $\vec{K}_-$ . In the chiral representation one then has

$$\mathcal{H}(\vec{q}) = \hbar v_F \nu^3 \vec{q} \cdot \vec{\tau}. \quad (9.190)$$

Note that other basis choices, such as the valley isotropic basis, have also found use in the literature [200].

The spectral degeneracy at the Brillouin zone vertices  $\vec{K}_\pm$  is required by point group symmetries [76, 201, 202], as is explained and demonstrated in Appendix A. The breaking of point group symmetries, such as for instance the threefold rotation  $C_3$ , will allow the degeneracy to move away  $\vec{K}_\pm$ , or will lead to the lifting of the degeneracy and consequently the opening of a spectral gap, which is allowed when

the reflection  $\sigma_v$  is broken. Even in case of rotational symmetry breaking, i.e.  $C_3$ , the gapless Dirac nodes are still protected by the combination of inversion  $C_2$  and time-reversal symmetry  $\mathcal{T}$ , but they are no longer required to be located at  $\vec{K}_\pm$ . In the language of [201], point group symmetries cause the degeneracies to be essential at the invariant points  $\vec{K}_\pm$ , while they are accidental under  $\mathcal{T}C_2$ .

The peculiar electronic properties of the honeycomb lattice have been known since long [199], but since the isolation of graphene [196], a single one-atom-thick layer of graphite realizing the two-dimensional honeycomb lattice structure, interest in the fundamental aspects of graphene physics has surged massively. Due to its particular low-energy electronic Dirac structure graphene has become a prime condensed matter playground to study and observe phenomena usually confined to the realm of high-energy physics. In addition, an impressive amount of research has been dedicated to the unique potential of graphene for technological application. Good reviews of graphene physics include [98, 179, 200, 203]. One of the main challenges is to make graphene semiconducting by opening a controllable spectral gap, which in the language of Dirac theory means making the low-energy electrons massive. Both from the fundamental and the applied perspective, the Dirac Hamiltonian of equation (9.190) is generally the starting point to study the electronic properties of electrons on the honeycomb lattice. What we will attempt here is, far from rediscovering widely known facts about the low-energy description of honeycomb lattice electrons, to establish a connection between the symmetry properties of lattice density waves, i.e. intrinsic condensed matter phenomena, and the impact at low energies of these density waves. In doing so we adopt the same approach as for the square lattice  $\pi$ -flux state in Section 9.3.2. We first classify all Dirac fermion bilinears based on their transformation properties under lattice symmetries and then associate them to the site, bond and flux ordered density waves modulated by  $\vec{K}$ -vectors. Based on this symmetry connection, and using the results of the square lattice Dirac theory, will argue for very general statements regarding the lattice symmetry properties of density waves and their low-energy interpretation.

In case of the honeycomb lattice, the effect of the generators of the group  $C_{6v}'''$  on the Dirac spinor (9.189) can be worked out to obtain a full representation of the symmetry group. In the same way as for the square lattice these are then used to classify the fermion bilinears  $\hat{\Phi}_i^\dagger M_{ij} \hat{\Phi}_j$  based on extended point group symmetry. The specifics of this can be found in the Appendix, as the technical details are not of general interest, and here we will simply draw from these results. Incidentally, a discussion of fermion fields not very dissimilar to the present one has appeared in the context of electron-phonon coupling in graphene [204, 205].

We divide the Dirac matrices and the density waves into two groups, i.e. one which collects all translationally invariant states and the other group collects the translational symmetry broken states. Starting with states that do not break translational

invariance, we find that in the chiral representation there are two mass terms, i.e. Dirac matrices which anti-commute with  $\nu^3\tau^1$  and  $\nu^3\tau^2$  and these are given by  $\nu^3\tau^3$  and  $\tau^3$ . It is shown in Appendix A.3 that  $\nu^3\tau^3$  is time-reversal invariant and transforms as  $B_2$ , while  $\tau^3$  breaks time-reversal and transforms as  $A_2$ . This allows for the immediate identification of these mass matrices with density wave states. Both the site ordered state of equation (9.138) and the next nearest neighbor bond ordered state of equation (9.4.1) transform as  $B_2$  and therefore correspond to a mass term in the low-energy theory. It is indeed a very well-known fact that making the two sublattices of graphene energetically inequivalent will open up a spectral gap. The time-reversal breaking bond density wave of equation (9.143) transforms as  $A_2$  and thus corresponds to the mass matrix  $\tau^3$ . Such a mass term was first discussed by Haldane [76] who went on to show that such a Dirac mass leads to a topologically nontrivial insulating state, providing the first example of a Quantum Hall state without external magnetic fields.

There are three more Dirac matrices which commute with the translations  $T(\vec{x}_1)$  and  $T(\vec{x}_1 + \vec{x}_2)$  and these are  $\nu^3$ ,  $\tau^1$  and  $\tau^2$ . The matrix  $\nu^3$  transforms as  $B_1$  and we can identify it with the bond ordered state of equation (9.4.1). This state preserves the reflections which leave the valleys  $\vec{K}_\pm$  invariant and we therefore expect the degeneracies not to be preserved as well. It does however make the valleys inequivalent, which causes the Dirac points at  $\vec{K}_+$  and  $\vec{K}_-$  to be no longer degenerate.

The two Dirac matrices  $(\tau^1, \tau^2)$  form a doublet together, transforming as  $E_2$ . We have found the the bond order components  $(\Delta_{x^2-y^2}, \Delta_{xy})$  of equation (9.4.1) to have precisely this symmetry and we therefore identify the doublet with this unit cell preserving bond order doublet. Working out the low-energy term in the low-energy mean field spectrum we find that

$$\mathcal{H}_{E_2} = -\Delta_{x^2-y^2}\tau^1 + \Delta_{xy}\nu^3\tau^2. \quad (9.191)$$

This may be rewritten slightly and combined with the free low-energy Hamiltonian of equation (9.190) to obtain

$$\mathcal{H}_0 + \mathcal{H}_{E_2} = \hbar v_F [\nu^3\tau^1(q_x - A_{5x}\nu^3) + \nu^3\tau^2(q_y - A_{5y}\nu^3)], \quad (9.192)$$

where  $\vec{A}_5$  has been introduced as an axial gauge field. It couples to an axial gauge charge  $\nu^3$ , which can be recognized as  $\gamma^5$  when writing everything in Lorentz covariant form (see for instance [102, 206]). We thus conclude that the two density-wave partners correspond to an axial gauge field at low energies

$$(\Delta_{x^2-y^2}, \Delta_{xy}) \leftrightarrow (A_{5x}, -A_{5y}). \quad (9.193)$$

Axial gauge fields in a honeycomb lattice system have been discussed to great extent in the context of strain fields in graphene [98, 179]. In fact, recent experimental

data shows the observation of such strain engineered gauge fields in graphene-like systems [81].

Proceeding to the translational symmetry broken states, we first observe that they all couple the two valleys and will therefore correspond to Dirac matrices proportional to  $\nu^1$  or  $\nu^2$ . Let us get organized by listing all Dirac matrices of this form. They are  $\nu^1\tau^i$  and  $\nu^2\tau^i$ , where  $i = 0, 1, 2, 3$  and so includes the unit matrix  $\tau^0$ . Density wave states which break translational symmetry we found to transform as  $G' = E_1 \oplus E_2$  for site order,  $E'_1 \oplus G' = A_1 \oplus B_1 \oplus E_1 \oplus E_2$  in case of bond order and  $E'_2 = A_2 \oplus B_2$  in case of flux order. We therefore have to consider the doublets  $E'_1$  and  $E'_2$ , which are further decomposed into  $1D$  irreducible representations, and  $G'$  which consists of two  $2D$  representations.

Starting with the two doublets  $E'_1$  and  $E'_2$ , it is shown in Appendix A.3 that the two Dirac matrices  $\nu^1$  and  $\nu^2$  transform according to  $E'_1$  and the matrices  $\nu^1\tau^3$  and  $\nu^2\tau^3$  transform according to  $E'_2$ . The former are time-reversal invariant while the latter break time-reversal symmetry. In addition, in Appendix A.3 we write the explicit basis functions of the representations  $A_1$ ,  $A_2$ ,  $B_1$  and  $B_2$  contained in  $E'_1$  and  $E'_2$ . Based on this we can write down the low-energy effective mean field Hamiltonian for the  $E'_1$  states as

$$\mathcal{H}_{\text{Kekule}} = (\Delta_{A_1}^{E'_1} \cos \theta - \Delta_{B_1}^{E'_1} \sin \theta) \nu^1 + (\Delta_{A_1}^{E'_1} \sin \theta + \Delta_{B_1}^{E'_1} \cos \theta) \nu^2. \quad (9.194)$$

where  $\theta = \pi/3$ . As these terms correspond to the condensate expressions of equation (9.154), we have chosen to label the Hamiltonian  $\mathcal{H}_{\text{Kekule}}$ . Indeed, it may be simply checked that both  $\nu^1$  and  $\nu^2$  anti-commute with the Dirac matrices of equation (9.190) and therefore constitute compatible masses. The two matrices  $\nu^1\tau^3$  and  $\nu^2\tau^3$  on the other hand, do not enter as masses and do not open up a spectral gap. Instead they enter equivalently as  $\nu^3$ , shifting the Dirac nodes energetically with respect to each other.

What is left to consider is the set of Dirac matrices corresponding to the  $G'$ -symmetric density wave states. The remaining translational symmetry breaking Dirac matrices are  $\nu^1\tau^1$ ,  $\nu^2\tau^1$ ,  $\nu^1\tau^2$  and  $\nu^2\tau^2$ , which indeed transform as a quartet according to  $G'$ . The low-energy Dirac structure of  $G'$  symmetric states is most powerfully demonstrated and explained by combining all Dirac matrices, and hence density wave states, which transform as  $2D$  representations of the point group  $C_{6v}$ . We had found the doublet  $(\tau^1, \tau^2)$  to transform as  $E_2$  and together with the  $G' = E_1 \oplus E_2$  symmetric matrices we have the six terms

$$\tau^1, \tau^2, \nu^1\tau^1, \nu^2\tau^1, \nu^1\tau^2, \nu^2\tau^2. \quad (9.195)$$

A key observation is that all of these Dirac matrices can be generated by the triple  $(\nu^1, \nu^2, \nu^3)$  in the following way. The two Dirac matrices appearing in (9.190) are

$\nu^3\tau^1$  and  $\nu^3\tau^2$ . The multiplication  $\nu^3\tau^1\nu^i$  and  $\nu^3\tau^2\nu^i$  then straightforwardly give all six Dirac matrices listed here. This means for the low-energy Dirac Hamiltonian that we can write a general expression incorporating the effect of these density waves, which reads

$$\mathcal{H}(\vec{q}) = \hbar v_F [\nu^3\tau^1(q_x - A_x^i\Omega^i) + \nu^3\tau^2(q_y - A_y^i\Omega^i)]. \quad (9.196)$$

Here we have defined the three matrices  $\Omega^i \equiv \nu^i$ , which then obey the  $su(2)$  algebraic relations generating the  $SU(2)$  gauge field  $\vec{A}^i$ , i.e.  $[\Omega^i, \Omega^j] = 2i\epsilon^{ijk}\Omega^k$ . We can put this differently by saying that density waves transforming as  $E_2$  or  $G'$ , all  $2D$  irreducible representations of  $C_{6v}$ , act as components of a non-Abelian gauge field in the low-energy description of the mean field spectrum.

The equations (9.148) and (9.149) provide explicit expressions for the site ordered states transforming as  $G'$  and per the above we can conclude that they enter, together with the bond ordered state of equation (9.4.1), as the components of one non-Abelian gauge field  $\vec{A}^i$ . The identification of translational symmetry broken charge density waves as components of a gauge was already reported in [180], which highlighted the possibility of a condensed matter realization of non-Abelian gauge fields in graphene. What we have shown here is how symmetry can be used to establish which density wave states correspond to gauge field components in the low-energy description of the electronic degrees of freedom. In demonstrating this, we have used the same approach and reasoning as for the case of the square lattice in Section 9.3.2, which dealt with the Dirac theory of the  $\pi$ -flux state with  $C_{4v}$ . The key observations which hold true in both cases and are therefore independent of symmetry class (square or hexagonal), can be summed up as follows.

When the low-energy electronic spectrum exhibits symmetry protected Dirac points, then the impact of additionally induces density waves on the low-energy Dirac theory can be predicted based on the lattice symmetry breaking properties of such density waves. Density waves which are either even or odd under the rotations and reflections, i.e. transform as  $1D$  representations, will either correspond to a Dirac mass gapping out the spectrum, or lift the degeneracy between the inequivalent Dirac nodes (the valleys). Density waves which have a partner and transform together as a  $2D$  representation of the group of rotations and reflections will have the low-energy interpretation of gauge fields. Constant gauge fields merely shift the Dirac nodes away from their high symmetry mandated location, while spatially dependent gauge fields give rise to pseudo-Landau level quantization [180]. We propose that these statements have general validity, independent of lattice and symmetry class. This means that decompositions such as in equations (9.131) and (9.133) already provide quite some information on properties of the mean field spectra, without the need to calculate them. For any specific lattice one may proceed to derive the lattice symmetry

group representation on the Dirac spinor  $\hat{\Phi}$  in order to classify the fermion bilinears in terms of lattice symmetries and obtain a more detailed identification of density waves and Dirac matrices. The full potential of such a symmetry perspective will be demonstrated with the help of a specific example below when we discuss the kagome lattice.

### Low-energy description: Van Hove-singularities

The Dirac points at  $\vec{K}_{\pm}$  provide a natural low-energy setting for discussing the impact of density wave states at these ordering momenta, as they couple the two inequivalent Dirac points. For the low-energy physics to be captured by the relativistic Dirac equation, the filling needs to be appropriate, i.e. one electron per two sites in case of spinless fermions. Ordering at the  $M$  points, contrary to  $K$ -point ordering, is expected not to couple the Dirac points, but instead couple Fermi surface arcs at filling  $n = 3/8$ . At this particular filling the Fermi surface on the honeycomb lattice is a hexagon inscribed in the Brillouin zone hexagon, as shown in Fig. 9.4, and is perfectly nested by the three vectors  $\vec{Q}_{\mu}$ . The  $M$ -point vectors  $\vec{Q}_{\mu}$  are also shown in Fig. 9.4 and are explicitly given in Appendix A. Condensation at finite  $M$ -point wave vectors is therefore expected to be relevant for this filling, and possibly other commensurate fillings  $n = p/8$ . We furthermore anticipate that such  $M$ -point condensation will address the nested Fermi surface in an analogous way as  $(\pi, \pi)$  ordering in case of the nested Fermi surface of the square lattice at half filling. We recall that the two  $s$ -wave condensates, i.e. charge and spin density waves, gap out the full Fermi surface, while the two  $d$ -wave condensates gap out the Fermi surface except for isolated points in momentum space. Here we take a detailed look at how  $M$ -point condensates alter the spectrum by focussing on energies and fillings appropriate for the nested hexagonal Fermi surface. We stress that even though we present the results in the honeycomb lattice setting, they pertain to all hexagonal lattices, a point we come back to below.

Figure 9.7(a) shows the folding of the nested Fermi surface in the reduced Brillouin zone for  $M$ -point ordering. In the reduced Brillouin zone the Fermi surface consists of line segments connecting  $\Gamma$  to all  $M'$ -points of the reduced Brillouin zone. It follows from the folding that each line segment is doubly degenerate in the reduced zone. The symmetry of density wave orders will determine the way in which the Fermi surface is altered. In general we expect two scenarios in the presence of at least a three-fold symmetry  $C_3$  of the physical system. They are schematically depicted in Fig. 9.7(b). The right side shows a full lifting of the Fermi surface degeneracy at generic  $\vec{k}$ , except for the high symmetry points  $\Gamma$  and  $M'$ , which may or may not have residual degeneracies protected by symmetry. The left figure depicts the scenario of a shifting and change in shape of the degenerate arcs in momentum

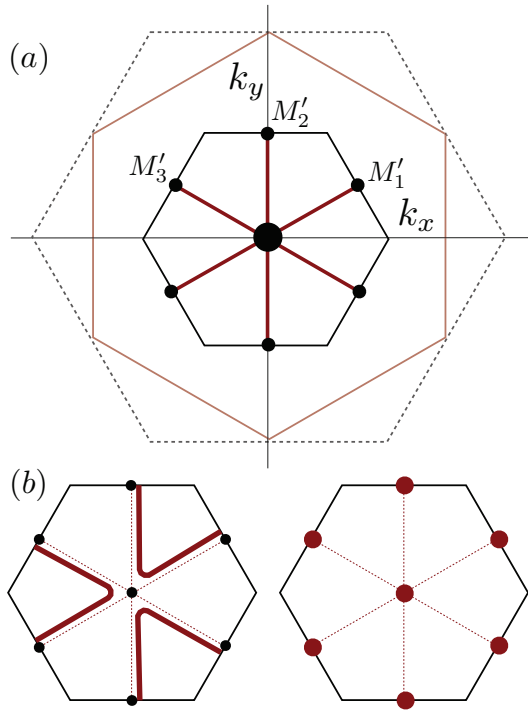


**Figure 9.7:** (Above) Folding of the Brillouin zone as a consequence of  $M$ -point order. Outer dashed transparent hexagon represents the hexagonal Brillouin zone, red transparent hexagonal is the  $M$ -point nested Fermi surface. Inner solid black hexagon is the reduced Brillouin zone and red lines in the reduced Brillouin zone represent the folded Fermi surface, which is doubly degenerate everywhere in the reduced BZ except  $\Gamma$  where it is threefold degenerate. (Below) A schematic picture of the possible effect of particle-hole condensation on the (mean field) spectrum with on the right the gapping out of the Fermi surface, i.e. lifting of the degeneracies, possibly except for high symmetry points  $\Gamma$  and  $M'$ . On the left the possible shifting of the degenerate arcs, a situation which requires the breaking of time-reversal symmetry.

space. It is clear that this is only possible when time-reversal symmetry and the six-fold rotation  $C_6$  are broken. In what follows we will focus on the first scenario as the singlet density waves we have identified so far cannot lead to the second scenario. We come back to the second scenario in the context of triplet condensates.

At the high symmetry points  $\Gamma$  and  $\vec{M}'_\mu$  degeneracies may be symmetry protected and due to this we examine these isolated points in more detail. Let us start with  $\Gamma$  and construct an 8-dimensional spinor  $\hat{\Phi}_\Gamma$  as

$$\hat{\Phi}_\Gamma = \begin{bmatrix} \hat{\psi}_j(\vec{0}) \\ \hat{\psi}_j(\vec{Q}_1) \\ \hat{\psi}_j(\vec{Q}_2) \\ \hat{\psi}_j(\vec{Q}_3) \end{bmatrix}, \quad (9.197)$$

with  $j = A, B$ . In the absence of any particle-hole condensation all point group operations  $C'''_{6v}$  are good symmetries and we can build a representation of this group by considering how the generators of  $C'''_{6v}$  act on  $\hat{\Phi}_\Gamma$ . For the translation  $T(\vec{x}_1)$  we have

$$T(\vec{x}_1) \rightarrow \begin{bmatrix} 1 & & & \\ & -1 & & \\ & & -1 & \\ & & & 1 \end{bmatrix} \hat{\Phi}_\Gamma, \quad (9.198)$$

while the six-fold rotation  $C_6$  leads to the matrix

$$C_6 \rightarrow \begin{bmatrix} \tau^1 & & & \\ & \tau^3 \tau^1 & & \\ & & \tau^3 \tau^1 & \\ & & & \tau^1 \end{bmatrix} \hat{\Phi}_\Gamma, \quad (9.199)$$

and the reflection  $\sigma_v$  gives rise to

$$\sigma_v \rightarrow \begin{bmatrix} \tau^1 & & & \\ & & & \tau^1 \\ & & \tau^1 & \\ & \tau^1 & & \end{bmatrix} \hat{\Phi}_\Gamma. \quad (9.200)$$

These operations define a reducible representation of  $C'''_{6v}$  which can be decomposed into irreducible representations as  $A_1 \oplus B_2 \oplus F_1 \oplus F_4$ . The two one-dimensional representations correspond to high energy modes coming from  $\hat{\psi}_j(\vec{0}) = \hat{\chi}_{0j}(\vec{0})$ , while the two 3D representations correspond to the folded  $M$ -points at  $\Gamma$ . The honeycomb lattice with nearest neighbor hopping only is particle-hole symmetric and a nested

Fermi surface exist both at filling  $n = 3/8$  and  $n = 5/8$ . Each of the two 3D representations corresponds to one of these fillings. The dimensionality of these two irreducible representations mandates a threefold degeneracy at  $\Gamma$ , which is just a restatement of the intuitively clear fact that energy levels at  $M$ -point in the original Brillouin zone must be degenerate for  $C_{6v}$  symmetry. When translational symmetry is broken by  $M$ -point ordering we are forced to consider the group of remaining symmetries and see how this group will affect degeneracies. If the group of remaining symmetries is  $C_{6v}$ , i.e. the density wave still has  $C_{6v}$  symmetry, we decompose  $F_1 \oplus F_4$  further into irreducible representations of  $C_{6v}$ , which we already know to result in  $A_1 \oplus B_2 \oplus E_2 \oplus E_1$ . From this we conclude that while the three-fold degeneracies in general will be lifted, two-fold degeneracies must remain at  $\Gamma$ . We can go one step further and assume an even smaller group of remaining symmetries, which is  $C_{3v}$ . There are two distinct possibilities corresponding to the two distinct sets of reflections which are part of  $C_{6v}$ . To put it differently, the particle-hole condensate lowering the symmetry down to  $C_{3v}$  may transform as  $B_1$  or  $B_2$  of  $C_{6v}$ . In case of the former, i.e.  $B_1$ , we find that  $F_1 \oplus F_4 = A_1 \oplus A_2 \oplus 2E$ , while in the latter we find that  $F_1 \oplus F_4 = 2A_1 \oplus 2E$ . Hence, even in case of  $C_{3v}$  symmetry the two-fold degeneracies are protected.

In the same way we can study the  $M'$ -points of the reduced Brillouin zone (see Fig. 9.7). The symmetry group is different from the  $\Gamma$  point, as the  $M'$ -points are left invariant only by the inversion  $C_2$  and two reflections, leading to a little group  $C_{2v}$ . The group  $C_{2v}$  only has 1D representations and therefore cannot protect degeneracies by itself. If translations are included to generate the group  $C_{2v}'''$  degeneracies are protected. Details are presented in Appendix A as they are of less significance. For our purposes at this point it is sufficient to conclude that particle-hole condensation will generally lift the  $M'$ -point degeneracy as it breaks translations.

Based on these considerations we make predictions concerning the spectral effects of particle-hole condensates with specific symmetries. For reasons of definiteness let us focus on the lower part of the honeycomb lattice spectrum, i.e. the filling  $n = 3/8$ . All condensates constructed from  $\vec{Q}_\mu$  components that transform as 1D representations of  $C_{6v}$  have  $C_{3v}$  as a remaining symmetry group, except for  $A_2$  states which we discuss separately below. Therefore, at  $\Gamma$  the three-fold degeneracy will generically be lifted and result in a non-degenerate energy level plus a two-fold level. Symmetry does not tell us a priori what the order is, i.e. whether the non-degenerate level is higher in energy or lower, but it is clear that there are only these two options. If the degenerate level is lower in energy, then for reasons of band connectivity we expect a full energy gap to develop. In contrast, if the non-degenerate level is lower in energy the existence of a Fermi surface is expected. These two different situations are graphically depicted in Fig. 9.8, where we plot the lowest four electron bands along a path in the reduced BZ for the site ordered density wave state transforming as  $A_1$

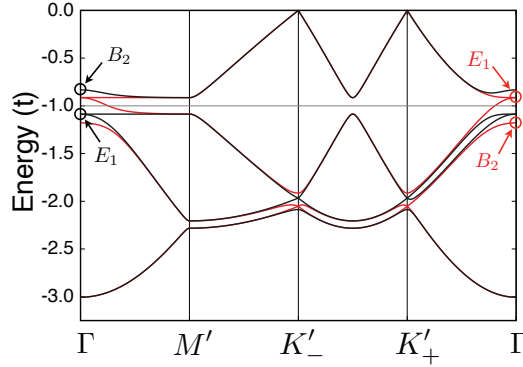


**Figure 9.8:** Folding of the Brillouin zone as a consequence of  $M$ -point order. Red lines in the reduced Brillouin zone represent the folded Fermi surface.

of equation (9.170), by way of example. Black and red spectra correspond to positive and negative sign of  $\Delta_{A_1}^{F_1}$ , respectively. At the relevant filling  $n = 3/8$  we see that the two spectra differ precisely as expected and the order in which the doublet and non-degenerate level split is apparently controlled by the sign of  $\Delta_{A_1}^{F_1}$ .

In order to gain more insight into the way particle-hole condensation affects the nested Fermi surface, effect let us take a closer look at the low energy description at  $\Gamma$ . First, we organize the components of  $\hat{\Phi}_\Gamma$  according to the triplets  $F_1$  and  $F_3$ . Using obvious notation, we find that

$$\hat{\Phi}_{F_1} = \begin{bmatrix} \hat{\chi}_{1A} - \hat{\chi}_{1B} \\ \hat{\chi}_{2A} + \hat{\chi}_{2B} \\ -\hat{\chi}_{3A} + \hat{\chi}_{3B} \end{bmatrix}, \quad \hat{\Phi}_{F_4} = \begin{bmatrix} \hat{\chi}_{1A} + \hat{\chi}_{1B} \\ \hat{\chi}_{2A} - \hat{\chi}_{2B} \\ -\hat{\chi}_{3A} - \hat{\chi}_{3B} \end{bmatrix}, \quad (9.201)$$

where  $\hat{\Phi}_{F_4}$  is relevant operator for  $n = 3/8$ , while is  $\hat{\Phi}_{F_1}$  is a basis for the three-fold degeneracy at  $n = 5/8$ . Expanding the Hamiltonian to second order in momentum and projecting into the bases  $\hat{\Phi}_{F_1}$  and  $\hat{\Phi}_{F_4}$  we obtain

$$\mathcal{H}(\vec{q}) = \pm \begin{bmatrix} -q_1 q_3 & & \\ & -q_2 q_1 & \\ & & -q_3 q_2 \end{bmatrix}, \quad (9.202)$$

where  $+$  ( $-$ ) refer to  $F_1$  ( $F_4$ ). We continue to rewrite the basis states  $\hat{\Phi}_F \equiv [\hat{\Phi}_1, \hat{\Phi}_2, \hat{\Phi}_3]^T$  in such way that they will be the proper basis states of the representations  $A_{1/2}$  and

$E$  of  $C_{3v}$ . This gives the generic states

$$\hat{\Phi}_A = \frac{1}{\sqrt{3}}(\hat{\Phi}_1 + \hat{\Phi}_2 + \hat{\Phi}_3) \quad (9.203)$$

$$\hat{\Phi}_E = \begin{cases} \frac{1}{\sqrt{6}}(\hat{\Phi}_1 + \hat{\Phi}_2 - 2\hat{\Phi}_3) \\ \frac{1}{\sqrt{2}}(-\hat{\Phi}_1 + \hat{\Phi}_2) \end{cases}. \quad (9.204)$$

Writing the Hamiltonian of equation (9.202) in this basis we obtain the diagonal blocks  $\mathcal{H}_A(\vec{q})$ , which is given by

$$\mathcal{H}_A(\vec{q}) = \mp(q_1q_3 + q_2q_1 + q_3q_2)/3, \quad (9.205)$$

and  $\mathcal{H}_E(\vec{q})$  which after implementing a unitary transformation is given by

$$\mathcal{H}_E(\vec{q}) = \pm \frac{1}{4}q^2 \pm \frac{1}{4}[(q_x^2 - q_y^2)\tau^3 + 2q_xq_y\tau^1] \quad (9.206)$$

Note that the blocks coupling these two sectors do not vanish. The clear advantage of the present basis is revealed when expressing the possible spectral impact of general density wave states. For all density wave states that have at least  $C_{3v}$  symmetry, the allowed term in the low-energy Hamiltonian at  $\Gamma$  reads

$$\mathcal{H} = \begin{bmatrix} \Delta_A & & \\ & \Delta_E & \\ & & \Delta_E \end{bmatrix}. \quad (9.207)$$

It is the sign of  $\Delta_A - \Delta_E$  that determines whether or not a gap will open up. At the filling  $n = 3/8$  a gap opens up if  $\Delta_A - \Delta_E > 0$ , while it is the other way around at  $n = 5/8$ .

Armed with this general framework we are in a position to take a specific look at the density wave states that were derived in the previous section. Starting with site ordered states, we recall that there are two states with  $\vec{Q}_\mu$  components which have residual  $C_{3v}$  symmetry. These are states transforming as  $A_1$  and  $B_2$ , both given in equation (9.170). The lower part of the spectrum of the  $A_1$  is presented in Fig. 9.8 and we have already pointed out the significance of the sign of the density wave strength  $\Delta_{A_1}^{F_1}$ . We note here that the situation is exactly opposite for  $n = 5/8$  to the one at  $n = 3/8$ . When a gap is opened up at  $n = 3/8$ , then a degeneracy remains at  $n = 5/8$  originating from the fact that the energetic order of the non-degenerate level and the degenerate levels is the same for both fillings. The  $B_2$  state exhibits a threefold degeneracy at  $\Gamma$ , both at  $n = 3/8$  and  $n = 5/8$ , and this is a purely accidental fact. The degeneracy is not symmetry protected. Apart from this degeneracy at  $\Gamma$ , the Fermi surface is completely gapped out.

Coming back again to the  $A_1$  site ordered state and restricting ourselves to  $n = 3/8$ , we notice that in case of  $\Delta_A - \Delta_E < 0$  the description of low-energy excitations close to  $\Gamma$  is fully governed by the Hamiltonian  $\mathcal{H}_E(\vec{q})$ , which we recognize to have the generic structure of a quadratic band crossing (QBC) Hamiltonian. The emergence of such a QBC point in the context of  $M$ -point ordering was first noticed in Ref. [163], which derived the QBC Hamiltonian for uniaxial spin density wave with  $\vec{Q}_\mu$ -vector modulations. In the present case we have established the existence of a QBC purely based on symmetry arguments and the particular case of the uniaxial spin density wave follows from these more general arguments. Indeed, even though we have assumed the absence of any structure in spin space so far, the result of Ref. [163] is readily understood based on the present discussion. The uniaxial spin density wave of [163] and [160, 162] can be thought of as two copies of the  $A_1$  site order state, one for each spin species with opposite sign. Hence, the spectrum is precisely that shown Fig. 9.8, where the colors can be interpreted as spin up and spin down bands. We have shown that the QBC point arising from particle-hole condensation is protected by the residual  $C_{3v}$  symmetry, which in case of the uniaxial spin density wave may be considered to apply to each species separately. In Section 10 we will discuss the symmetries of spin triplet condensates in more detail in the context of  $M$ -point order on the triangular lattice. Here we just conclude that in the spinless case the only option apart from the appearance of a full spectral gap, is the emergence of a QBC point in the low energy description of the  $M$ -point.

We have obtained three bond ordered states with residual  $C_{3v}$  symmetry, an  $A_1$ ,  $B_1$  and  $B_2$  state, originating from the triplets  $F_1$ ,  $F_3$  and  $F_4$ , and collectively represented in equation (9.185). Per the above, we can ask a simple question to find out what the spectral effects of these density waves are. What is the sign of  $\Delta_A - \Delta_E$ ? We find the remarkable result that for both  $B_1$  and  $B_2$  symmetric bond density waves the non-degenerate level is higher in energy than the degenerate doublet at  $n = 3/8$  (and vice versa for  $n = 5/8$ ), amounting to the opening of a full energy gap. For these two states this is independent of the sign of  $\Delta_{B_1}^{F_3}$  or  $\Delta_{B_2}^{F_4}$  and as a result the situation of a QBC point does not occur. Even the simple triplet version of these bond density waves, which is just two copies of the density wave state for each spin species but with opposite sign, is gapped due to the sign independence. In addition, we can argue that the spectral gaps caused by these distinct density waves are compatible, in the sense that if a density wave develops which is an arbitrary combination of these states, the total energy gap is always larger than the individual gaps. This follows in part from the fact that to lowest order, the structure of the low-energy Hamiltonian at  $\Gamma$  associated to the density waves, is given by equation (9.207), in a basis which is valid for all three density waves. Since we find that both these bond orders have the same order of energy levels, the values of  $\Delta_A - \Delta_E$  simply add. We find the same to be true at the  $M'$ -points, which indeed shows that the gaps are compatible. In case

of the  $A_1$  bond density wave both situations  $\Delta_A - \Delta_E > 0$  and  $\Delta_A - \Delta_E < 0$  can occur, depending on the sign of  $\Delta_{A_1}^{F_1}$ . It is therefore not necessarily compatible with the  $B_1$  and  $B_2$  induced gaps, but instead, its spectral impact is equivalent with the site ordered  $A_1$  state. In particular, creating a uniaxial spin-bond ordered state out of the  $A_1$  state results in a QBC point for one spin species and gapped excitations for the other.

Up to this point the emphasis has been on the assumption of residual  $C_{3v}$  symmetry, which holds for the states we have considered to far. We have not treated the case of  $C_6$  symmetry (representation  $A_2$ ), or the doublet states contained in the  $F$  representations of  $C_{6v}'''$ . If only  $C_6$  rotational symmetry is left no degeneracies can be symmetry protected as Abelian groups such as  $C_6$  have only  $1D$  representations. We had derived one density wave with  $C_6$  symmetry, given in equation (9.186). Indeed, the mean field spectrum of this density wave does not show any degeneracies at  $\Gamma$  or  $M'$ . Following equation (9.186) it was already noted that the spectrum is fully gapped, with nontrivial topological ground state. Insofar as the doublets are concerned the remaining symmetry is at most  $C_{2v}$ , which cannot lead to any symmetry protection of degeneracies either. An interesting common property of all doublet states we have verified, is that none of them lead to an immediate opening of a mean field spectral gap. Instead, we find that doublet states transforming as partners of  $E_1$  or  $E_2$  all have a mean field spectrum with a remaining Fermi surface at the van Hove filling for weakly developed density waves.

We conclude this discussion of the spectral effects of  $M$ -point modulated density waves at the Van Hove filling, by stressing the general validity and applicability of the results presented here. The dispersion of electrons hopping on the triangular or kagome lattices, two other ubiquitous examples of lattices with hexagonal symmetry, exhibits the same Fermi surface with Van Hove singularities for appropriate fillings as the honeycomb lattice. The  $\vec{Q}_\mu$  vectors again connect arcs of the Fermi surface and  $M$ -point order is therefore expected to alter the spectrum in similar ways as outlined above. In order to gain deeper insight into the general, i.e. lattice independent, features of  $M$ -point order, we review a number of observations detailed above which hold true for the triangular and kagome lattice as well.

Based on the example of the honeycomb lattice, we showed that in the absence of translational symmetry (extended point group elements  $T(\vec{x}_1)$  and  $T(\vec{x}_2)$  are broken) the two-fold degeneracy at the  $M'$ -points and the threefold degeneracy at  $\Gamma$  are generally lifted. This statement only relies on symmetry, as it follows from the dimensionality of irreducible representations, and therefore directly applies to other lattices with hexagonal symmetry. In particular, by focusing on the  $\Gamma$  point, we have demonstrated that in the presence of at least  $C_{3v}$  symmetry, a two-fold degeneracy at  $\Gamma$  is protected. For any of the lattices with hexagonal symmetry the Van Hove singularities are located at  $\Gamma$  of the reduced Brillouin zone and the state vectors corresponding

to this subspace can be denoted as  $\hat{\Phi}_F \equiv [\hat{\Phi}_1, \hat{\Phi}_2, \hat{\Phi}_3]^T$ . Full symmetry makes these three states partners of a  $3D$  representations causing the three-fold degeneracy. Lowering the symmetry down to  $C_{3v}$  lifts this degeneracy to a  $2 + 1$  degeneracy, with corresponding states given by equation (9.203). The low-energy theory in terms of these basis states takes the generic form presented in equations (9.205) and (9.206), meaning in particular that all  $C_{3v}$  symmetric density waves will enter as (9.207). The sign of  $\Delta_A - \Delta_E$  will then determine whether a full gap exists or the low-energy theory is captured by a QBC theory. Hence, many of the spectral effects and effective low-energy descriptions of electronic degrees of freedom in the presence of density wave states are very general. We will come to this briefly in Section 9.4.3) when focusing on the triangular lattice. It should be stressed though that these considerations are based on symmetry. There may be accidental degeneracies at  $\Gamma$  or even  $M'$  in addition to the degeneracies required by symmetry.

### 9.4.2 Kagome lattice

After this long and detailed discussion of honeycomb lattice density waves, we focus attention on the second example of a well-known lattice with hexagonal symmetry, the kagome lattice. The kagome lattice has three inequivalent sites in its unit cell, instead of two in case of the honeycomb lattice, which leads to more possibilities for both site and bond ordered states. The specific aim of this section is not only to provide the symmetry-based framework for classifying kagome lattice density waves, but also to highlight the utility and power of the lattice symmetry perspective. The insight into the strong link between organizing density waves as basis functions of irreducible representations and physical electronic properties of these condensates, gained both from the the square lattice and honeycomb lattice cases, will be applied to the kagome lattice. Therefore, the structure of this kagome lattice section will be as follows. We start by listing the decompositions of site, bond and flux order in the same way as for the square and honeycomb lattices, and both for  $K$ -point ordering and  $M$ -point ordering. Then we briefly discuss the prominent features of the free kagome lattice spectrum which make the kagome lattice a desirable object of study. These are the presence of Dirac fermions at the touching of the lowest two bands, a QBC point at the touching between the upper two bands, and van Hove singularities in combination with a nested Fermi surface in each of the lower two bands. Armed with the decompositions of site, bond and flux order we can make predictions concerning the mean field spectral effects of the condensates. Before we then come to a more elaborate discussion of translationally invariant order, i.e.  $K$ -point order, and  $M$ -point orderings, we introduce the sublattice functions, i.e. the kagome lattice equivalents of the Pauli matrices  $\tau^i$ , and show how their transformation properties can be used to straightforwardly write down explicit condensate functions corresponding to the

irreducible representations obtained from group theory. The more detailed discussion of density waves, the construction of their explicit expression and electronic properties is divided into two parts. The first part deals with translationally invariant and  $K$ -point ordered density waves, as both of these classes affect the low-energy physics at the Dirac points, while the second part will deal with  $M$ -point ordering relevant for Fermi surface instabilities at van Hove fillings. In both of these parts we will not attempt an exhaustive characterization of all density waves, but instead limit ourselves to interesting examples. In case of the honeycomb lattice we have discussed the mean field spectrum of the density waves in a separate section. Here we integrate this part into the discussion of the density waves, their explicit form and their characteristics.

Following the same group theoretical recipe that was used for the honeycomb lattice, details of which are presented in Appendix C, we find the irreducible representations of the extended groups  $C''_{6v}$  and  $C'''_{6v}$  present in the decompositions of site, bond and flux order representations. The decomposition for kagome lattice site order with  $K$ -point ordering vectors is given by

$$\mathcal{P}_s^K = A_1 \oplus E_2 \oplus E'_1 \oplus G' \quad (9.208)$$

whereas we have for  $M$ -point ordering

$$\mathcal{P}_s^M = A_1 \oplus E_2 \oplus F_1 \oplus F_3 \oplus F_4. \quad (9.209)$$

The translationally invariant content of these two decompositions is  $A_1 \oplus E_2$ , which shows that in addition to the trivial  $A_1$  state there is a translationally invariant site order doublet. For  $K$ -point order the translational symmetry broken states transform as  $E'_1 \oplus G'$ , which differs from the honeycomb lattice decomposition [equation (9.131)] in the presence of  $E'_1$  states. Both the  $K$ -point and  $M$ -point site order decompositions are seen to be identical to the honeycomb lattice bond order decompositions, i.e. equations (9.133) and (9.134), which is a consequence of the kagome lattice being the line graph of the honeycomb lattice.

Moving on to bond order decompositions, we find that  $K$ -point order can be broken up into the following representations,

$$\mathcal{P}_b^K = A_1 \oplus B_2 \oplus E_1 \oplus E_2 \oplus E'_1 \oplus E'_2 \oplus 2G', \quad (9.210)$$

while the  $M$ -point order decomposition reads

$$\mathcal{P}_b^M = A_1 \oplus B_2 \oplus E_1 \oplus E_2 \oplus 2F_1 \oplus F_2 \oplus F_3 \oplus 2F_4. \quad (9.211)$$

The translationally invariant part of the decomposition, i.e.  $A_1 \oplus B_2 \oplus E_1 \oplus E_2$ , tells us that there is a  $1D$  representation present, in addition to the fully symmetric  $A_1$  state. We come back to these decompositions below, after we have briefly introduced

the low-energy physics corresponding to electron filling fractions where these density waves are expected to have significant impact.

The third type of order, flux order, leads to the following decomposition for translational symmetry breaking at  $K$

$$\mathcal{P}_\phi^K = 2A_2 \oplus B_1 \oplus E'_2 \oplus G', \quad (9.212)$$

and for translational symmetry breaking at  $M$ -points one finds

$$\mathcal{P}_\phi^M = 2A_2 \oplus B_1 \oplus 2F_2 \oplus F_3. \quad (9.213)$$

Contrary to all the other examples of flux order decompositions we have seen so far, the translationally invariant part contains the representation  $A_2$  twice. This suggests the possibility of a realizing a density wave state breaks both time-reversal symmetry and all reflections, while at the same time leading to a flux pattern that averages to zero over the unit cell and corresponding to an insulating QAH state. The existence of such a state has in fact been known for some time [85], and here we see why it is particular to the kagome lattice. In addition to this QAH state, symmetry-based flux order decompositions teach us there are translational symmetry broken candidates for such insulators, which are contained in  $E'_2 = A_2 \oplus B_2$  ( $K$ ) and  $F_2 = A_2 \oplus E_2$  ( $M$ ). From the symmetry of these density waves we can actually make more precise statements concerning their characteristics as we now proceed to argue in the context of low-energy spectral effects.

In case of the kagome lattice there are a number of interesting electron fillings worth considering, reflecting the spectral features of electrons hopping in the kagome lattice. For the filling  $n = 1/3$  the Fermi surface consists of isolated points, i.e. Dirac points, which are located at the vertices of the Brillouin in the same way as for the honeycomb lattice. Therefore, in much the same way we can expand the spectrum around these Dirac points to obtain an effective Dirac theory capturing the electronic properties at low energies. The only technical difference is the fact that at both  $\vec{K}_\pm$  one has to project the three-component eigenstates into the subspace corresponding to the Dirac nodes. If we label the set of states spanning the space of the Dirac nodes as  $|+, j\rangle$  and  $|-, j\rangle$  ( $j = 1, 2$ ) for  $\vec{K}_+$  and  $\vec{K}_-$ , respectively, then we derive a Dirac Hamiltonian which has exactly the same structure as for the honeycomb lattice (details in Appendix A.4),

$$\mathcal{H}(\vec{q}) = \hbar v_F \nu^3 \vec{q} \cdot \vec{\tau}, \quad (9.214)$$

[compare also equation (9.190)] where here we have  $\sqrt{3}at/\hbar$ . The Dirac spinor is

given by

$$\hat{\Phi}(\vec{q}) = \begin{bmatrix} \hat{\psi}_1(\vec{K}_+ + \vec{q}) \\ \hat{\psi}_2(\vec{K}_+ + \vec{q}) \\ \hat{\psi}_1(\vec{K}_- + \vec{q}) \\ \hat{\psi}_2(\vec{K}_- + \vec{q}) \end{bmatrix}. \quad (9.215)$$

As the structure is indeed equal to the honeycomb lattice Dirac theory, we can borrow the interpretation of Dirac matrices  $\nu^i \tau^j$  from Section 9.4.1, where it should be understood that the  $\nu^i$  act on the valley degree of freedom, i.e.  $\pm$ , and  $\tau^j$  on the effective sublattice degree of freedom labeled by  $j = 1, 2$ . For instance, we directly conclude that the Dirac matrices  $\nu^3 \tau^3$ ,  $\nu^1$  and  $\nu^2$  constitute the compatible Dirac masses, while  $\nu^1 \tau^3$  and  $\nu^2 \tau^3$  make the two valleys inequivalent by separating the two nodes in energy.

Can the symmetry decompositions of equations (9.208), (9.210) and (9.212) assist us in assigning the density waves to the Dirac matrices describing their effect at the Dirac nodes? The answer to this question is yes. Let us look at site order and take the states  $E'_1 = A_1 \oplus B_1$  as an example. These can be written as basis functions of 1D representations of the bare point group  $C_{6v}$  and according to our proposition they must therefore couple to mass matrices. Indeed, as site order does not break time-reversal symmetry, valley mass terms must be excluded. As is detailed in Appendix A.4, an organization of the Dirac masses in terms of lattice symmetries indeed establishes the Dirac masses  $\nu^1$  and  $\nu^2$  as terms coupling to  $E'_1 = A_1 \oplus B_1$ . This immediately implies the same interpretation of the bond density waves transforming as  $E'_1$ . Furthermore, there is a bond density wave which does not break translational symmetry and transforms as  $B_2$ . We can directly assign it the same character as the honeycomb lattice site order state with that same symmetry, i.e. the third Dirac mass. Another assignment that is easy to make in light of the symmetry perspective, is that of the translationally invariant site order doublet  $E_2$  as a gauge field component. Some of these states have been found and discussed in mean field treatments or related studies [169, 170, 207]. The symmetry perspective adopted here provides a complete classification of density waves and their mean field spectral effects in the context of a Dirac theory.

Apart from Dirac nodes at filling  $n = 1/3$  the kagome lattice spectrum exhibits two other types of spectral regimes which we have already encountered in this study. At filling  $n = 2/3$ , when two of the three bands are filled, the second filled band and the upper empty touch at the  $\Gamma$  point, making this degeneracy point a QBC. Even though this is an interesting property of the kagome lattice, as all the generic and peculiar features of a QBC apply directly, we will not address this point in more detail for the kagome lattice. Instead, we will be interested in the other special fillings

fractions, i.e.  $n = 3/12$  and  $n = 5/12$ , which are the van Hove fillings of the kagome band structure. At these van Hove points the Fermi surface is shape-equivalent to the Fermi surface of the honeycomb and triangular lattice for corresponding fillings, meaning a hexagon nested by the three inequivalent  $M$ -point vectors.

Before we zoom in on the specific density waves both at  $K$ -points and at  $M$ -points and explain how to obtain explicit expressions using symmetry, it will be helpful to take a look at the kagome generalizations of the Pauli matrices, i.e. matrices which encode the sublattice structure of the lattice. For any lattice with two sublattices the Pauli matrices (in this work we consistently use the set  $\tau^i$ ) form a set of functions which transform as irreducible representations of the point group. In case of the kagome lattice, which has three sublattices, the appropriate set of functions is the collection of Gell-Mann matrices. The latter span the space of  $3 \times 3$  Hermitian matrices and are listed in Appendix A.4. We have organized them in three distinct sets, i.e.  $\vec{\Lambda}_a$ ,  $\vec{\Lambda}_b$ , and  $\vec{\Lambda}_c$ . The first two sets only have off-diagonal elements and therefore connect two sites, making them bond order functions. The set  $\vec{\Lambda}_a$  is real while  $\vec{\Lambda}_b$  is imaginary, meaning that the former preserves and the latter breaks time-reversal symmetry. The third set collects matrices with diagonal entries only and therefore pertains to site order. We can extract the irreducible representations of the point group  $C_{6v}$  contained in these three sets and with this information one can straightforwardly write down condensate function, which will be demonstrated in the next subsection.

We use the set  $\vec{\Lambda}_a$  as example. Using equation 9.6, in particular the matrices  $U_R^{\text{sl}}$  ( $R$  being an element of the point group), we can derive how the  $\vec{\Lambda}_a$  transform under point group operations. In the present case of the kagome lattice, the matrices  $U_R^{\text{sl}}$  are generated by the two permutations  $X$  and  $Y$  as defined in equations (9.160) and (9.160). Take the six-fold rotation  $C_6$  for instance. It corresponds to  $U_{C_6}^{\text{sl}} = X$  and we therefore have

$$U_{C_6}^{\text{sl}\dagger} \Lambda_{1a} U_{C_6}^{\text{sl}} = X^T \Lambda_{1a} X = \Lambda_{3a}, \quad (9.216)$$

and similarly we find for the other  $\Lambda_a$  that  $\Lambda_{2a} \rightarrow \Lambda_{1a}$  and  $\Lambda_{3a} \rightarrow \Lambda_{2a}$ . This can be summarized as

$$C_6 \rightarrow X \vec{\Lambda}_a. \quad (9.217)$$

We can proceed in this way to find the representation of  $C_{6v}$  acting on  $\vec{\Lambda}_a$ , which for definiteness we write as  $\mathcal{P}_a$ . It is then a simple matter to decompose  $\mathcal{P}_a$  into irreducible representations and one finds  $\mathcal{P}_a = A_1 \oplus E_2$ , which does not surprise given the translationally invariant content of the bond order decompositions. Repeating the same calculation for the representation  $\mathcal{P}_b$  acting on  $\vec{\Lambda}_b$  we find that  $\mathcal{P}_a = A_2 \oplus E_2$ . Similarly we find  $\vec{\Lambda}_c$  to transform according to  $E_2$ .

We are now in the possession necessary ingredients to find and characterize the kagome lattice density waves and we will do so in the next two sections. Instead of aiming for a complete listing of all density obtained from group theory, we will focus on the most illustrative cases in order to demonstrate the utility and relevance of the symmetry-based organization.

### Density waves at $\Gamma$ and $\vec{K}_\pm$

Consider first the site ordered doublet  $E_2$  of equation (9.208) representing a translationally invariant state. Since it transforms as  $E_2$  it is  $d$ -wave-like. We have seen that there is precisely such a doublet among the sublattice matrix functions, given by  $\vec{\Lambda}_c$ , and as these are the only functions corresponding to site order, we can directly use them to write down the condensate functions

$$\begin{aligned}\langle \hat{\psi}_{i\sigma}^\dagger(\vec{k}) \hat{\psi}_{j\sigma'}(\vec{k}) \rangle &= \Delta_{x^2-y^2} [\Lambda_{1c}]_{ij} \delta_{\sigma\sigma'} \\ \langle \hat{\psi}_{i\sigma}^\dagger(\vec{k}) \hat{\psi}_{j\sigma'}(\vec{k}) \rangle &= \Delta_{xy} [\Lambda_{2c}]_{ij} \delta_{\sigma\sigma'}.\end{aligned}\quad (9.218)$$

As a density wave doublet, which does not couple the low-energy Dirac nodes, we expect the presence of these condensates to alter the mean field spectrum at the Dirac points as an effective axial gauge field. This is analogous to the bond order  $E_2$  doublet of the honeycomb lattice. Indeed, such site ordered states we indeed found to have the interpretation of an axial gauge field at low energies [169, 207], and in the chiral representation chosen here (just as for the honeycomb lattice) the Dirac matrices are  $\tau^1$  and  $\tau^2$ .

There is one bond ordered state and one flux ordered state we wish to mention explicitly here. Both transform as  $1D$  representations, do not break translational symmetry, and both are obtained from the sublattice functions  $\vec{\Lambda}_b$  which break time-reversal symmetry. For bond order these sublattice should acquire a momentum dependence and for each functions we are naturally presented two choices, i.e.  $\cos k_i$  and  $\sin k_i$ , where  $k_i = \vec{\delta}_i \cdot \vec{k}$  with  $\vec{\delta}_i$  the nearest neighbor vectors defined in Appendix A.4. It is important to note here that the use of the sine and cosine functions imply the standard tight-binding gauge, which we have avoided consistently throughout this paper. In this particular case we temporarily adopt this gauge as it makes the presentation a great deal more transparent. For instance, it easy to convince oneself that the cosine functions,  $\cos k_i$ , transform into each other under point group operations and are always even. The sine functions on the other hand,  $\sin k_i$  transform into each as well, but acquire a minus sign for the six-fold rotations the reflection  $\sigma_d$  (and its threefold equivalents). We can exploit this to construct combinations of sublattice and orbital momentum functions which yield the condensate functions of

desired symmetry. As an example consider the combination

$$\sin k_1 \Lambda_{1b} + \sin k_2 \Lambda_{2b} + \sin k_3 \Lambda_{3b}. \quad (9.219)$$

It is a symmetric superposition of  $\Lambda_b$  matrices and therefore its basic symmetry is  $A_2$ , as the decomposition of  $\mathcal{P}_b$  shows. However, the sine functions provide additional minus signs for all the elements which are odd under  $B_1$ . This leads to an overall symmetry of  $\sim B_1 \otimes A_2 = B_2$ , and we have consequently identified the  $B_2$  bond order state. Note that the sine functions compensate the oddness of  $\vec{\Lambda}_b$  under time-reversal. Physically this density wave corresponds to alternating bond modulations. Depending on the strength of the density wave, the order parameter  $\Delta_{B_2}$ , the up triangles acquire stronger (weaker) bonds while the down triangles have weaker (stronger) bonds.

In contrast, the cosine functions preserve time reversal and are even under all point group operations (they do of course transform into each other). Hence, forming an analogous combination with the  $\cos k_i$  one obtains

$$\cos k_1 \Lambda_{1b} + \cos k_2 \Lambda_{2b} + \cos k_3 \Lambda_{3b}, \quad (9.220)$$

which inherits all its symmetry from the  $\vec{\Lambda}_b$  set, i.e. it transforms as  $A_2$ . We have therefore identified the time-reversal breaking  $A_2$  flux ordered state.

For completeness we write down the full condensate functions for both density wave states,

$$\begin{aligned} \langle \hat{\psi}_{i\sigma}^\dagger(\vec{k}) \hat{\psi}_{j\sigma'}(\vec{k}) \rangle &= \Delta_{B_2} \left( \sum_n \sin k_n \Lambda_{nb} \right)_{ij} \delta_{\sigma\sigma'} \\ \langle \hat{\psi}_{i\sigma}^\dagger(\vec{k}) \hat{\psi}_{j\sigma'}(\vec{k}) \rangle &= \Delta_{A_2} \left( \sum_n \cos k_n \Lambda_{nb} \right)_{ij} \delta_{\sigma\sigma'}. \end{aligned} \quad (9.221)$$

We had already identified the  $B_2$  state as a Dirac mass, i.e. the  $\tau^3 \tau^3$  matrix, and based on symmetry it is a rather simple matter to identify the  $A_2$  state with the time-reversal breaking mass  $\tau^3$ , sometimes known as Haldane mass.

Let us now consider translational symmetry broken density waves with  $K$ -point ordering vectors. Here we will limit ourselves to site ordered states as they provide particularly nice examples of the way in which symmetry arguments can be employed to find explicit expressions for density waves.

Consider first the site ordered doublet  $E'_1$ . We know from the honeycomb lattice that this representation can be further decomposed as  $E'_1 = A_1 \oplus B_1$ , meaning that it contains two states transforming as  $1D$  representations of the bare point group. All  $1D$  representations of the hexagonal point group preserve the threefold rotation  $C_3$  and, in addition, the ordering vectors  $\vec{K}_\pm$  are invariant under the threefold rotations.

This motivates the definition of a vector of phase factors, which was already encountered in equation (9.158), in order to describe the translational symmetry breaking at  $K$ . Such a vector of phase vectors is given by

$$\vec{d} = \begin{bmatrix} d_1 \\ d_2 \end{bmatrix} = \frac{1}{\sqrt{2}} \begin{bmatrix} \frac{1}{\sqrt{3}}(\omega + \omega^{-1} - 2) \\ \omega - \omega^{-1} \end{bmatrix} \quad (9.222)$$

Here the cubic roots of unity,  $\omega$ ,  $\omega^{-1}$  and 1 come from the Fourier transform of the real space cosine functions  $\cos(\vec{K} \cdot \vec{x} + j\vartheta)$  which modulate the site order. The key point to stress here is that the vector  $\vec{d}$  can be thought of as (i) encoding the  $K$ -point modulations, and (ii) to transform as the  $2D$  representation  $E$  of the group  $C_{3v}$ , which is the group that leaves unit cells invariant. At the same time, the sublattice matrices  $\vec{\Lambda}_c$  transform as  $E$  as well. This allows for a rather elegant derivation of condensate functions. It is clear that in order to write down these functions we need a sublattice part (the  $\vec{\Lambda}_c$  matrices) and a translational symmetry breaking part (the vector  $\vec{d}$ ). Both transform as  $E$  and therefore products of them will transform as  $E \otimes E = A_1 \oplus A_2 \oplus E$ . The  $1D$  representations  $A_1 \oplus A_2$  correspond to the  $A_1 \oplus B_1$  representations of  $C_{6v}$  that are contained in  $E'_1$ . Using standard recipes from group theory designed to obtain basis functions of tensor product representations, we find straightforwardly

$$\begin{aligned} A_1, A_1 &\sim d_1 \Lambda_{1c} + d_2 \Lambda_{2c} \\ A_2, B_1 &\sim d_1 \Lambda_{2c} - d_2 \Lambda_{1c}. \end{aligned} \quad (9.223)$$

These expressions are all we need as ingredients for the condensate functions belonging to the doublet  $E'_1$ . They take the form

$$\begin{aligned} \langle \hat{\psi}_{i\sigma}^\dagger(\vec{k} + \vec{K}_\pm) \hat{\psi}_{j\sigma'}(\vec{k}) \rangle &= \Delta_{A_1} (d_1 \Lambda_{1c} \pm d_2 \Lambda_{2c})_{ij} \delta_{\sigma\sigma'} \\ \langle \hat{\psi}_{i\sigma}^\dagger(\vec{k} + \vec{K}_\pm) \hat{\psi}_{j\sigma'}(\vec{k}) \rangle &= \Delta_{B_1} (d_1 \Lambda_{2c} \mp d_2 \Lambda_{1c})_{ij} \delta_{\sigma\sigma'}. \end{aligned} \quad (9.224)$$

Note that  $\langle \hat{\psi}_{i\sigma}^\dagger(\vec{k} + \vec{K}_+) \hat{\psi}_{j\sigma'}(\vec{k}) \rangle$  is related to  $\langle \hat{\psi}_{i\sigma}^\dagger(\vec{k} + \vec{K}_-) \hat{\psi}_{j\sigma'}(\vec{k}) \rangle$  by complex conjugation and therefore these are not independent.

These two charge density waves modulated by  $K$ -point vectors are the kagome lattice equivalents of the honeycomb lattice Kekule bond ordered states. They share the same symmetry and consequently they also have the same impact on the low-energy electrons. Indeed, as we already mentioned, they correspond to the compatible Dirac masses  $\nu^1$  and  $\nu^2$ . In fact, these site ordered states have been found in a mean field study of the kagome lattice where the band structure was doped to the Dirac points [169]. Based on symmetry grounds we concluded that there is an equivalent correspondence between the bond ordered states with  $E'_1$  symmetry and

the Kekule bond density waves of the honeycomb lattice. For both these types of density waves we therefore expect the same intriguing physics to be possible as for the Kekule distortions. Most notably, topological defects in the order parameter of the two compatible mass states should come with fractionally charged excitations and anyonic statistics.

In case of the honeycomb lattice we had found the translational symmetry broken site ordered states to correspond to low-energy gauge fields. This originated from their point group representation, which we found to be  $G' = E_1 \oplus E_2$ . Site ordered states of the same symmetry exist for the kagome lattice, as equation (9.208) shows, and they have the same low-energy interpretation. All charge density waves on the kagome lattice constituting doublets, i.e.  $E_2 \oplus G'$ , are components of a non-Abelian  $SU(2)$  gauge field within the low-energy Dirac theory. The translationally invariant states we already identified and it is straightforward to find the other two doublets. Actually, one of them we already obtained when decomposing the products of  $\vec{d}$  and  $\vec{\Lambda}$  into  $E \otimes E = A_1 \oplus A_2 \oplus E$ . The doublet on the right hand side is one of the gauge field components. Using the same group theory recipe the condensate functions of the doublet are spanned by

$$E \sim \begin{cases} d_1\Lambda_{1c} - d_2\Lambda_{2c} \\ d_1\Lambda_{2c} + d_2\Lambda_{1c} \end{cases} \quad (9.225)$$

### Translationally symmetry breaking at $\vec{Q}_\mu$

Let us finally come to the  $M$ -point ordered density waves, which are composed of the ordering vectors  $\vec{Q}_\mu$  pictorially shown in Fig. 9.4 and specified for the kagome lattice in Appendix A.4. We will discuss the site ordered, bond ordered and flux ordered states of equations (9.209), (9.211) and (9.213), but instead of presenting the derivation of explicit based on the real space formalism laid out in Section 9.4.1, we will show these density waves graphically and analyse their mean field spectral characteristics based on symmetry. In the same way as for  $K$ -point order this will serve to illustrate that obtaining information on electronic properties is intimately related to knowing the symmetry of a density wave state.

As was highlighted in Section 9.4.1, the honeycomb lattice has been presented as a study case for both  $K$ -point and  $M$ -point order, but the general conclusions apply to all hexagonal lattices. In particular, the low-energy description of electronic degrees of freedom at the  $M$ -points given in Section 9.4.1 is valid for the kagome lattice as well. The kagome lattice has two van Hove fillings corresponding to the saddle points of band structure with a Fermi surface looking exactly like Fig. 9.7. These fillings are given by  $n = 3/12$  and  $n = 5/12$ . In the same way as for the honeycomb lattice we can project into the low-energy subspace at  $\Gamma$  by choosing

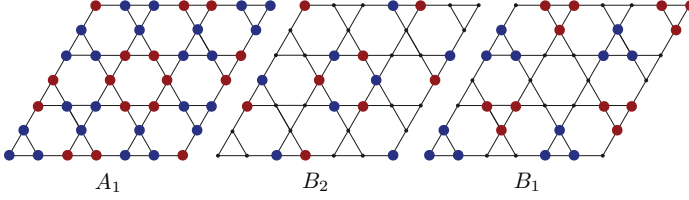


**Figure 9.9:** Graphical representation of kagome lattice site order with  $M$ -point ordering vectors. (upper left) the  $A_1$  state, (upper right) the  $B_2$  state and (below) the  $B_1$  state.

state vectors that transform according to the  $3D$  representations  $F_j$ . This yields the generic basis states  $\hat{\Phi}_F \equiv [\hat{\Phi}_1, \hat{\Phi}_2, \hat{\Phi}_3]^T$ , the explicit form of which in terms of  $\hat{\chi}_{\mu j}$  depends on the lattice and the specific van Hove filling. We can always perform a basis transformation which leaves us with the combinations

$$\hat{\Phi}_A = \frac{1}{\sqrt{3}}(\hat{\Phi}_1 + \hat{\Phi}_2 + \hat{\Phi}_3) \quad (9.226)$$

$$\hat{\Phi}_E = \begin{cases} \frac{1}{\sqrt{6}}(\hat{\Phi}_1 + \hat{\Phi}_2 - 2\hat{\Phi}_3) \\ \frac{1}{\sqrt{2}}(-\hat{\Phi}_1 + \hat{\Phi}_2) \end{cases}. \quad (9.227)$$

We have demonstrated that in case of  $C_{3v}$  symmetry, the double degeneracy of the  $\hat{\Phi}_E$  is protected. For the kagome lattice, as well as for the honeycomb lattice, the only allowed term in the low-energy Hamiltonian is

$$\mathcal{H} = \begin{bmatrix} \Delta_A & & \\ & \Delta_E & \\ & & \Delta_E \end{bmatrix}. \quad (9.228)$$

Having reviewed these basic features of  $M$ -point spectral features, we come to the specific density wave states.

The translational symmetry broken content of the kagome lattice site order decomposition is  $F_1 \oplus F_3 \oplus F_4$  and this gives the  $1D$  bare point group representations  $A_1$ ,  $B_1$  and  $B_2$ . The density wave states transforming as such are shown in Fig. 9.9. The  $A_1$  state has the same mean field spectral properties as the honeycomb lattice  $A_1$  states, both the site and bond ordered states. The sign of the order parameter  $\Delta_{A_1}^{F_1}$  determines the sign of  $\Delta_A - \Delta_E$  and therefore decides between a gap and a QBC at the lower van Hove filling ( $n = 3/12$ ), while at  $n = 5/12$  the doublet is always lower in energy leading to a QBC. In case of the  $B_1$  and  $B_2$  states we find the mean field

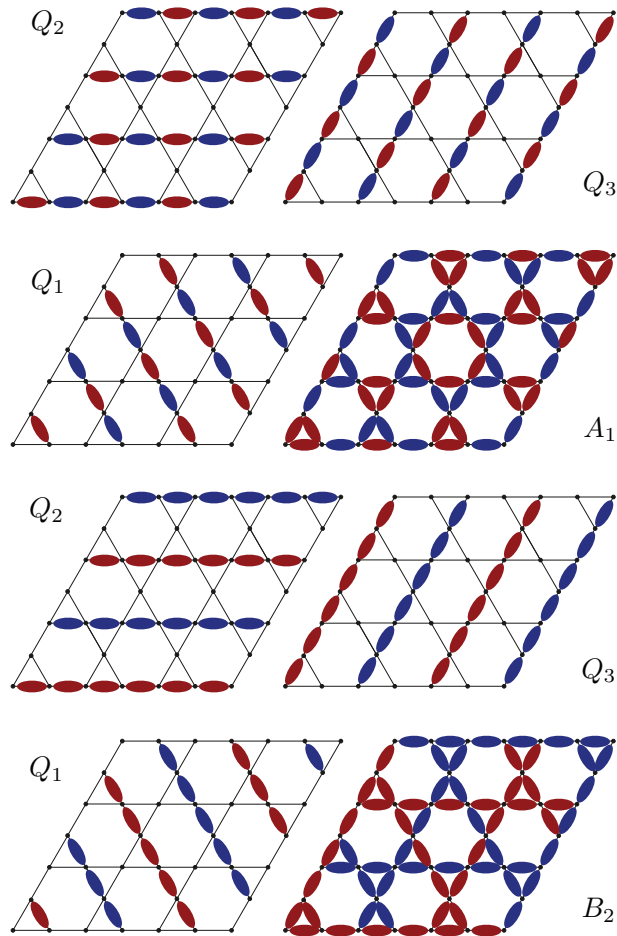


**Figure 9.10:** Graphical representation of kagome lattice bond order with  $M$ -point ordering vectors. We show the three individual components of  $F_1$  (above) and  $F_4$  (below) which transform as basis functions of these representations, in addition to the combination of these three components yielding the  $A_1$  and  $B_2$  states, respectively. We label the three components by their corresponding ordering vector  $Q_\mu$ . As before, red (blue) bonds represent stronger (weaker) bonds.

spectrum not to depend on sign of the order parameter, in accordance with results of the honeycomb lattice. The mean field spectrum of the  $B_1$  shows QBC's at both can Hove fillings while in case of the  $B_2$  state the lower van Hove point is gapped out and the one at  $n = 5/12$  shows a QBC. We note that in both cases,  $B_1$  and  $B_2$ , the low-energy terms are not first order in the density wave strength (order parameter), but higher order.

Moving on to bond order, we recall that the translational symmetry broken states transform as  $2F_1 \oplus F_2 \oplus F_3 \oplus 2F_4$ . Note the appearance of the  $F_2$  representation, which we had only encountered in time-reversal symmetry breaking flux order decompositions so far. A closer look at these states reveals that they can be organized in two series, which are  $2F_1 \oplus F_2$  and  $2F_4 \oplus F_3$ , where the second is obtained from the first by multiplication with  $B_2$ . As mentioned, explicit expressions are worked out in Appendix A.4, and here we show them graphically in Figs. 9.10, 9.11 and 9.12. For convenience and completeness we have chosen not only to show the 1D states contained in the  $F_i$  representations, but instead to show the three components transforming as  $F_i$  as well.

The generic spectral features of these states again depend on symmetry only. The mean field spectra of both the  $A_1$  states derived from the two  $F_1$  representation and given in Figs. 9.10 and 9.11 depend on the sign of the order parameter, which in case of the van Hove filling  $n = 3/12$  always decides between a gap and QBC. For the other van Hove filling,  $n = 5/12$ , the  $A_1$  state of Fig. 9.11 always leads to a QBC. The mean field spectra of the two  $B_2$  states obtained from these states (shown the same figures) does not depend on the sign of the order parameter. For both of these states the van Hove point at  $n = 3/12$  is gapped out as the doublet is lower in energy. Instead, at  $n = 5/12$  a QBC emerges, with an accidental degeneracy of the doublet  $\hat{\Phi}_E$  and  $\hat{\Phi}_A$  state in case of the  $B_2$  state given in Fig. 9.10.

The other two bond order representations related to each other are  $F_2$  and  $F_3$ , which contain the 1D representations  $A_2$  and  $B_1$ . They are shown in Fig. 9.12. The appearance of a time-reversal invariant state with  $A_2$  symmetry is new. So far we only found flux ordered states with  $A_2$  symmetry. For the latter type of states we noticed that degeneracies are in general not protected as the point group is Abelian. In the presence of time-reversal symmetry the situation changes and we can use the low-energy description at  $\Gamma$  to elucidate how. In the absence of  $C_{3v}$  symmetry the doublet states  $\hat{\Phi}_E$  corresponding to the Hamiltonian (see also Section 9.4.1)

$$\mathcal{H}_E(\vec{q}) = \pm \frac{1}{4}q^2 \pm \frac{1}{4} [(q_x^2 - q_y^2)\tau^3 + 2q_x q_y \tau^1] \quad (9.229)$$

are no longer protected by pure point group operations. However, the combination of  $C_6$  symmetry and time-reversal symmetry robustly protects a QBC [86] and the double degeneracy is therefore still protected. This is indeed reflected in the mean

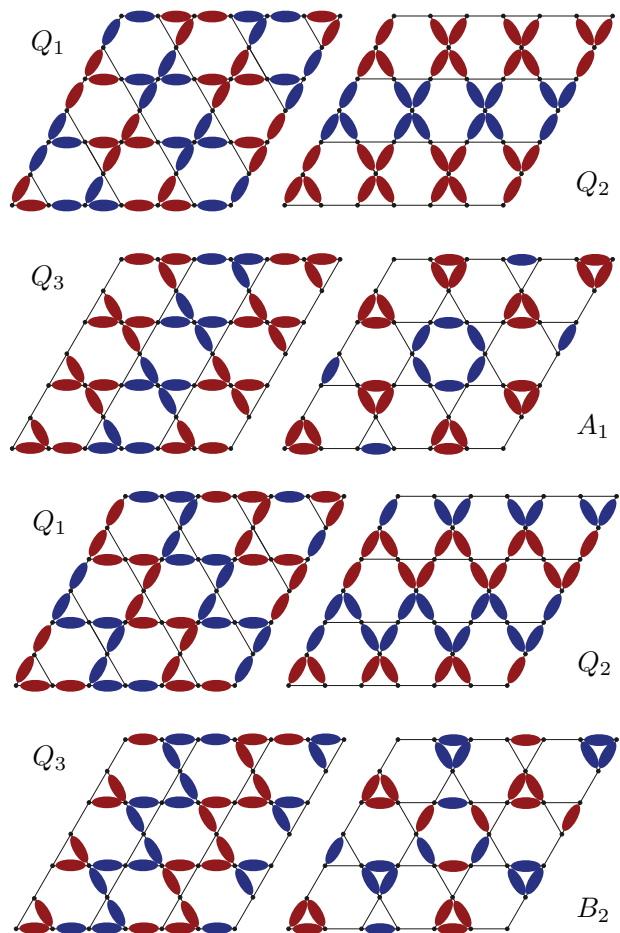


**Figure 9.11:** Same as in Fig 9.10, but for the other  $F_1$  and  $F_4$  representations contained in the bond order decomposition.

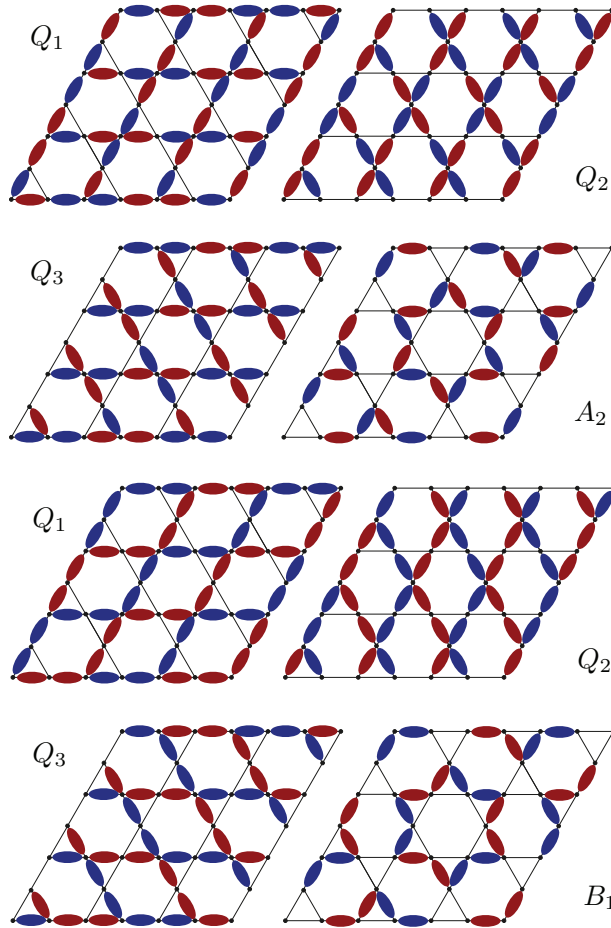


**Figure 9.12:** Same as in Fig 9.10 and Fig. 9.11, but for the  $F_2$  and  $F_3$  bond order representations. The  $A_2$  and  $B_1$  states that can be formed as linear combinations of the three components are shown as well.

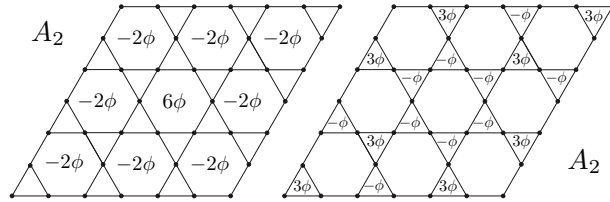


**Figure 9.13:** Graphical representation of kagome lattice flux order with  $M$ -point ordering vectors. On the left and right we show the two independent flux ordered states which transform as  $A_2$  and come from the two  $F_2$  representations contained in the flux order decompositions.

field spectrum. In particular, in case of the  $A_2$  density wave state the low-energy theory at both van Hove points is that of a QBC. In contrast, for the  $B_1$  state the order of singlet and doublet is such that a gap emerges for both van Hove points. For both states the sign of the order parameter is immaterial.

Finally, we come to  $M$ -point flux order on the kagome lattice. There are two independent  $F_2$  representations contained in the flux order decomposition, both leading to  $A_2$  time-reversal breaking  $1D$  representations. In Fig. 9.13 we show these two independent  $A_2$  states. For both states the original three-fold degeneracy at  $\Gamma$  is fully lifted and no degeneracies remain. Both of these states can and do in fact lead to a fully gapped mean field spectrum and an insulating QAH ground state.

The kagome lattice  $M$ -point states provide additional evidence that the symmetry of density wave allows to make specific statements regarding the low-energy electronic properties. They show that while details may depend on lattice, states of the same symmetry have the same generic features, independent of lattice.

### 9.4.3 Triangular lattice

In this last part of the present section focusing lattices with hexagonal symmetry, we turn to the simplest of them, the triangular lattice. Even though the lattices considered up to this point, honeycomb and kagome, have already served to uncover the general structure and shared features of density waves on hexagonal lattices at specific ordering vectors, for completeness, but most of all as a warm up for the spin triplet condensates, we treat the triangular lattice case as well. The triangular lattice does not have a sublattice, which makes it similar to the square lattice. Nevertheless, its hexagonal symmetry puts it on the same footing with the honeycomb and kagome lattices, as we will demonstrate below. The hexagonal symmetry of the triangular

lattice is its most fundamental property in the context of density waves.

Contrary to the honeycomb and kagome cases, we will restrict ourselves to ordering at the  $M$ -points. As mentioned, all three hexagonal lattices here presented have a Fermi surface nested by the  $\vec{Q}_\mu$  vectors and a logarithmically diverging density of states for appropriate filling. For the triangular lattice this filling is  $n = 3/4$  and we therefore present the potential condensates for this filling in what follows.

The recipe is well-established and familiar by now, and we content ourselves with quoting the symmetry decomposition for site, bond and flux order. For site order we find the irreducible representations  $A_1$  and  $F_1$ , i.e.

$$\mathcal{P}_s^M = A_1 \oplus F_1. \quad (9.230)$$

The triangular lattice has no basis and  $M$ -point ordering quadruples the unit cell, which yields the four distinct site ordered states. We have already seen a number of times that the representation  $F_1$  decomposes further into  $A_1$  and  $E_2$  of the point group  $C_{6v}$ . For bond order we find the decomposition

$$\mathcal{P}_b^M = A_1 \oplus E_2 \oplus F_1 \oplus F_3 \oplus F_4, \quad (9.231)$$

which is equal to the decomposition for honeycomb bond order. Not surprising, as there is an equal number of bonds in the enlarged unit cell and both lattices do have the same symmetry. Hence, in the same way as for the honeycomb lattice, there will be three condensates transforming as  $1D$  representations of  $C_{6v}$ , which are  $A_1$ ,  $B_1$  and  $B_2$ , coming from  $F_1$ ,  $F_3$  and  $F_4$ , respectively. To conclude, in case of flux order we find

$$\mathcal{P}_\phi^M = A_2 \oplus B_1 \oplus F_2 \oplus F_3. \quad (9.232)$$

For the purposes of this work we will be interested exclusively in the state transforming as  $A_2$  and coming from the triplet  $F_2$ . This state has the potential of having nonzero Chern number, see Section 9.1.4, and based on the results obtained for honeycomb and kagome lattices, we strongly suspect that it will be a gapped state carrying a QAH effect.

For triangular lattice condensates, the compatibility and consistency relations of equations (9.92) and (9.95) carry over in the same form. In addition, since we focus on  $M$ -point ordering, the definitions and formalism of Section 9.4.1 apply directly to the present case.

Starting with site order we can write the generic condensate expression in real space as

$$\langle \hat{\psi}_\sigma^\dagger(\vec{x}) \hat{\psi}_{\sigma'}(\vec{y}) \rangle = \Delta \vec{\zeta} \cdot \vec{\xi}(\vec{x}) \delta_{\vec{x}, \vec{y}} \delta_{\sigma\sigma'}, \quad (9.233)$$

We are looking for a state which respects all operations of  $C_{6v}$  and this leads immediately to the requirements that  $X\vec{\zeta} = \vec{\zeta}$  and  $Y\vec{\zeta} = \vec{\zeta}$ . There is only one vector satisfying this and it is  $\vec{\zeta} = (1, 1, 1)^T/\sqrt{3}$ . The density wave corresponding to  $F_1$  and transforming as  $A_1$  is therefore given in momentum space as

$$\langle \hat{\psi}_\sigma^\dagger(\vec{k} + \vec{Q}_\mu) \hat{\psi}_{\sigma'}(\vec{k}) \rangle = \frac{1}{\sqrt{3}} \Delta_{A_1}^{F_1} \delta_{\sigma\sigma'}. \quad (9.234)$$

The site ordered doublet contained in  $F_1$  is straightforwardly obtained by solving the equation  $(-2 + X + X^T)\vec{\zeta} = \vec{\zeta}$ , but we will leave it at this for now and continue to bond order.

In line with the approach so far we write down a general real space expression and evaluate the constraints imposed by symmetry. For the bonds in the  $\vec{x}_1$  direction we can write down the general bond order form

$$\langle \hat{\psi}_\sigma^\dagger(\vec{x}) \hat{\psi}_{\sigma'}(\vec{y}) \rangle = \Delta \vec{\zeta} \cdot \vec{\xi}(\vec{x}) (\delta_{\vec{x}+\vec{x}_1, \vec{y}} + \delta_{\vec{x}, \vec{y}+\vec{x}_1}) \delta_{\sigma\sigma'}. \quad (9.235)$$

For the other bond directions,  $\vec{x}_2$  and  $\vec{x}_3$ , the corresponding expressions are automatically obtained using the threefold rotation, which yields  $X\vec{\zeta}$  and  $X^T\vec{\zeta}$  respectively. In order to find the unique expressions for  $\vec{\zeta}$  corresponding to the translational symmetry broken states  $A_1$ ,  $B_1$  and  $B_2$  we study the effect of the inversion  $C_2$ . The state transforming as  $A_1$  should be invariant under inversion, while the other two should be odd. Applying  $C_2$  we find the condition  $G_1\vec{\zeta} = \pm\vec{\zeta}$  and this immediately fixes the  $\vec{\zeta}$  vectors. The solution associated to the plus sign is given by  $\vec{\zeta} = (0, 0, 1)^T$  and constitutes the  $A_1$  state. There are two solutions associated to the minus sign, which are given by  $\vec{\zeta} = (1, \pm 1, 0)^T/\sqrt{2}$  and they correspond to  $B_1$  (+) and  $B_2$  (-).

In order to write compact expressions in momentum space we define the triad of vectors  $\vec{\zeta}_1 = \vec{\zeta}$ ,  $\vec{\zeta}_2 = X\vec{\zeta}$  and  $\vec{\zeta}_3 = X^T\vec{\zeta}$ , where  $\vec{\zeta}$  is one of the three vectors just identified. Furthermore, we define the functions  $\cos k_j = \cos \vec{k} \cdot \vec{x}_j$  with  $\vec{x}_3 = -\vec{x}_1 - \vec{x}_2$ . Then, choosing  $\vec{\zeta} = (0, 0, 1)^T$ , we have the  $A_1$  condensate expression

$$\langle \hat{\psi}_\sigma^\dagger(\vec{k} + \vec{Q}_\mu) \hat{\psi}_{\sigma'}(\vec{k}) \rangle = \Delta_{A_1}^{F_1} \zeta_j^\mu \cos k_j \delta_{\sigma\sigma'}. \quad (9.236)$$

Very similar expressions are then simply obtained for the  $B_1$  and  $B_2$  states. Substituting the proper vectors  $\vec{\zeta}$  one has

$$\langle \hat{\psi}_\sigma^\dagger(\vec{k} + \vec{Q}_\mu) \hat{\psi}_{\sigma'}(\vec{k}) \rangle = i \Delta_{B_{1/2}}^{F_3/4} \zeta_j^\mu \sin k_j \delta_{\sigma\sigma'} \quad (9.237)$$

The last state of the triangular we present here is the flux state transforming as  $A_2$  and coming from  $F_2$ . We must have imaginary hoppings in this state and we therefore start from the Ansatz

$$\langle \hat{\psi}_\sigma^\dagger(\vec{x}) \hat{\psi}_{\sigma'}(\vec{y}) \rangle = \Delta i \vec{\zeta} \cdot \vec{\xi}(\vec{x}) (\delta_{\vec{x}+\vec{x}_1, \vec{y}} - \delta_{\vec{x}, \vec{y}+\vec{x}_1}) \delta_{\sigma\sigma'}. \quad (9.238)$$

Again the other directions are obtained using the threefold rotation. The state  $A_2$  must be invariant under the inversion  $C_2$  and we find this demand to yield the constraint  $G_1 \vec{\zeta} = -\vec{\zeta}$ , which we have seen to give solutions  $\vec{\zeta} = (1, \pm 1, 0)^T / \sqrt{2}$ . Evaluating the action of the reflection  $\sigma_v$  shows that the correct choice for  $A_2$  is  $\vec{\zeta} = (1, -1, 0)^T / \sqrt{2}$ . In momentum space the condensate expression is

$$\langle \hat{\psi}_\sigma^\dagger(\vec{k} + \vec{Q}_\mu) \hat{\psi}_{\sigma'}(\vec{k}) \rangle = i \Delta_{A_2}^{F_2} \zeta_j^\mu \cos k_j \delta_{\sigma\sigma'}. \quad (9.239)$$

Inspecting the momentum space expressions just derived from a real space perspective, we see that for each order parameter component  $\vec{Q}_\mu$  they transform according to an irreducible representation of the group of  $\vec{Q}_\mu$ , which is  $C_{2v}$ . Indeed,  $\cos k_2$  is invariant under all operations leaving  $\vec{Q}_1$  invariant. In the same way the functions  $\sin k_3 \pm \sin k_1$  and  $\cos k_3 - \cos k_1$  transform according to irreducible representations of  $C_{2v}$ . Individually these components are basis functions of the 3D  $F_i$  representations of  $C_{6v}'''$  and forming proper combinations gives basis functions of the 1D and 2D representations of  $F_i$ . In particular for the triangular lattice, which has no basis, an alternative way to construct the condensates is therefore to work directly in momentum space, find functions transforming as the group of the wave vector  $\vec{Q}_\mu$  use the compatibility and consistency relations of equations (9.92) and (9.95) and form the proper combinations.

We close this section with some remarks on the spectral effects of the site, bond and flux ordered states. To this end we can use the general features of the low-energy structure applicable to a Fermi level close to the Van Hove singularities of hexagonal lattices, which we discussed in the context of the honeycomb lattice in section 9.4.1. First, we note that at the Van Hove singularities the perfectly nested Fermi surface (only nearest-neighbor hopping) has exactly the same form in the reduced Brillouin zone as depicted in Fig. 9.7. The relevant high symmetry points, where degeneracies may be symmetry protected are the  $\Gamma$  point and the  $M'$  points. The degeneracy protection is the same as was found for the honeycomb lattice. Specifically, in the presence of full  $C_{6v}'''$  symmetry, the two-fold degeneracy at each  $M'$  point is protected, while breaking of translational symmetry lift this degeneracy in general. At the  $\Gamma$  point, the representation of the symmetry group  $C_{6v}'''$  on  $\hat{\Phi}_\Gamma = [\hat{\chi}_0, \hat{\chi}_1, \hat{\chi}_2, \hat{\chi}_3]^T$  can be decomposed into  $A_1 \oplus F_1$ . Losing translational symmetry but retaining  $C_{6v}$  symmetry then yields  $2A_1 \oplus E_2$ , which is replaced with  $2A_1 \oplus E$  in case of residual  $C_{3v}$  symmetry. Furthermore, as was mentioned already in section 9.4.1, expanding the dispersion around the  $\Gamma$  gives the same low-energy structure that was obtained for the honeycomb lattice. At  $\Gamma$  the basis states corresponding to the non-degenerate and

doubly degenerate levels are given by

$$\hat{\Phi}_A = \frac{1}{\sqrt{3}}(\hat{\psi}(\vec{Q}_1) + \hat{\psi}(\vec{Q}_2) + \hat{\psi}(\vec{Q}_3)) \quad (9.240)$$

$$\hat{\Phi}_E = \begin{cases} \frac{1}{\sqrt{6}}(\hat{\psi}(\vec{Q}_1) + \hat{\psi}(\vec{Q}_2) - 2\hat{\psi}(\vec{Q}_3)) \\ \frac{1}{\sqrt{2}}(-\hat{\psi}(\vec{Q}_1) + \hat{\psi}(\vec{Q}_2)) \end{cases} . \quad (9.241)$$

In terms of these states, the lowest order term of density wave states in the effective low-energy theory is precisely given by equation (9.207). Therefore, it is again the sign of  $\Delta_A - \Delta_E$  which decides between the two possibilities of a full gap and a symmetry protected QBC point. For the triangular lattice, we find that both the site ordered and the bond ordered  $A_1$  states lead to either a gap or a QBC depending on the sign of  $\Delta_{A_1}^{F_1}$ , in way equivalent to honeycomb lattice  $A_1$  site order. The two bond ordered states transforming as  $B_1$  and  $B_2$  both have a threefold degeneracy at  $\Gamma$ , which is consequence of the sine functions: at  $\Gamma$  the density wave state does not alter the Hamiltonian. This degeneracy is not symmetry protected. To conclude we mention here that the flux ordered state  $A_2$  gaps out the full Fermi surface. Due to the absence of reflection symmetries there is no two-fold degeneracy at  $\Gamma$ . Direction calculation reveals that the energy gap at filling  $n = 3/4$  is a nontrivial gap and the insulating state hosts a Quantum Hall effect marked by a nonzero Chern number.